Investigation of a Novel MPCM-S Based PV/T System

Samira Abdulla Ali

Submitted in partial fulfilment of the requirements for the degree of Doctor of Philosophy

Institute of Energy and Sustainable Development

De Montfort University

July 2017

ABSTRACT

In order to meet energy conservation targets and minimize global warming effects, this research is aimed to rise the efficiency of the PV/T system. This research investigates the usage of microencapsulated phase change slurry (MPCM-S) to replace conventional cooling fluids such as water. The phase change materials (PCMs) are encapsulated in a polymer shell forming microencapsulated phase change materials (MPCM) to prevent leakage of the PCMs as well as increasing the thermal conductivity. Mixtures of (5%, 10% and 15%) of microencapsulated phase change materials in water (slurries) were investigated. The use of phase change materials (PCM) improves heat absorption from the PV module due to their high latent heat, consequently increasing thermal output of the system, and electrical output because the PV panel temperature is reduced.

The research started with an intensive literature review covering all elements involved, and then the conceptual design of the experimental rig was developed. Theoretical investigations including a steady-state computerized simulation module were developed, this simulation validated depending on a previous research and showed good agreement with results from that published experimental study. This suggested that the computer module could successfully predict the operational performance of the module with satisfactory accuracy. A series of laboratory-based tests were conducted for a wide range of conditions and slurry concentrations. The results were compared to the computer simulation with the same parameters. It was found that the root mean square percentage deviations (RMSPE) between experimental and simulated results were generally under 4%, so considered acceptable for engineering application of PV/T system. A slurry concentration of 10% was found to give the best results.

Under operational conditions of 10% MPCM concentration, 3000 Reynolds number and 600W/m^2 solar radiation, an experimental test was conducted. The electricity and heat outputs of the system were 108 and 520 W respectively, the associated electrical and thermal efficiency were 14.1% and 68.8%, giving an overall efficiency of 82.9%.

The economic analysis was carried out to investigate the feasibility of the MPCM-S based PV/T system in two different climates of Europe. It showed that the system generates higher annual electrical and heat of 488.29 and 2184.93 kWh in a hot climate

(using Madrid as an example) than the annual electrical and heat of 323.12 and 1262.1 kWh for colder climate (Stockholm as an example). Consequently, the life cycle cost of MPCM-S based system per kWh were -0.068 and 0.019 GBP for Madrid and Stockholm respectively, and for water-based PV/T system were -0.038 and 0.028 GBP for Madrid and Stockholm respectively. Finally, the environmental effect of the system was investigated by calculating the life cycle CO_2 emission reduction of MPCM-S based PV/T system in both climates, they were 11.75 and 6.9 tonnes for Madrid and Stockholm respectively, and for water-based PV/T system were 7 and 3.5 tonnes for Madrid and Stockholm respectively.

Generally, the MPCM-S based PV/T system is more efficient than the conventional water-based PV/T systems as predicted, especially if it runs with 10% MPCM-S. It delivers higher electrical and heat outputs in hot climates in comparison with colder climates of Europe, consequently better economically and environmentally.

AKNOWLEDGEMENTS

"All praise and thanks are for God almighty, the One who, by His blessing and favour, good works are accomplished".

I would like to express my sincere and appreciation to my first supervisor, Dr Andrew Wright, for his keenness on my success by continuous support, guidance, detailed and constructive comments and advice. His experience, wide knowledge and logic thinking have provided a good basis for the present thesis.

I am sincerely indebted and thank my external supervisor Professor Xudong Zhao, for his backing, suggestions and immense knowledge even after moving to another university. His contributions, suggestions and insight have been of great value to me and for his important support throughout this work.

Thanks to my great mother and deepest gratitude and love for her dedication and support for every successful step during my life.

Finally, I would like to thank and dedicate this thesis to my beloved husband for his unselfish, encouragement, care and endless love. I could never have accomplished so much without him.

PUBLICATIONS AND CONFERENCE PROCEEDINGS

1. Samira Ali, Andrew Wright, Xudong Zhao, Zhongzhu Qiu, Experimental Rig and Test Procedure Of Novel Microencapsulated Phase Change Materials Slurry (MPCM-S) Based Building Integrated Photo Voltaic/Thermal (BIPV/T) , the 1st faculty of technology PGR conference ,De Montfort University, Leicester, July 2016, **[Best paper award winner]**.
2. Zhongzhu Qiu, Xiaoli Mab, Xudong Zhao, Peng Li , Samira Ali . Experimental investigation of the energy performance of a novel Micro-encapsulated Phase Change Material (MPCM) slurry basedPV/T system. Appl Energy 2016;165:260–71. doi:10.1016/j.apenergy.2015.11.053.
3. Zhongzhu Qiu,Xudong Zhao, Peng Li , Xingxing Zhang , Samira Ali , Junyi Tan. Theoretical investigation of the energy performance of a novel MPCM (Microencapsulated Phase Change Material) slurry based PV/T module. Energy 2015;87:686–98. doi:10.1016/j.energy.2015.05.040.
4. Ali Algaddafi ,Nei Brown ,Rupert Gannon, Saud Al Tuwayjiri, Abdulla Rahil, Samira Ali. An Analogue Computation based Photovoltaic Emulator for realistic Inverter testing. Proceedings of third International Conference on Energy Engineering Faculty of Energy engineering - Aswan University - Aswan - Egypt December 28-30, 2015.
5. Zhongzhu Qiu, Xudong Zhao, Samira Ali. Microencapsulated Phase Change Suspension (MPCS): Newtonian or non-Newtonian fluid? 12th International Conference on Sustainable Energy technologies (SET2013) 26-29 August 2013.

CONTENTS INDEX

LIST OF FIGURES

LIST OF TABLES

ABBREVIATIONS

ASHRAE	*American Society of Heating, Refrigeration and Air Conditioning Engineers*
BIPV	*Building Integrated Photo Voltaic*
CC	*Cooled Ceiling*
CNG	*Compressed Natural Gas*
DHW	*Domestic Hot Water*
DSC	*Differential Scanning Calorimetry*
RCO_2	*Reduction of Dioxide Carbon*
EU	*European Union*
GBP	*Great British Pound*
GHG	*Green House Gas*
HVAC	*Heating, Ventilation and Air Conditioning*
LCC	*Life Cycle Cost*
LHS	*Latent Heat Storage*
MPCM	*Micro-encapsulated Phase Change Materials*
MPCM-S	*Micro-encapsulated Phase Change Materials Slurry*
PBT	*Pay Back Time*
PCM	*Phase Change Materials*
PV	*Photo Voltaic*
PV/T	*Photo Voltaic / Thermal*
SEM	*Scanning Electron Microscope*
SHS	*Sensible Heat Storage*
TES	*Thermal Heat Storage*
TPT	*Tedlar Polyester Tedlar*
VAT	*Value Added Tax*

NOMENCLATURE

Am	*Module area, m^2*
Aø	*Dependent constant on size and shape of MPCM*
Cb	*Bond conductivity* $W \cdot m^{-1} \cdot k^{-1}$
cp	*Specific heat capacity,* $kJ \cdot kg^{-1} \cdot k^{-1}$
D	*Diameter (* m *)*
d	*Diameter (m)*
F	*Standard fin efficiency*
F`	*Thermal efficiency factor of the collector*
g	*Gravity acceleration (m/s^2)*
H	*Height (m)*
h	*Heat transfer coefficient(W/m.K)*
hc	*Convection heat transfer coefficient (W/m.K)*
h_R	*Radiation heat transfer coefficient (W/m.K)*
hx	*Heat exchanger*
I	*Solar irradiance (*W / m^2*)*
K	*Thermal conductivity (* $W \cdot m^{-1} \cdot k^{-1}$ *)*
L	*Length (m)*
m	*Fin variable*
$\dot{m}$	*Mass flow rate (* kg / s *)*
n	*number*
Nc	*Number of covers*
Nu	*Nusselt number*
Np	*Number of pipes*
p	*Pressure (pa)*
Pr	*Prandtl number*
Ra	*Rayleigh number*
Re	*Renaults number*

Se	*Standard deviation of the groups of testing results*
t	*temperature (^{o}C)*
T	*Temperature (^{o}C)*
U	*Uncertainty*
$\overline{U}$	*Mean Uncertainty*
U_L	*Overall heat loss coefficient (W/mK)*
V	*Velocity (m/s)*
W	*mass fraction (%)*
w	*Width (m)*
xe	*Experimental value*
xs	*Simulation value*
$\bar{x}_e$	*Arithmetic mean experimental value*

Subscripts

a	*Air*
abs	*Absorbed*
c	*Cover, convection*
c-a	*Cover to air*
core	*Core of MPCM particles*
e	*Electrical*
f,i	*Inlet fluid*
fin	*Fin*
g,pv	*Glass layer of PV lamination*
L	*Loss*
m	*mean*
n	*Number*
o	*Overall, outer*
p	*Absorbed pipe*
p,i	*Pipe inlet*

p,o	*Pipe outlet*
particle	*Particle of MPCM*
pv	*PV cell*
pv-c	*PV to cover*
rt	*Reference temperature*
shell	*Shell of the MPCM particles*
slurry	*MPCM slurry*
th	*Thermal*
u	*Useful*

Greek

α	*Absorption ratio*
β_p	*Packing factor*
β_{pv}	*PV cell efficiency temperature coefficient*
δ	*Thickness (m)*
ε	Emissivity
η	*Efficiency*
θ	*Collector slop (deg)*
ρ	*Density (kg/m^3)*
σ	*Stevan - Boltzman constant*
μ	*Dynamic viscosity (kg/m.s)*
Ø	*Particle volumetric concentration of the slurry*
τ	*Visual transmittance*

CHAPTER 1: INTRODUCTION

1.1 Background

Climate change is the main challenge to be faced in the 21st century, due to the fast progress of its effect. The forecasts show that the surface temperature could rise to between 1.4 °C and 5.8 °C if action is not taken [1]. Such grow will doubtless cause droughts, glacier melting, sea level rise, floods etc. So a serious solution is needed to reduce the green gases emission, this could be achieved by swapping many traditional energy resources to renewable energy[2] .In 2015 the United Nations Climate Change Conference held in Paris, 195 countries made a plan for reducing the effect of global warming by reducing the CO2 and other greenhouse gases (Methane, Ozone, Chlorofluorocarbons…etc.) emission. Their aim is to limit the global temperature to rise to below 2°C [3]. "Greenhouse effect" introduces the link between CO2 emission and global warming as shown in **Figure 1–1**. According to the United Nations Environmental Program UNEP-2009 , buildings are responsible for more than 40% of global energy consumption, and 30% of global greenhouse gas emissions[4]. In the EU countries, buildings (commercial and residential) cover 38.7% of the total energy consumption[5], and 36% of the CO2 emissions, thus EU stated that all new buildings shall be almost zero energy buildings by 31 December 2020[6].

The International Renewable Energy Agency (IRENA) planned a project named RE map, which aims to double the world's usage of renewable energy by 2030. They expect that in 2030 renewable energy consumption in China reach 20%, in the U.S. 15% and in the E.U. 14%, so they will become the three largest renewable energy consumers, eventually getting a united global share of 49%. According to the plan of (IRENA), the usage of coal will drop to 25% by 2030. By depending on the same scenario the photovoltaic power will increase from 1% to 7% from 2014 – 2030 [7]. Mostly the energy demand of buildings originates from heat and electricity, and mainly used for space heating and cooling, hot water, lighting and ventilation.

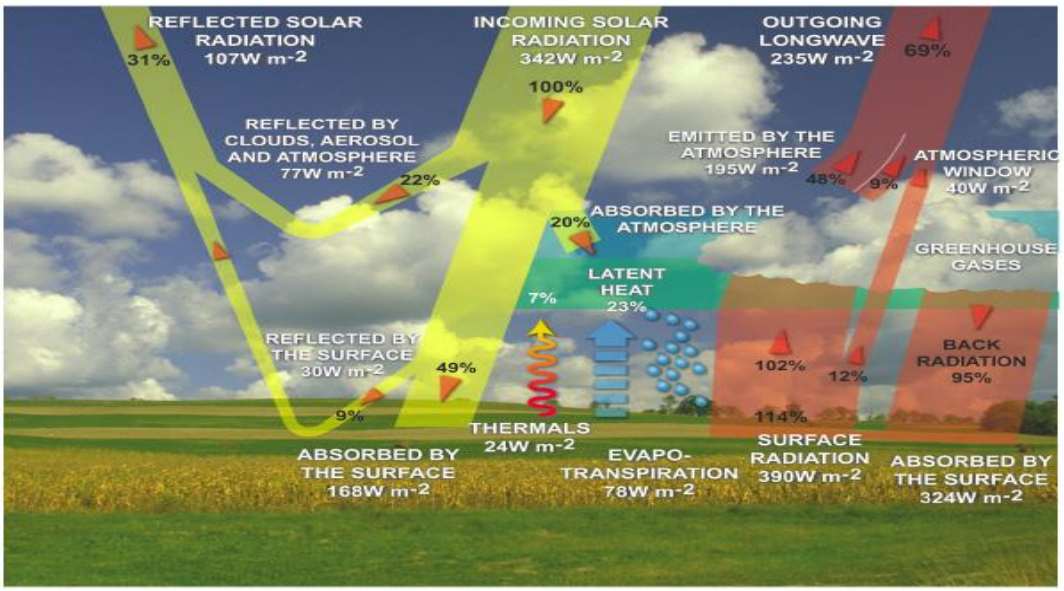

Figure 1–1: "Greenhouse effect" the trapping of the sun's warmth in the planet's lower atmosphere[8]

Because of the high-energy consumption in the building sector, especially in the EU, reducing the energy demand and improving the energy resources are the main challenges, which need to be faced. In October 2014 the European Council approved the target plan of 2030 for greenhouse gas reduction of 40% at least, depending on renewable energy by at least 27%, this is the extension of the European Council 2020 target[9]. Further action has been taken by the EU which is setting a long term energy roadmap of 2050 that aims to reduce the green gas emission by 80 – 90% in comparison with 1990 levels[10]. According to a report by International Energy Agency, solar power could reach the top commercially within a decade and could shift the fossil fuels and become the number one energy resource in the world by 2050 [11]. Renewables 2015 Global Status report stated that the most rapidly grown renewable sector between 2009 – 2015 is Photovoltaic [12] as shown in **Figure 1–2.**

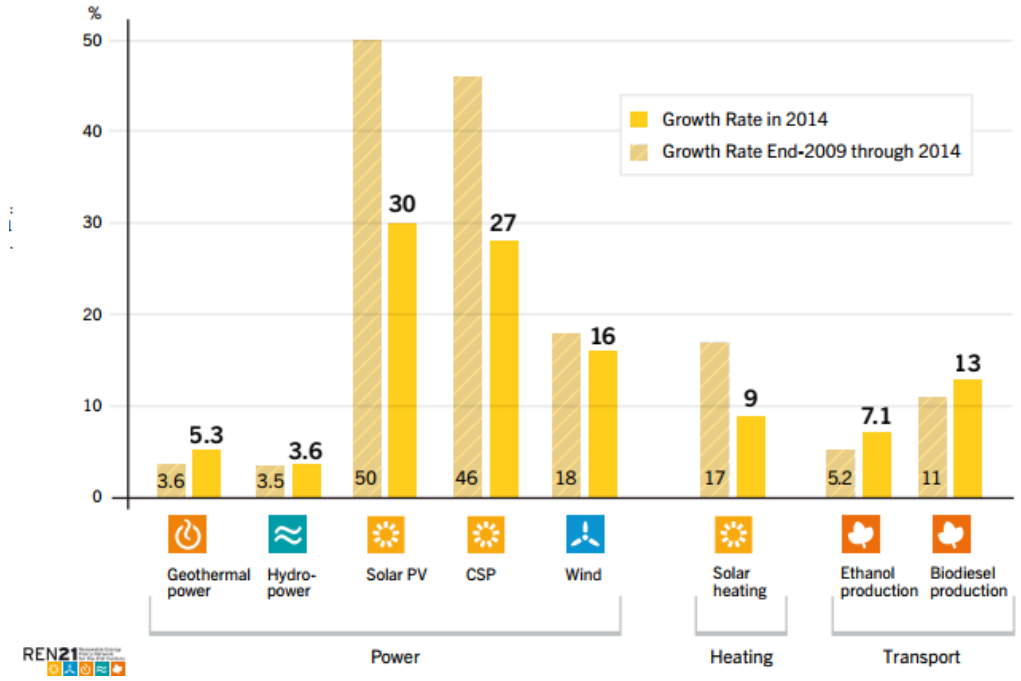

Figure 1–2: Average annual growth rate of renewable energy capacity and Biofuels production[12]

1.2 General description of the research concept

The main purpose of the research is to increase the efficiency of the PV/T system by using a novel MPCM-S as a cooling fluid. The slurry contains phase change materials to improve the cooling capacity of the system. Phase change materials with a high latent heat can absorb more heat than a conventional cooling medium without a significant change in the temperature, it changes the phase from solid to liquid while absorbing the heat and returns to the solid phase when releasing it. Consequently, the PV cells stay colder and the electrical output of the system increase. Then it could be stored in batteries or could be connected to the national grid.

Meanwhile, the thermal output of the system could be employed in several ways, depending on the amount of cooling the slurry needs to change the phase of its main content (PCM) from liquid to solid and recirculate through the pipe attached behind the PV module. There are three ways for the heat to be employed, i) air based heat exchanger could be used if the slurry temperature is not too high, the output air could be used for heating. (ii) The slurry could pass through a water-based heat exchanger if it needs more cooling, the water could be employed for the domestic use. (iii) If the slurry needs further cooling, the heat pump is the best choice to be used. Heat pump has a very

high cooling ability, it upgrades the heat and the hot water produced from the condenser (a part of the heat pump) could be used for the domestic use. In this research, the heat pump has been chosen to be used. **Figure 1–3** illustrates the concept of the PV/T system.

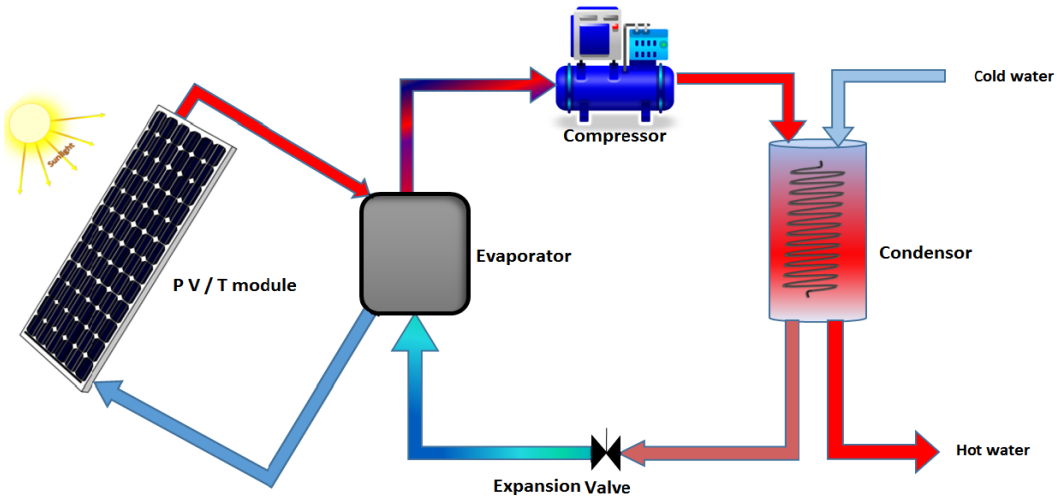

Figure 1–3: The concept of the PV/T system

1.3 Aim and Objectives

As the Photovoltaic /Thermal system considered a developed renewable energy resources, which introduce electricity and heat together, that encouraged the researchers to do further development to remove the weak points associated with this kind of systems. From the engineering point of view, PV/T system still has some problems that need investigation such as; inadequate energy supply, low efficiency, irregular fluid distribution, leakage etc. This research is a step forward in solving one of the problems, which is low efficiency by replacing the conventional cooling fluid mostly air or water by a novel Phase Change Materials Slurry. The overall aim of the project is to improve the overall efficiency of the PV/T system toward decreasing GHG emission, consequently involving in the efforts for limiting global warming. The objectives for achieving the goal are illustrated as below:

1- To carry out a literature review on PCMs and PV/T systems, hence detect the challenges and barriers not solved up to date, and show the recommendations for solving it.

2- To design PV/T rig for laboratory testing of Microencapsulated Phase Change Materials Slurry (MPCM-Slurry).

3- To develop, as part of research team effort a computerized simulation of the PV/T module for the steady state flow condition, and validate it depending on a similar system from a published resource, then using the cooling fluid (MPCM-S) to optimise the design and predict the performance of the system.

4- To construct and set up the PV/T system rig in the laboratory, and test under a range of steady state flow condition, then compare results with the simulation module outputs under same operation conditions.

5-To investigate the environmental and economic effect of the system application in two different European climates.

1.4 Methodology

The planned project involves a review of literature for investigating the novel cooling media of the system (MPCM-S) and its contents, also the potential of using it in building energy systems. The literature identifies the PV/T operational mechanism and classifies them according to the used cooling fluid. This enables carrying out the main methods to process the scientific and technical works of the study including:

Conceptual design of the PV/T energy system: The project planned to include laboratory-based experiments, so the preparation of a rig design is required. This approach includes (i) preparing the sketch up of the PV/T system; (ii) preparing the list of the system components, investigating the geometrical size and materials of the components, then suggest the potential variation depending on the fundamental knowledge, established experience and availability in market; and (iii) identifying the MPCM-S as a cooling fluid to be used in the PV/T system. The design is detailed in **Chapter 3**.

Theoretical investigation and developing a computer model: The computerized simulation model has to be developed, because none of the available software could represent a slurry based PV/T system. This approach predicts the system's operating

performance and optimises its configuration. It includes; (i) analysing the fluid flow, power generation and heat transfer of the entire system; (ii) identifying the optimal size of the system components specially the serpentine pipe size; (iii) recommending the optimal system operating conditions such as radiation, flow rate state of the MPCM-S and MPCM concentration percentage in the slurry, these obtained by comparing various predictions for different operational conditions and climates; and (iv) comparing the overall and net efficiency of the novel MPCM-S base PV/T system with the efficiencies of the conventional water-based PV/T system. All the formulas representing the system performance and the algorithm are detailed in **Chapter 4**.

Laboratory-based experiments: Carrying out the experiments under laboratory conditions for the steady state flow condition, to provide the outputs that are more reliable, and to validate the computerised model, which is viable for different climates applications. The approach includes; (i) determine the net efficiency of the module which includes electrical and thermal efficiencies under various radiation, flow rate and MPCM concentration conditions; (ii) calculating the overall system's Coefficient of Performance (COP) by taking into account the power consumed for pump which used for the slurry circulation and the heat pump for cooling module; and (iii) validate the developed computer simulation model to reach the satisfactory accuracy of prediction. Details about the experiments are presented in **Chapter 5**.

Economic and environmental analyses: Choosing two locations in Europe with different climate conditions and compare the performance and viability of the novel PV/T system within each climate condition. The approach steps toward this objective are; (i) collecting weather data of two different climates and calculating the annual heat and electricity yields; (ii) calculating the life cycle cost (LCC) for economic analysis; and (iii) determining the annual CO2 emission as environmental analyse. Details about economic and environmental analysis are illustrated in **Chapter 6**.

1.5 Overall thesis structure

Chapter 1 (Introduction): This chapter provides overall information about the project that covers background, objectives, general concept of the project and methodology.

Chapter 2 (Literature review): This chapter includes detailed information and reviews about the MPCM-S and PV/T technology and investigation of current and possible future statues of the PV/T systems. It illustrates the potential opportunities for developing PV/T technology in the future.

Chapter 3 (Experimental rig design): This chapter defines the working principle of the proposed system and the diagram for the main components. It shows the proposed main parts of the system such as (PV/T module, heat pump and MPCM-S) and the actual once used in the laboratory respectively. In addition, it illustrates the experimental instrumentation used for measuring the operational parameters of the experiments.

Alternative structures, materials, geometric and operating conditions of the system are recommended for the further input of theoretical simulation.

Chapter 4 (Theoretical analysis and development of the computer simulation model)*:* This chapter analysis a set of heat transfer, fluid flow, solar transmittance, photovoltaic and energy balance equations to support the development of the computerized model for the steady state simulation. This simulation offers a valuable outcomes and recommendation for recognizing the optimum geometry of the components and operational conditions.

Chapter 5 (Experimental performance under Laboratory conditions): This chapter shows the experimental rig construction and the test procedure with all the problems and difficulties associated with the process. Also it analysis the experimental results especially the effect of the radiation slurry flow condition and the MPCM particles concentration in the slurry on the performance of the system. Then comparing these reliable results with the simulation output to make a set of comparison curves for further discussion and validating the results from the computerized module. Finally determining the performance of the overall PV/T based heat and power system with the optimum operational conditions.

Chapter 6 (Economic and environmental analysis): This chapter illustrates the application of the system for two European cities with different climates, then calculating the heat and electrical output for each city, to find the viability of the system in different climate conditions. For analysing the economic effect life cycle cost (LCC)

needs to be calculated. Finally, annual CO_2 emission needs to be determined for investigating the environmental effect of this new system's application.

Chapter 7 (Conclusion and further works): This chapter summarises the main finding and results of the research. It discusses the problems and challenges facing the technology and the available opportunities for developing it.

CHAPTER 2: LITERATURE REVIEW

2.1 Basic concept of PCM

2.1.1 Classification and its Thermal and Physical properties

The increase of energy demand urged the scientists to discover new renewable energy sources, so energy storage device was one of the developed areas for the aim. Thermal energy storages (TES) could attain the aim as a renewable resource, consequently, reduce the environment impact by overuse energy. There are two main kinds of thermal energy storages, sensible heat storages (SHS) and latent heat storage (LHS). The former utilizes the change in temperature and the heat capacity of the material during charging and discharging processes. The temperature changes and amount of the material as well as the specific heat of the medium specify the amount of stored thermal energy. The latter (LHS) uses phase change materials which absorb and release the heat during phase changing process and provides higher energy storage density [13].

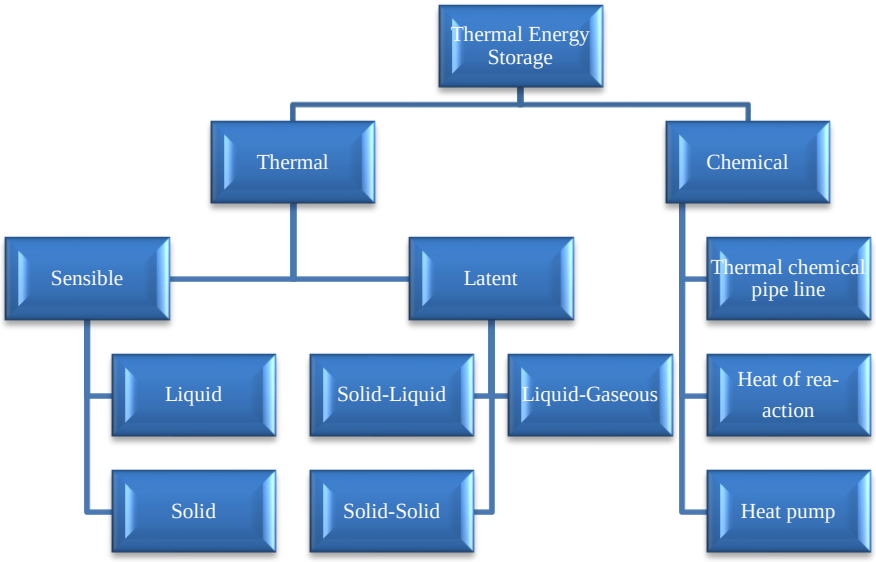

Figure 2–1: Types of thermal storage [14]

A Phase change material (PCM) is a substance which possesses a high latent heat of fusion, it melts when absorbing heat and solidifies when releasing it, this process happens without a significant change in temperature as shown in **Figure *2–2***, and could be repeatedly switched between these two phases. PCMs are available for a wide range of fusion temperature between -5 to 150 ºC [15]. They enhance the heat storage by 5–14

times heat per unit volume compared to sensible storage materials such as masonry or water [16].

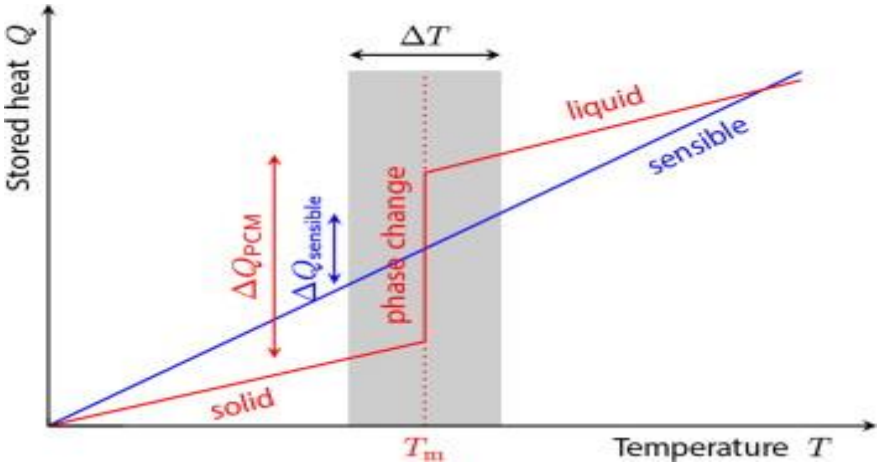

Figure 2–2: Graphic representation of the variation of stored heat of a PCM with increasing temperature[17]

The desirable properties or the selection criteria of phase change materials to be used for latent heat are [18]:

Thermodynamic properties:

- High latent heat of fusion per unit volume.
- Melting temperature matches the operating temperature range.
- Small volume changes during phase transformation and small vapour pressure.
- High specific heat, high density, high thermal conductivity.
- High nucleation rate to avoid super cooling of the liquid phase.

Kinetic properties:

- The high rate of crystal growth.

Chemical properties:

- Completely reversible freeze/melt cycle.
- Chemical stability.
- Non-corrosiveness, non-toxic, non-flammable, non-explosive materials.

- No degradation with time after a large number of freeze/melt cycle.

iv) Economic properties:

- Low cost.
- Large-scale availability.

Phase change materials are recognized by some merits to be the best up to date for thermal energy storage and its applications such as high latent heat, small volume requirements for latent heat storage and melt -solidify processes occur at a constant temperature[19]. All the previous advantages, even more, lead to a high rate of energy saving, which is the aim of most scientists working in the energy field. Beside all these advantages the phase change materials have some problems such as super cooling, complex thermodynamic properties and lack of investigated thermodynamic properties, low thermal conductivity and high pressure drop are the most important problems of phase change materials which have to be solved [20].

Super cooling is one of the major problems in the inorganic phase change materials [13], it is a phenomenon that occurs when the liquid or gas reach the temperature below freezing point and still at their phase (liquid or gas) and do not solidify [21], so it's the difference between melting and solidifying temperature [22][23]. The PCMs have super cooling throughout their freezing process, the main factors influencing degree of super cooling are; (i)heterogeneous nucleation which refers to the nucleation at the surface of external bodies alike heat exchangers, suspended particles and containers.(ii) homogenous nucleation, refers to forming embryos of a new phase and (iii) the rate of cooling [24].

Generally, phase change materials are classified into four types: solid-liquid, solid- gas, solid-solid and liquid-gas phase change materials as shown in **Figure *2–3***. Liquid-gas phase change materials have higher latent heat during phase changing than solid-liquid one, but because of containment problems and high gas volume of liquid – gas phase change materials while phase changing are the main reasons to let the solid- liquid phase change materials to be more desirable [16].

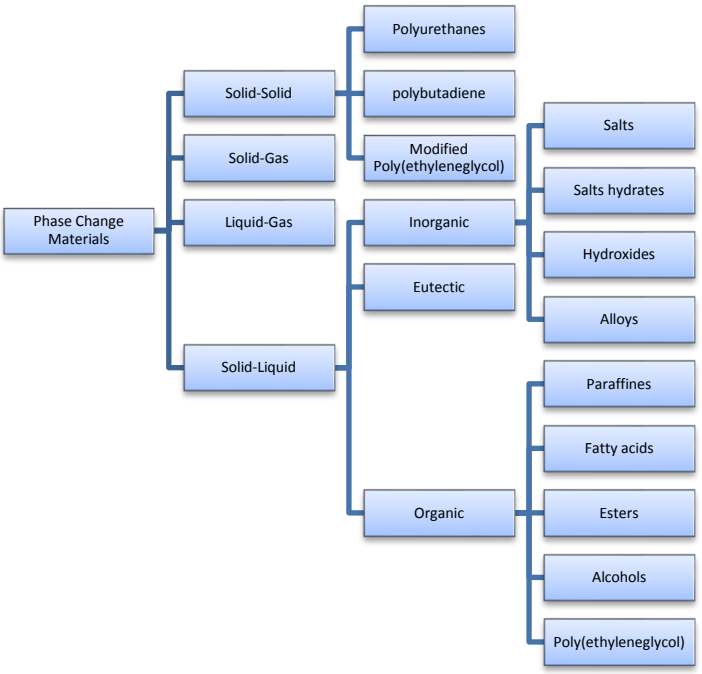

Figure 2–3: Classification of Phase Change Materials [13]

So most of the energy-related researches concentrated on the solid-liquid phase change materials due to its suitability for energy applications. It is generally classified to (Organic, Inorganic and Eutectics) as below:

1-Organic phase change materials [16]:

(a)-Paraffin: possess lots of desirable characteristics as thermal storage material such as negligible super cooling, chemically stable, high latent heat, low vapour pressure, no phase segregation, self-nucleating, and commercially available. Nevertheless, it has some demerits such as a large change of volume during phase transmission and low conductivity**.**

(b) Non-paraffin: Includes a wide variety of organic phase change materials such as esters, fatty acids, glycols and alcohols. They show an excellent (melting /freezing) characteristic without super cooling

2- Inorganic phase change materials [25]:

The main type of inorganic PCMs is salt hydrates. These PCMs have some attractive advantages such as, the high latent heat of fusion, high water content, hence they are

cheap and available and they are safe and not flammable. However, they have some disadvantages like instability, corrosiveness and tendency to super cooling. These disadvantages made the researchers to concentrate on organic PCMs rather than these PCMs.

3-Eutectics:

Eutectic is a composition includes two or more components.

The general advantages and disadvantages of the three main types of solid –liquid PCMs are listed in **Table 2-1.**

Table 2-1 :Comparison of different types of PCMs [26]

Classification	Advantages	Disadvantages
Organic PCMs	1. Available in a large temperature range	1. Low thermal conductivity (around 0.2 W/m K)
	2. High heat of fusion	2. Relative large volume change
	3. Low super cooling	3. Flammability
	4. Chemically stable and recyclable	
	5. Good compatibility with other materials	
Inorganic PCMs	1. High heat of fusion	1. Super cooling
	2. High thermal conductivity (around 0.5 W/m K)	2. Corrosion
	3. Low volume change	
	4. Availability at low cost	
Eutectics	1. Sharp melting temperature	Lack of currently available test data of thermo-physical properties
	2. High volumetric thermal storage density	

A perceptible number of studies have been done in the last decade to improve the phase change materials to verify the best results and solve the associated problems, an example is shown in **Table 2-2**.

Table 2-2: The methods of solutions for the main problems associated with PCMs [27]

	Methods of Solution	
	Material Developments	Microencapsulation
Problems to be solved	• Incongruent Melting • Suitable melting temperature • Super cooling	• Liquid-solid Phase • Low-thermal conductivity • Volume change • Incongruent Melting

2.1.2 MPCM, and MPCM- Slurry preparation and properties

Microencapsulation is a method in which the particles of the phase change material are coated by a film of polymeric material, forming a shell with a diameter of a few micro meters, called microcapsule, it is usable for phase change materials with a melting point between -10 to 80 ºC [28]. Microencapsulation is introduced as the main method to overcome the major problems associated with phase change materials, it increases the heat transfer process by using a capsule material with higher thermal conductivity than the PCM [29], and it solves the liquid migration in some applications[30]. Sizes between 1 µm and 1 mm are called micro PCM, if it is less than 1 µm it called Nano PCM [31]. An extra layer could be added on the microcapsules, which called double layered microencapsulated phase change materials, this extra external layer is for enhancing the electrical conductivity in addition to the thermal conductivity, this external layer could be silver [32]. These microencapsulated phase change materials have higher resistance to damage and are stronger when their diameters are less than 10 µm [33].The heat transfer process of the MPCM is explained in **Figure 2–4**.

Figure 2–4: The heat transfer process of MPCM [34]

The most common methods of preparing microencapsulation phase change materials are:

1. Physical method: (air-suspension coating, centrifugal extrusion, vibrational nozzle, pan coating, spray drying and solvent evaporation).
2. Physic-chemical methods :(Ionic gelation, coacervation, and sol-gel).
3. Chemical methods: (interfacial polymerization, emulsion polymerization and suspension polymerization).

Choosing a suitable method depends on the materials of the core and the shell, the required capsule size, the thickness of the shell and the chemical and thermal properties of the capsule[35].

Organic phase change materials are more stable than inorganic ones after about 1000 thermal cycles [36]. Paraffin is an n-alkane with a chain of a different number of carbon. It is a suitable phase change material to be encapsulated due to the large latent heat of fusion, suitable phase change temperature for most applications , chemical stability and its capability to be encapsulated [37] ,also microencapsulation needs a hydrophobic core materials like paraffin which is another reason for its suitability for microencapsulating[30].

Though the heat storage and release depend on the core material of the microencapsulated phase change materials, it is important not to underestimate or ignore the role of shell material and its effects on the properties of the microencapsulated phase change materials like shell mechanical strength, morphology, thermal stability and heat capacity[31].The requirements of shell materials are i) high thermal conductivity, ii)

good flexibility, iii) good sealing tightness and high endurance. So due to the better thermal and mechanical stabilities as well as higher thermal conductivity than the organic phase change materials , researchers prefer inorganic phase change materials as shell material[38], the availability of the microencapsulated phase change materials in markets is limited, **Table 2-3** illustrates the commercially available m-PCM.

Table 2-3:Commercially available m-PCMs*[39]*

Manufacturer	Product	Type of product	PCM	Concentration	Particle/droplet size	Melting temperature	Latent heat
BASF	DS 5000	mPCM slurry	Paraffin	42%		26 °C	45 kJ/kg
	DS 5007	mPCM slurry	Paraffin	42%		23 °C	41 kJ/kg
	DS 5030	mPCM slurry	Paraffin	42%		21 °C	37 kJ/kg
	DS 5001	Powder	Paraffin			26 °C	110 kJ/kg
	DS 5008	Powder	Paraffin			23 °C	100 kJ/kg
	DS 5030	Powder	Paraffin			21 °C	90 kJ/kg
Microtek Laboratorie	MPCM-30D	Powder	n-Decane		17–20 µm	−30 °C	140–150 kJ/kg
	MPCM-10D	Powder	n-Dodecane		17–20 µm	−9.5 °C	150–160 kJ/kg
	MPCM 6D	Powder	n-Tetradecane		17–20 µm	6 °C	157–167 kJ/kg
	MPCM 18D	Powder	n-Hexadecane		17–20 µm	18 °C	163–173 kJ/kg
	MPCM 28D	Powder	n-Octadecane		17–20 µm	28 °C	180–195 kJ/kg
	MPCM 37D	Powder	n-Eicosane		17–20 µm	37 °C	190–200 kJ/kg
	MPCM 43D	Powder	Paraffin mixture		17–20 µm	43 °C	100–110 kJ/kg
	MPCM 52D	Powder	Paraffin mixture		17–20 µm	52 °C	120–130 kJ/kg
Capzo	Thermusol HD35SE	Powder	Salt hydrate			30–40 °C	200 kJ/kg
	Thermusol HD60SE	Powder				50–60 °C	160 kJ/kg

In last few years, a new method developed for producing PCMs in industries such as BASF and EPS [40].According to this method, the PCM particles are encapsulated in polymer shells size (0-1000 µm) forming micro encapsulated phase change materials(MPCM). This MPCM s then mixed into a carrier fluid (e.g., water) with the particular additives (e.g., anti-freezing fluid), thus forming a microencapsulated PCM slurry (MPCM-S), the size of the shells depends on the application used for. Usage of this kind of slurries qualifies much higher thermal conductivity of the fluid [41][42].

These microcapsules need an energy transfer medium fluid to be dispersed in, mostly water is used for this purpose, this mixture of water and capsules is called microencapsulated phase change materials slurry, or MPCMs [43], the increase in MPCM ratio (mass concentration) in the slurry enhances its latent heat [44] , it leads to increase the heat storage capacity and time [45]. Although MPCM- slurry possesses higher heat transfer coefficient and specific heat than pure water, these benefits could be offset by consuming more power for pumping it due to its higher viscosity which leads

to higher pressure drop. Other challenges include high maintenance cost, poor durability and super cooling [14].

Table 2-4: Objective magnitudes and influential parameters at the time of selection of a PCM emulsion or mPCM slurry as heat transfer fluid or thermal storage materials [39].

Influential factors or parameters	**Objective magnitudes**	**Influence when the factor increases**	
		Positive influence	**Negative influence**
Particle Diameter	Rupture of microcapsules		Rupture pressure of microcapsules decreases, higher number of ruptured capsules
	Super cooling	Greater probability of existing nucleation agents, and, therefore, lower sub cooling	
	Apparent hysteresis		Possible non-equilibrium between PCM and water temperatures, possibility of hysteresis
	Heat transfer	Improvement in convection coefficient.	
	Stability of emulsions		Creaming speed increases
PCM concentration	Heat capacity	Increase in heat capacity<comma> increases in transported heat	
	Pressure drop		The increase of viscosity, increase of pressure loss and pumping work. Up to PCM concentrations of 15–20% the increase is slightly superior to water.
	Heat transfer	Decrease in Stefan number and, therefore, improvement of convection coefficient.	Increase in viscosity, decrease in turbulence degree, and, therefore, worsening or convection coefficient.
			The decrease of thermal conductivity, occasioning deterioration in heat transfer.
Operation temperature range	Heat transfer	The operation temperature range must fit with the phase change temperature range, and be the narrowest possible.	

For any application of MPCM-s, the thermal, physical and rheological properties of the bulk should be known, each application needs a slurry with different ratio of particle to the carrier fluid, this apart of a particular thickness of the microcapsule shell and its ratio to the core material which is PCM. Any change of the above contents leads to change in a thermal and physical property of the bulk (slurry). The formulas for calculating the specific heat and density of the microcapsules and the slurry were resulting from mass and energy balance principle, these formulas [4-1] to [4-6] are shown in section **4.1**.

2.1.3 Overview of researches about PCM, MPCM and MPCM-S

Any system employs MPCM slurry as a cooling medium needs intensive investigation about such a complex fluid, due to the high number of parameters affecting the performance of the system. Containing PCM is relatively new in engineering that is apart from the other complexity accompanied with making MPCM and later on preparing the MPCMS. Different proportions of the materials and the methods used in the preparation of the slurry lead to a different thermal, physical and rheological property of the slurry.

Temperature-dependent properties of PCM such as viscosity, heat transfer, density ...etc., are important to be investigated in PV/T studies. Currently, the thermal analysis of incomplete phase change processes is rarely investigated, but often occurs in the actual PCMs applications. Li et al [46] have studied the heating/cooling rate of eight organic commercial and non-commercial, encapsulated and non- encapsulated PCMs by using the differential scanning calorimetry (DSC) method for the thermal analyses results, concentrating on the incomplete phase change processes including partly freezing, partly melting and partly melting and freezing processes. Generally, up to date the enthalpy as a function of temperature for completed and non-completed phase change process assumed same, this assumption effects on the accuracy of any study outputs. The study by Li et al proved that the heating/cooling rate had a big effect on the phase change temperature range and the enthalpy as a function of temperature of PCMs, regarding to the commercial PCM that include different constituents with different phase change temperature cause the incongruent solidification of the different PCMs with temperature, consequently different melting process than the freezing one. Finally, they concluded that incomplete melting or/and freezing of PCMs made the DSC results greatly different from the complete phase change processes also extremely discounted the effect of thermal storage. Sattari et al. [47] have conducted CFD simulation to investigate the melting process and melting fraction in different time of n- octodecane PCMs in spherical containers, depending on the results from the simulations the change in surface temperature has the most effect on melting time, melting rate as well as the heat transfer rate. Tang et al. [48] investigated the encapsulating n- octodecane in silica shell, and done it successfully, the melting and freezing temperature of the satisfactory

MPCM were 28.32℃ and 26.22℃, with a latent heat of 226.26 kJ/ kg. Temiral et al. [49] have investigated solidification of PCMs with and without Nano additives experimentally in spherical enclosures under a convective cooling condition in water and air, they concluded that solidification time decreases with enlarging the Nano additive percentage , because it enhances the thermal conductivity of PCM. In addition, it found that the Nano additives are more effective in water for solidification in comparison with air.

The slurries with very little PCM particles mostly are non-Newtonian fluid (its viscosity and behaviour are changed by applying force or stress), due to the flocculation of the particles however, for particles diameter between 2-13 μm the slight flocculation is prevented by adding less than 1 wt. % anionic surfactant [23]. Delgado et al [39] found that the smaller capsules 2-10 μm with thicker diameter exhibits less damage with forced circulation by the pump. Liu et al. [50] proved that the thinner MPCM particle shell enhances the heat transfer more, it is preferred in case of higher heat transfer requirements.

Alvarado [33] confirms that the particles smaller than 10 μm are more impact resistant and durable, and that the MPCM-slurry shows a Newtonian behaviour with a mass fraction less than 17.7%. R. Zeng et.al have investigated MPCM-S with mass concentration up to 15%, they concluded that MPCM-S is Newtonian fluid at that range of concentration [51]. Chen [14] has concluded that the MPCM-S with a mass fraction of MPCM up to 30% is considered Newtonian fluid in case. Zhang [52]confirmed that within the shear rate greater than 200 $s^{-1}$and mass fraction smaller than 35%, the MPCM slurry could be considered as a Newtonian fluid. Mass concentration of MPCM in the slurry has merits and demerits at the same time, because the greater is the MPCM concentration in the slurry the greater is heat capacity and also is the greater viscosity which makes the slurry difficult to be pumped , so it causes more pumping power consumption also reduction of heat transfer ability of the MPCM.(because it cannot reach the turbulent flow state), so an appropriate mass concentration in vital in preparing the MPCM-S for a specific application, and not to offset the high heat transfer of the phase change materials by more energy consumption for pumping [53].

The MPCM-S need to be stable, it means the MPCM stay suspended in the carrier media for a long time, for that a suitable surfactant at the smallest rate need to be added, just to keep the capsules suspended for a long time and not to get high viscosity which is accompanied with the demerit operational condition. The structural stability is another issue with MPCM-S, it depends on the microcapsule diameter, the smaller size microcapsules tolerated the pressure of the slurry flow and the volumetric growth during the phase change, but the slurry with small microcapsules have a higher viscosity which need to be prevented. The microcapsules face the stress of pumping, which is the main cause that leads to the breakage of the microcapsules, the small diameters up to 5 μm are strong enough to face 5000 pumping cycles without rupture [54]. The centrifugal pumps is the best kind for MPCM circulation, as they are able to pump the MPCM- for a long period of time without damage to the shells of the microcapsules [55].

Zhang et al [45] experimentally studies heat storage characteristic of microencapsulated phase change material slurry for concentration of PCM particles 10%, 20%, 30% and 40% as shown in **Figure 2–5(a)**, shows that the thermal conductivity increases with decreasing the PCM concentration, so 10 % shows the higher thermal conductivity at same temperatures in comparison with the other higher concentrations, **Figure 2–5(b)** shows the relation between temperature and density for these concentrations, the density decreases with increasing the temperature, and the individual curves show the sharper decrease in density with increasing the mass concentration.

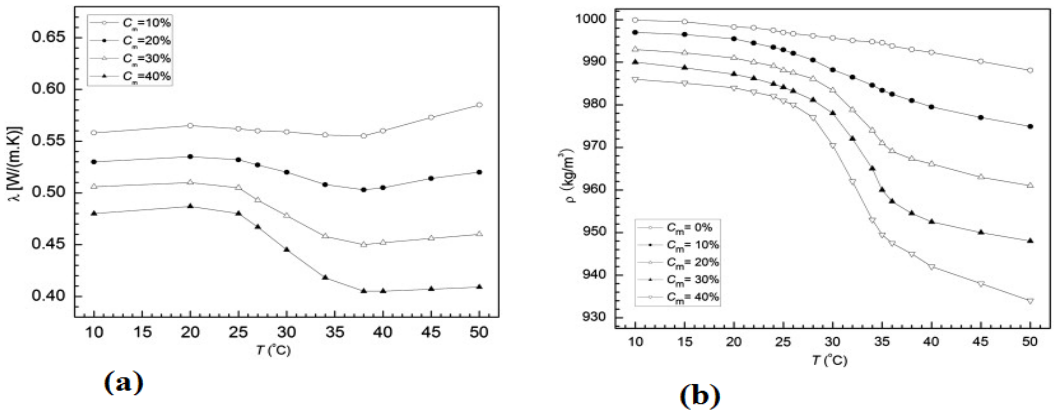

Figure 2–5:(a)Thermal conductivity with temperature at various mass concentration,(b) relation between measured density and temperature [45]

Heat transfer is one of the most important parameters that need to be enhanced in fields using MPCM slurry. Wang et al [56] have investigated the heat transfer behaviour of 5% to 27% particle concentration slurry, they found that 5% mass concentration have higher average Nusselt number than 10% mass concentration , this is because of the degradation of turbulent degree with higher concentration as shown in **Figure 2–6** , also the figure shows a very small difference in the local Nusselt number between pure water and slurry depending on two equations for water and slurry.

Eq 1 in (fig. 2-6):$\mathrm{Nu(water)} = 0.00425\ \mathrm{Re}_{lb}^{0.4}\ \left(\mu_{lw}/\mu_{lb}\right)^{-0.11}$

Eq 2 in (fig. 2-6) $\mathrm{Nu\ (slurry)} = \frac{\text{Nu MPCM slurry}}{\text{Nu Shan and London}}$

Note: equations adapted from the reference..

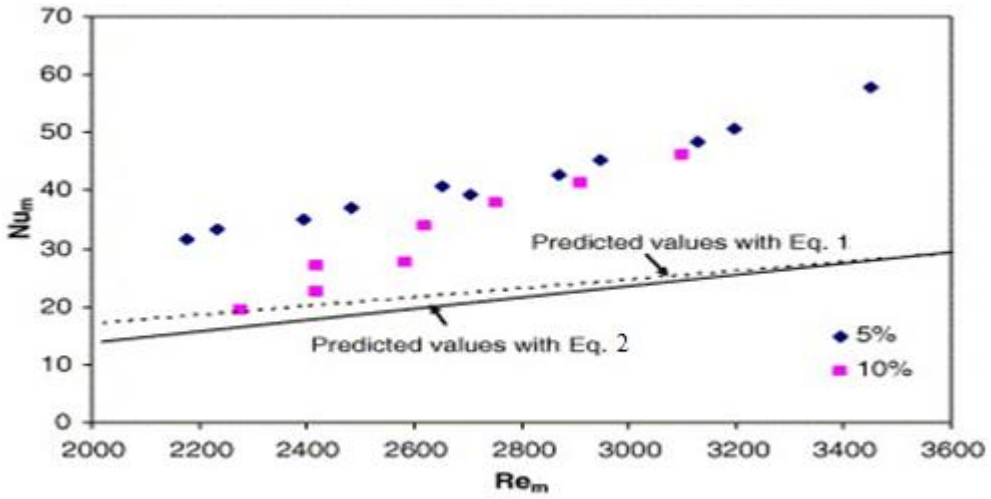

Figure 2–6:Average Nusselt number of two different slurries with p=0.05and 0.1 at Reynolds number=2100-3452, *[56]*

Ma et al [57] have modelled heat transfer characteristics of slurry flow in a circular tube and melting amount of PCM , they found that even at temperatures above the melting temperature range, some particle remain solid. Roy et al [58] concluded that heat transfer characteristics of MPCM-S is same as PCM emulsion in forced laminar convective condition, because at laminar flow the MPCM wall doesn't significantly affect heat transfer performance. Yamagishi et al [54] conducted several experiments of MPCM -S, with octadecane (C18H38) as core material , with turbulent condition and

uniform heat flux, the results showed that the increase in mass fraction leads to change in flow condition from turbulent to laminar, that changes the heat transfer feature of the slurry. Wang et al [59] have concluded some experiments to investigate the heat characteristics of MPCM slurries in horizontal tubes under constant heating rate condition, they concluded that heat transfer coefficient for laminar flow are always higher than the single phase fluid , however in the turbulent condition the heat transfer enhanced by the turbulent degree. The average Nusselt number is 1 to 2.5 times higher for the slurry in turbulent flow compared to water at same flow condition. Gschwander et al.[55] confirmed that for low temperature difference applications, the microencapsulated phase change material slurry is more advantageous than other fluids such as water or oil, but for the high temperature difference application water is better heat transfer medium also its much cheaper. Minsuk et al. [60] studied the performance characteristics of microencapsulated phase change material slurry in a helically coiled tube, the study showed that the specific heat of MPCM slurry rises with the mass fraction. When the phase change occurs, the improvement in specific heat also rises up to 80% when compared with water, leading to the increased heat transfer performance as shown in **Figure 2–7**.

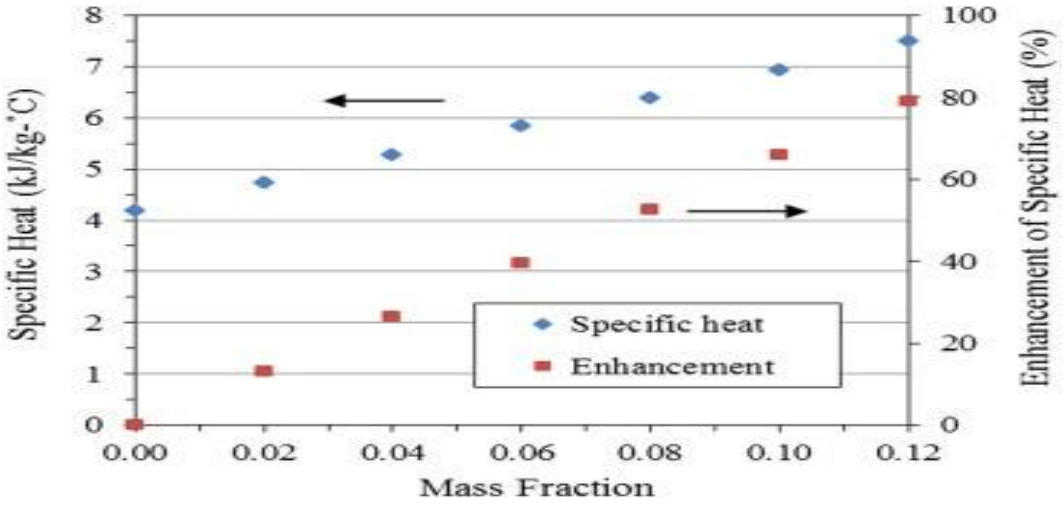

Figure 2–7: Specific heat and its enhancement as a function of mass fraction [60]

Wang et al. [61] have studied the natural convective heat transfer of tube immersed in MPCM suspensions, the PCM has the melting and solidifying temperatures of 58.11and 50.85 °C respectively and latent heat of 152.8 J/g. they tested the MPCM suspensions behaviour and characteristics, the suspension was Newtonian, the viscosity decreased with temperature rise and increased with enlarging the mass fraction of the MPCM in the suspension. The more important outcome of the study was the increase in thermal conductivity with temperature followed by a sudden decrease following the phase change region.

Most researches confirm that the MPCM enhanced the performance of the slurry in comparison with the single-phase fluids, due to higher heat capacity. However, the higher concentrations of MPCM in the slurry can also reduce the rate of heat transfer, it is preferred to choose lower concentrations to give good heat transfer performance, and the slurry to remain Newtonian.

So, flow and heat transfer characteristics depend on the change of other properties such as density, viscosity, thermal conductivity, latent heat of fusion and phase change point. The latter properties differ by PCM type, coating material, the particle concentration, carrier fluid and the flow parameters of the slurry. Turbulent flow of the slurry looks better than laminar condition due to the heat transfer enhancement in this condition.

2.1.4 Phase Change Materials for Building energy systems

There are numerous PCM application fields, and it is finding use in new fields. PCMs are most attractive in textile [62][63][64], medical and chemical [65], and building materials fabrications[66][67] fields. Engineering is one of the beneficial fields of using PCM, MPCM and MPCM–S. In building energy applications the organic phase change materials are more desirable due to its stability, availability in a good range of temperature and low super cooling, especially for latent heat thermal energy storage [13], **Figure 2–8** shows the rapid concentration on PCMs study in the recent years.

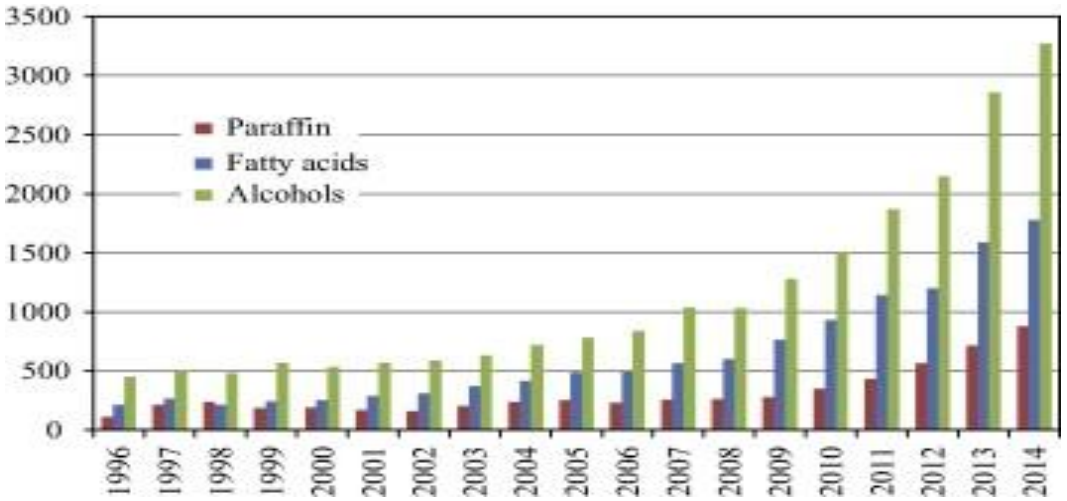

Figure 2–8:The number of articles published for organic PCMs as thermal energy storage for the period of 1996–2014. Source: Science Direct, ''paraffin'', ''fatty acids'', ''alcohols'' and ''thermal energy storage'[13]

The ASHRAE (American Society of Heating, Refrigerating and Air-Conditioning Engineers) has a list of airflow rate and temperatures for several types of buildings and for both summer and winter. They suggest 21.0–23 ºC in the winter and 23.5–25.5 ºC for summer condition [26], so it puts a limit on the types of the phase change materials used in building applications. A PCM for a particular application needs to be carefully chosen. Rastogi et al [68] have tried to rank different commercial PCMs for ventilation, heating and air-conditioning applications. They used a Multiple Criteria Decision Making (MCDM) method for that. The materials were first shortlisted depending on the phase change and followed by a selection of two advantages or merits of the PCM about the heat capacity and thermal inertia, they concluded that using MDCM approach for PCM selection is economic and instant alternative method for ranking of materials. Malvi [69] states that the climate is one of the important element that should be considered when choosing a PCM for general building energy application and especially PV/T systems. As example, choosing inappropriate melting temperature could reduce the PV output by 2%, because in this case, the PCM might spend more time as liquid or solid. The optimal melting point for air temperature between 10-20 ºC is 28 ºC, and it is 32 ºC when the air temperature is between 20-30 ºC. The latent heat of the chosen PCM should also be taken into consideration, **Figure 2–9,** shows the latent heat of a large range of PCMs with different melting temperatures, it shows that majority of the

organic PCMs are in the melting temperature range of 200-400K, in case the in-organic PCMs are available in wider range of melting temperature 200-2000 K. Barreneche et al.[70] have developed a new database including properties of PCMs with phase change materials between -50 to 150 ° C for both commercial and non-commercial PCMs, in addition to the two main property of PCMs (melting temperature and latent heat) the database includes other property such as thermal conductivity, thermos physical, density and wholesale cost.

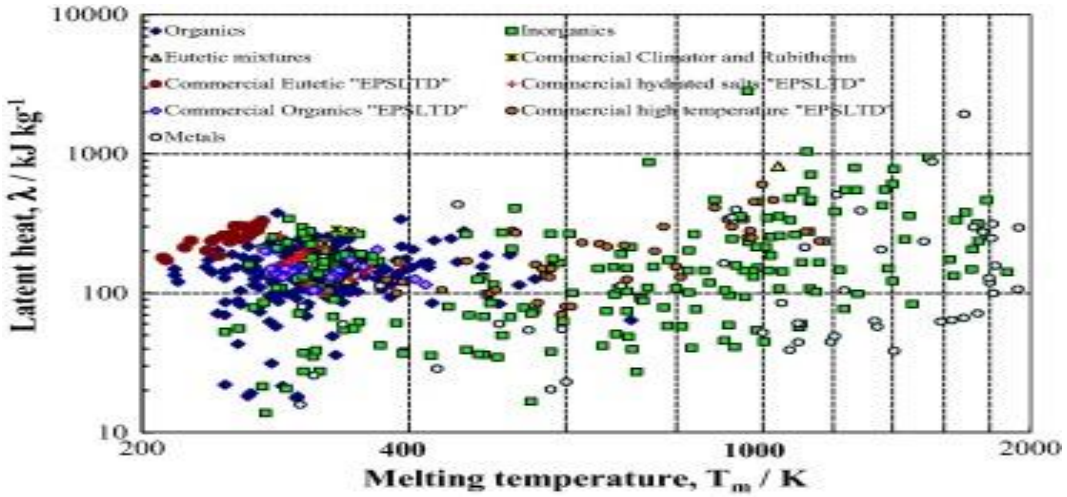

Figure 2–9:Energy density maps as a function of melting temperatures [71]

Li et al [72] note that n-octodecane is one of the best choices in building application, because of its high latent heat and suitable phase change range (21-27) ºC . Zhao et al.[73] investigated the fabrication and properties of microencapsulated n-octadecane in TiO2 shell to be used as thermal energy storage material, the prepared sample showed good phase-change act with suppressed super cooling amount and good thermal reliabilities. The preparation process was efficient, simple and the most important point it was environmentally friendly. This sample could be a candidate material for thermal energy storage in engineering fields, specially building air conditioning system, waste heat recovery, and solar energy storage, , etc. Zhou et al[26] confirmed that for indoor comfort the phase change temperature of PCM should be between (18-30) ºC. Madssa et al [74] believe that using PCM which melts at room temperature can reduce the overheating of indoor temperature above 26 ºC . Flammability of the PCM is considered

another important factor that restricted its applications in building and building energy systems. Flame retardant could be added to solve the problem, but it needs to be selected very carefully in a way not to affect negatively on the latent heat capacity of the PCM and also prevent any chemical interaction [75].

As microencapsulating of Phase change materials gives it a big enhancement and overwhelming the major problems such as low thermal conductivity and incongruent melting, it could be used in HVAC, hot water and solar systems as the main parts of building services. Takahiro et al. [76] have illustrated a general figure of reported MPCMs with diameters smaller than 50 µm , it shows the shell and core materials of the MPCMs and their typical application with a wide range of different melting temperature PCMs, this is summarized in **Figure 2–10**. Jamekhurshid et al. [77] illustrated that the microencapsulating is the best technique to prevent the leakage of PCM during the melting process, the polymer or inorganic PCM shell gives a non – diffusible barrier for leakage problem associated with PCMs.

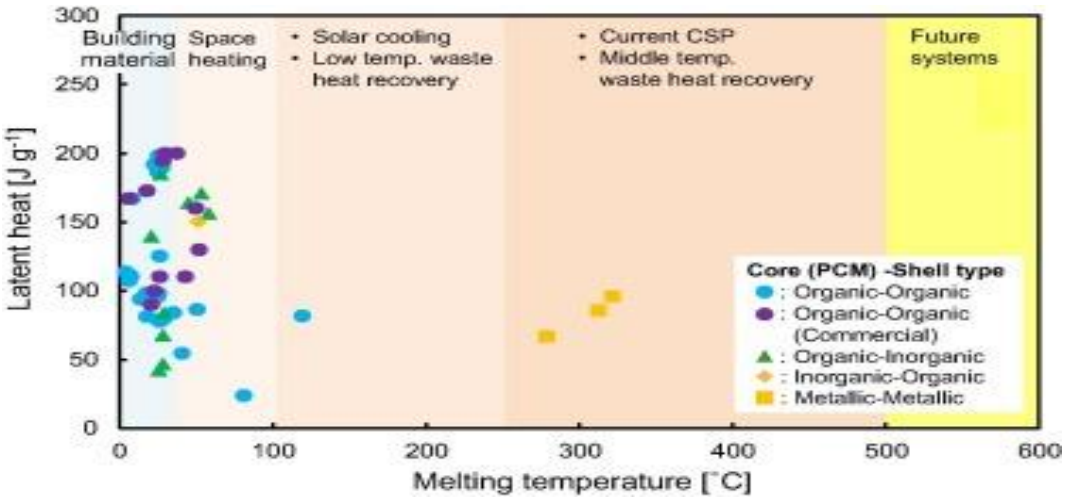

Figure 2–10;Relationship between Tm and latent heat of the reported MEPCMs which have diameters <50 µm, together with their typical applications in each temperature range[76]

Wang et.al [27] have used Hexadecane (C16H34) micro-encapsulated slurry for low energy building system as TES for the cooling tower of the residential building. The outcome of the study indicated significant enhancement of the heat transfer with using of MPCM particles. Li [78] has studied a proposed design of a hybrid system for office room, which contains three parts, Cooled Ceiling(CC) system, evaporative cooling

system and MPCM slurry storage tank. Hexadecane (C16H34) particles with pure water have been used to synthesize the MPCM slurry which stores the evaporative cooling at 24-hour operation mode at any time the wet bulb temperature reaches the pre-set point. As a result of the investigations on five different cities with different climates, it is concluded that this proposed hybrid system is best for dry climates with the high diurnal temperature difference.

Wang [79] has selected MPCM slurry containings encapsulated Hexadecane(C16H34) PCM particles and pure water as the carrier fluid to study the performance of cooled ceiling (CC) operating with that slurry. Water type ceiling panels are installed for an office room in Hong Kong to remove the sensible heat from the room. Air is supplied at minimum ventilation rate from the low level of the room by the conventional air handling unit (AHU). The chiller works at night time to store the cooling power as a latent heat in the MPCM slurry. Three different systems have been compared in this study, CC combined with MPCM slurry storage, CC combined with ice storage and CC without any thermal storage. It showed that the CC combined with MPCM slurry storage is a most energy efficient system for Hong Kong's climate, and its yearly energy consumption smaller than the other cases, because its heat transfer coefficient is 2 to 2.5 times higher than the pure water.

Sari [19] has used a eutectic mixture of the meristic and palmitic acids in the weight ratio of 58:42 for heating under the climate of Turkey. This PCM mixture with the high latent heat of fusion gives the high ability for heat storage in passive solar rooms devices and greenhouses. Kousksou et al [80] have numerically studied solar based domestic hot water system DHW system involving phase change materials, the concluded that involving PCM in this system is not beneficial, because the losses overnight is greater than the gain , the result was not expected because including PCM probably beneficial in such field, so more investigations need to be done to find the weak parts of the study. Huang et al [81] have studied the microencapsulated phase change slurries for thermal energy storage in a residential solar energy systems, they have tested a conventional hot water cylinder storage, it filled with water and three different volume concentration of the phase change slurry with melting temperature of 65 ºC is used. A heat exchanger circuit has been put in the system to know the store

performance when the inlet temperature of the fluid and the flow rates were changed. They concluded that slurries with a volume concentration of 50% is not appropriate for this application and was not successful, so the change of the heat exchanger size, location and kind, or the volume concentration of the phase change slurry could give a better and improved result.

2.1.5 Summary of the Current PCM Research

The researches in the PCM field still at their early stages especially in energy area , however in the last few years has become a desirable area of research due to the urgent need for limiting the energy usage rate , toward controlling the global warming. PCM possessing high latent heat became an attractive substance for building energy applications, especially solid-liquid PCM. Organic solid-liquid PCM is the most desirable type, particularly Paraffin due to a big number of desirable properties such as, negligible super cooling, chemically stability, high latent heat, low vapour pressure, no phase segregation, self-nucleating, and commercially available. However, it has some demerits such as low thermal conductivity, which could easily treat by encapsulating in higher thermal conductivity shell. Generally, because of the lack of information about the PCM properties, intensive investigation has been done for choosing the right PCM for the research application, the investigations from established studies are summarized as:

- Limited phase change temperature range are available for solar applications and building energy applications generally, the best choice is the organic PCM (octodecane) with a melting point of 28 °C with polymer shell for encapsulation.
- The MPCMs have higher resistance to damage and are stronger when their diameters are less than 10 μm, but flocculation should be considered in very small diameters that could be prevented by adding less than 1 wt. percentage anionic surfactant.
- Small MPCM particles with thick shells exhibit less damage with forced circulation by the pump, but thinner MPCM particle shell enhance the heat transfer more, it is preferred in case of higher heat transfer requirements.

- The centrifugal pumps are the best kind for MPCM circulation, as they are able to pump the MPCM- for a long period without damage to the shells of the microcapsules.
- For preparing the MPCM-S, water is the best carrier fluid, because it is cheap and easy to handle.
- The slurry of 5% and 10% of weight MPCM particle concentration are the best regarding the studies because they are without a doubt considered Newtonian fluid. Higher concentration increase the viscosity which makes the slurry difficult to be pumped , so it causes more pumping power consumption also reduction of heat transfer ability of the MPCM because it cannot reach the turbulent flow state.

2.2 General Concepts of PV/T system

2.2.1 General theory of PV/T operation

Photovoltaic (PV) cells are electricity generating semiconductors (commonly silicon) and their atomic structure could be multi-crystalline, nanocrystal or amorphous. The junction between p-type and n-type silicon junction is used to make PV cell. The electrons (-) and holes (+) are free to move, when the photon strikes on the junction, it produces an electron-hole pair. The doping in junction area reduces the chance of recombination, so the electrons and the holes will move away from the junction creating a flow of current. If the n and p layers are connected creating a circuit, it will produce electrical energy, the process illustrated in **Figure 2–11**.

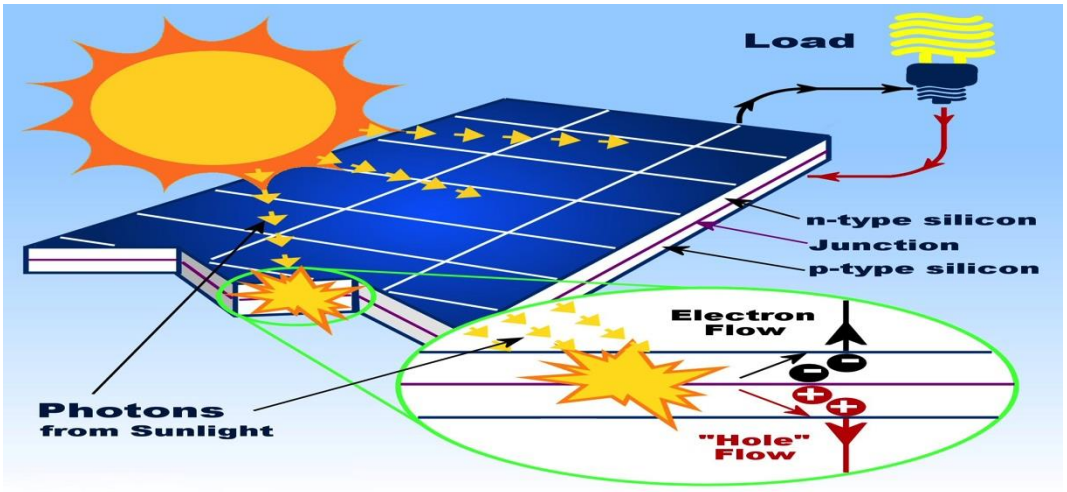

Figure 2–11: The photovoltaic effect in PV cells [82]

The percentage of solar irradiation converted into useful energy is increased because of the different technologies operating in various ranges of the solar spectrum. Solar photovoltaic cells are absorbers that work in a wavelength range of 350- 1200nm which could be mainly considered a visible light lower end of infrared and UVA as shown in **Figure 2–12**, and the solar energy outside this wavelength range could be collected in form of heat energy [83].

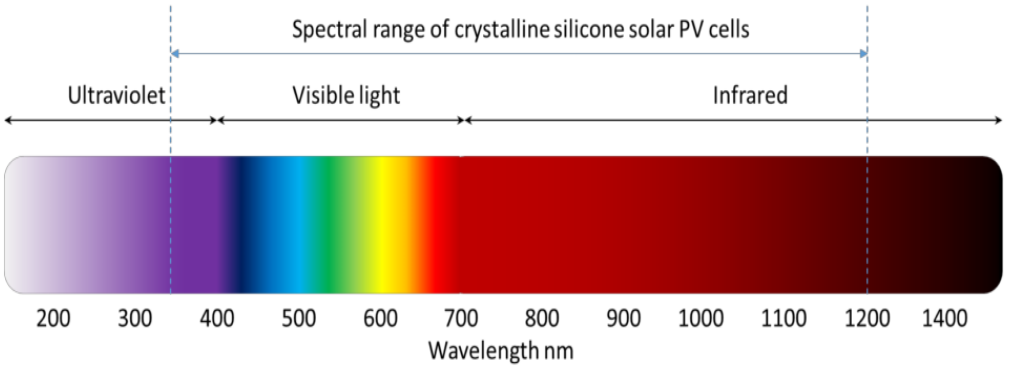

Figure 2–12: Operational range of spectrum for solar PV cells *[83]*

The commercially available photovoltaic cells or films that cover the market needs are[84]:

- **Monocrystalline silicon PV cell:** Is the greatest efficient photovoltaic cell, normally the electrical efficiency is around 15%. The industrial process for this

kind of cells is very complicated leading to higher cost in comparison with the type of PV cells.

- **Polycrystalline silicon PV cell**: Occasionally known as (multi-crystalline cell), it is very thin wafers assembled to cells of photovoltaics. Normally it is cheaper than monocrystalline cells because of the simple manufacturing procedure comparing to the monocrystalline cells, also it is less efficient, and the average efficiency is about 12%.

- **Thick film silicon PV cell:** It has a sparkling appearance. Similar to all crystalline photovoltaics, it is encapsulated in a clear protecting polymer.
- **Amorphous silicon PV cell:** It is a thin homogenous layer, so it called (thin film PV) as well, it has higher light absorption efficiently than crystalline silicon, consequently it can be thinner that make it flexible and more applicable for curved surfaces or bending. If the roof space is not limited and the maximum output per square meter is not required, then an amorphous cell product is a good option. Otherwise, the crystalline silicon is a better choice due to the low efficiency of an amorphous cell (6%).
- **Other thin-film PV cells:** Different materials like cadmium telluride (CdTe) and copper indium dieseline (CIS) and are now used for PV production. Manufacturing of these cells is cheap especially in comparison to crystalline silicon technologies but it is less efficient. But it could offer higher efficiency than amorphous silicon, as CdTe is normally efficient around 8 or 9% and CIS around 10-13%. The demerits of these technologies are the highly toxic metals like Cadmium, end of life disposal and carefully controlled manufacturing. Even though a classic CdTe module includes only 0.1% Cadmium, which is lesser than the rate in a single (AA) sized NiCad battery.

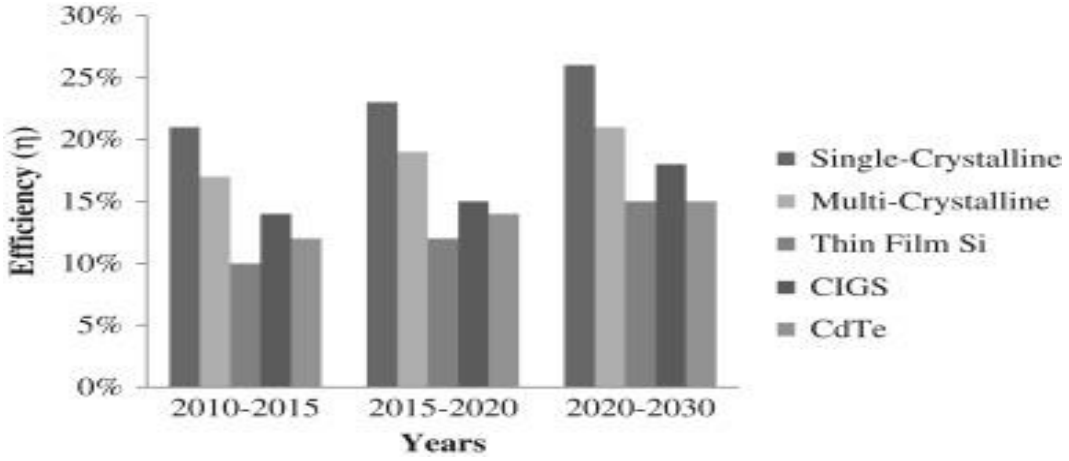

Figure 2–13:Projected improvements of PV efficiency with different technology *[85]*

The efficiency of the PV panel depends on three factors: solar cell materials, solar radiation intensity and its operation temperature. The solar radiation intensity is not under human control; the other two factors need to be investigated more to get higher solar energy conversion of PV. The panel temperature plays a main role in the photovoltaic conversion process[86].The efficiency of PV solar panels decreases with increasing its temperature above the standard operating temperature which is usually 25 °C [87], the efficiency reduction percentage depends on the material of the panels, so with each 1 ºC temperature rice of Monocrystalline and Polycrystalline cells the efficiency drops by 0.45% to 0.50%, for the Hybrid solar cells the efficiency drops by 0.32%,and for amorphous based thin film panels it drops by 0.20% to 0.25% [88] . At the nominal operating cell temperature(1m/s of wind speed, 20 ºC of ambient temperature, and 0.8 kW/m^2 of solar radiation) the PV electricity efficiency is between 6-18% [89].

So an improved cooling system for the PV panels is one of the most important points to gain a higher electrical efficiency and employ the heat removed to get higher thermal efficiency, concluded in getting higher overall efficiency, especially in hot regions, **Figure 2–14** shows the effect of cooling PV system on the output power.

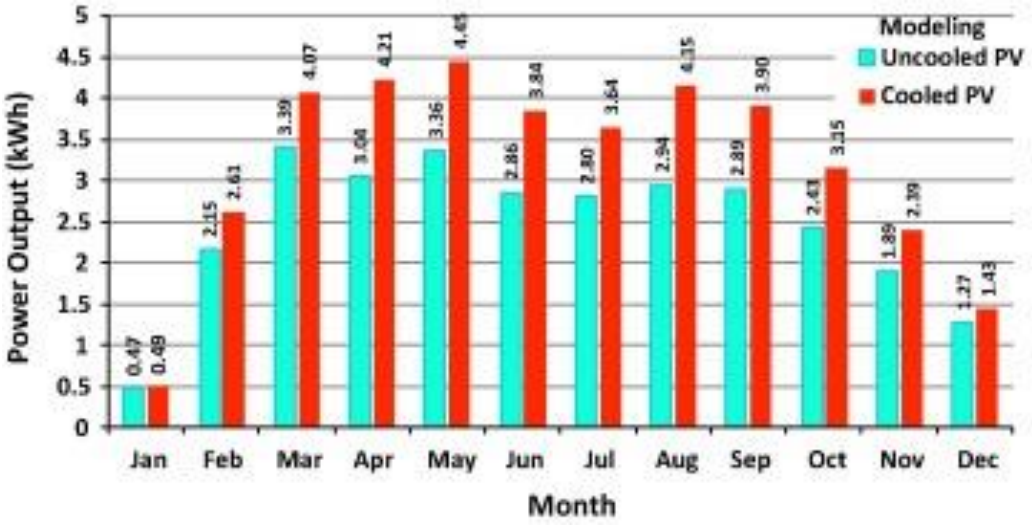

Figure 2–14:Annual energy yield simulation for uncooled and cooled PV in Saudi Arabia [90]

Solar collector systems transport the thermal energy from solar to the agent fluid. They can be combined with PV module to form a hybrid photovoltaic thermal PV/T system which introduces electrical and thermal energy [91].Usually the PV/T panel has several layers, first top layer is clear glazing, then a layer of photovoltaic cells with a small gap between them, for absorbing the sun heat there is an absorber layer adhered to the photovoltaic cell, then the piping system adhered to the absorber sheet for heat removal purpose, then the insulation layer, all these layers are combined in a fixed frame as shown in **Figure 2–15**. Investigation about the PV/T started in the mid-1970s [92].

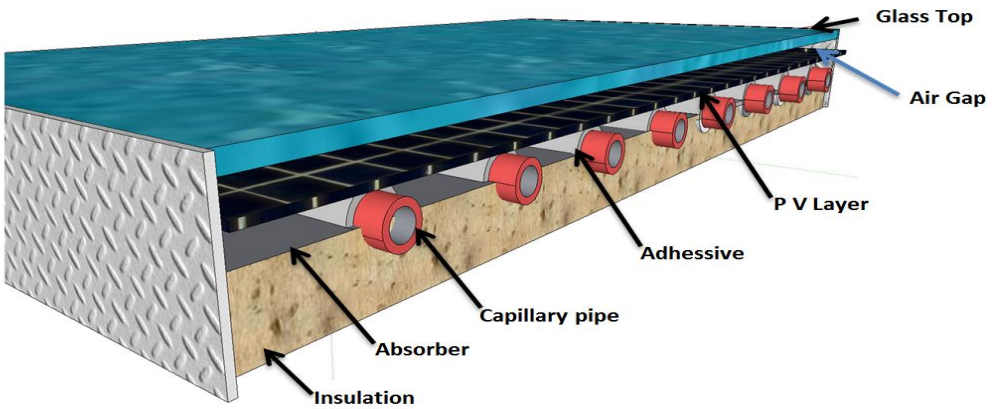

Figure 2–15: The cross-section of a standard PV/T module

Building Integrated Photovoltaic (BIPV) technology converts building from energy consumer to energy producer. It gives more advantages in case of merging instruction of buildings with this technology. At this point, the photovoltaic modules turn out to be a right construction element serving as building exteriors, such as façade, roof, or skylight. It could be considered as weather and noise protection, as well as the thermal insulation for buildings… etc. The technology lessens the total building material and mounting expenses, because it does not require brackets and rails. For the best outcome of BIPV technology, many factors should be taken into consideration such as installation angle, PV module temperature, partial shadowing, and orientations… etc.[85].

The operating temperature of the BIPV cells is usually higher than that of the PV exposed at free air. As a result, the solar electrical efficiency of the BIPV lower than that of the PV exposed in free air; consequently, the cost per unit electricity generation (£/kWh) by the BIPV will be higher than that by the free-air-exposed PV, and electricity generation per unit surface [93]. Therefore, the BIPV system requires a more effective cooling system than PV system exposed to air. It is important to define the optimum parameters required for PV or PV/T systems integrated to buildings. The key parameters such as air gap, mass flow rate, air channel dimensions or fluid pipe dimension (in water-based system) ...etc. will affect the general performance of the BIPV or BIPV/T systems.

Cartmail et al [94] concluded that main assistances to space heating and hot water supply can be obtainable throughout the year from building integrated combined PV/T collectors which were installed in Leicester. Touni et al [95] , and Zondag et al [96] have proved that PV/T module have higher electrical and thermal energy in comparison with individual PV and thermal modules.

The Hottel-Whillier model for thermal analysis of flat plate collectors has become a reference to the analysis of combined PV/T collectors, with some simple change of the parameters of the original model, all the information and relations still strongly applied for progression in this field [97]. The correlations of PV/T are derived from both thermal solar collectors to calculate the thermal efficiency and photovoltaic panel for

calculating the electrical efficiency. As a result, the overall efficiency of the PV/T module could be calculated as below:

$$\eta_o = \eta_e + \eta_{th} \tag{2-1}$$

Where η_o is overall efficiency, η_e is electrical efficiency and η_{th} is thermal efficiency

Thermal efficiency: could be defined as the ratio of the useful thermal energy to the incident radiation absorbed by the panel and represented as below:

$$\eta_{th} = \frac{Q_{th}}{A_m I} = \frac{Q_u}{A_m I} \tag{2-2}$$

Where η_{th} is the thermal efficiency, Q_{th} is the thermal energy, Q_u is the useful energy, I and A_m are the incident radiation and effective area of the module.

As PV/T module with a flat plate solar collector, produces electricity and collects the heat as thermal energy, the Hottel–Whillier [98] model needs to be modified slightly to predict the useful heat yield of the module, the following formula represents the useful heat of the PV/T system:

$$Q_u = LW F'\left[S - U_L'\left(t_f - t_a\right)\right] \tag{2-3}$$

Where,

S= $q_{abs} - q_e$ and t_f is the fluid temperature

$$U_L' = \frac{T_{pv} - T_a}{T_{fin} - T_a} U_L \tag{2-4}$$

$$F_R = \frac{\dot{m} c_p}{LWU_L'}\left[1 - \exp\left(-\frac{U_L' F' LW}{\dot{m} c_p}\right)\right] \tag{2-5}$$

Where,

$$F' = \frac{1/U_L'}{\frac{W}{N_p}\left\{\frac{1}{U_L'\left[(W/N_p - D_{p,o})F + D_{p,o}\right]} + \frac{1}{C_b} + \frac{1}{\pi D_{p,i} h_c}\right\}} \quad (2\text{-}6)$$

F which is the standard fin efficiency, is calculated as:

$$F = \frac{\tanh\left[m(W/N_p - D_{p,o})/2\right]}{m(W/N_p - D_{p,o})/2} \quad (2\text{-}7)$$

The variable (m)[99], is defined by:

$$m = \sqrt{\frac{U_L'}{K_f \delta_f}} \quad (2\text{-}8)$$

In terms of the physical inference, F_R signifies to the ratio of the system's actual useful heat gain to the overall converted solar heat at a definite working fluid temperature. The system's thermal efficiency factor F', is a constant under fixed operational and physical condition. However, F' varies as follows: it decreases with the increase in the fin width, increases with the increase in the material thicknesses and thermal conductivities, and decreases with the increase in the overall heat loss coefficient. The convection heat transfer coefficient of the working fluid in the heat absorber could be found by the following equation:

$$h_c = \frac{Nu_f K_f}{D_{p,i}} \quad (2\text{-}9)$$

Electrical Efficiency: The PV cells' electrical efficiency largely depends on the back surface temperature of the PV:

$$\eta_c = \eta_{rt}\left[1 - \beta_{pv}(T_{pv} - T_{rt})\right] \quad (2\text{-}10)$$

The overall electricity yield is given by:

$$Q_e = \eta_c f_{pv} \tau_c \tau_{g,pv} \alpha_{pv} IA \quad (2\text{-}11)$$

The electrical efficiency could be represented in terms of power as its more applicable practically as below:

$$\eta_e = \frac{P_o}{A_m I} \quad (2\text{-}12)$$

2.2.2 Categorization of the PV/T systems and applications

The classification of PV/T collector modules could be done by several ways depending on their temperature level, or cooling medium. To elevate the PV modules' solar electrical efficiency, the main aim to be achieved is removing heat from concealed PV surface, which could be employed for ventilation and heating of buildings, this will result in increasing the overall solar efficiency of the BIPV up to 80% [100]. **Figure 2–16** shows the categorization of BIPV/T systems[101].

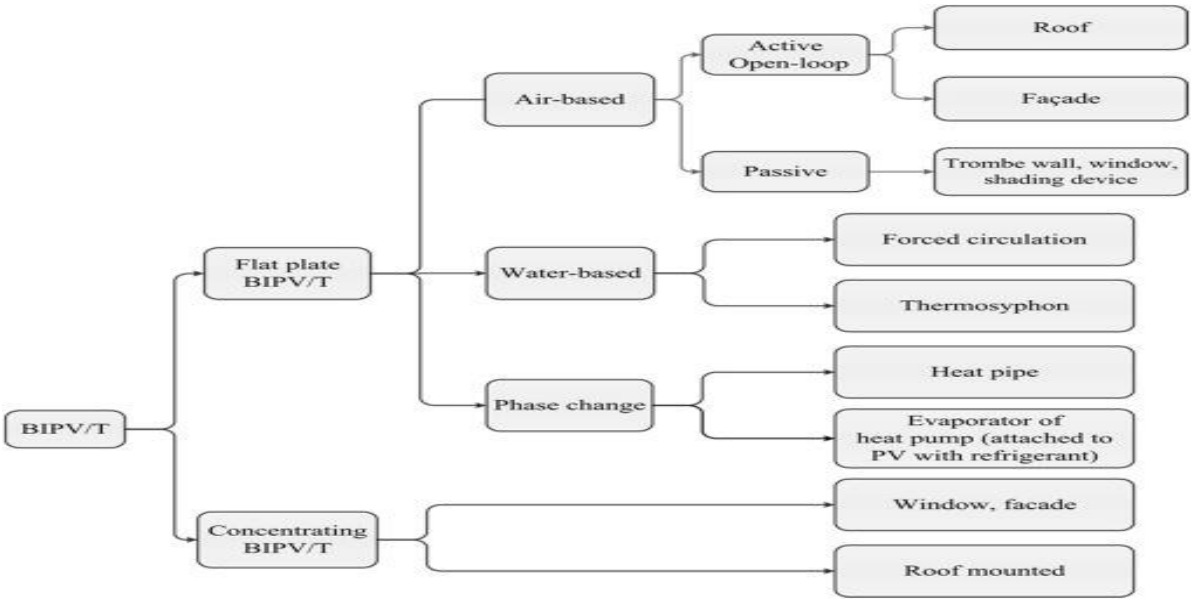

Figure 2–16: Classification of BIPV/T systems [101]

In this study, concentration is on the cooling medium or fluid of the cooling system of PV/T panels, so by depending on this aspect the PV/T systems could be divided into four types (air, water, refrigerants and phase change materials) based PV/T systems.

Air-based PV/T : this type PV/T technology usually used when there is need of hot air for heating systems, the system could be natural ventilation or forced air, which pass below, above or on the both sides of the plate absorber [102]. It is very popular in tropical countries for food industries, and both naturally or mechanically ventilated air is the most popular technique among researchers and engineering practice [103][104][105][106] to be used for the cooling purpose of the BIPV system by passing air between the building fabric and the rear surface of the PV module .Using air for cooling is associated with lots of disadvantages like low heat transfer due to the low heat conductivity and heat capacity, high volume transfer and noisy, also it is less effective when the air temperature is over 20 ºC [107]. With taking economic and environmental effect of this kind of collectors , the values of the cost pay back time (PBT) and CO2 PBTare high due to the low ability of heat extraction of this kind of PV/T systems [108]. In spite of these disadvantages, it is the most popular collector because of the low cost, no boiling or freezing, and no leakage risk. Also, the light weight of air makes this kind of technology more applicable for BIPV/T systems by integration with several building elements including façade, roof, window and skylight [101]. Generally a typical air-based PV/T has 8% electrical efficiency and 39% thermal efficiency[109].

Figure 2–17: Air-based PV/T collector [110]

Sopian et.al [111] have studied the performance of single pass and double pass air solar collector, the concluded that the double pass air collector is more efficient, as the solar cell temperature is lower which leads to higher efficiency. But the operation cost of the double-pass is higher due to the higher pressure drop in comparison with the single-pass one. Tonui et al [95] have investigated PV/T air collectors by comparing the efficiency of the typical single-pass air channel system which referred by (REF)with two modified thin metallic sheet (TMS) and fin (FIN) air cooling systems as shown in **Figure 2–18**. They concluded that with forced convection of the FIN type is most efficient with 30% thermal efficiency followed by TMS then REF with thermal efficiencies of 28% and 25% respectively. The thermal efficiency of FIN is greater than TMS, because of the extra shade of TMS. Therefore, for the best choice of application, FIN is better for the regions or countries which need more heat gain for heating, and TMS is appropriate for countries needing cooling.

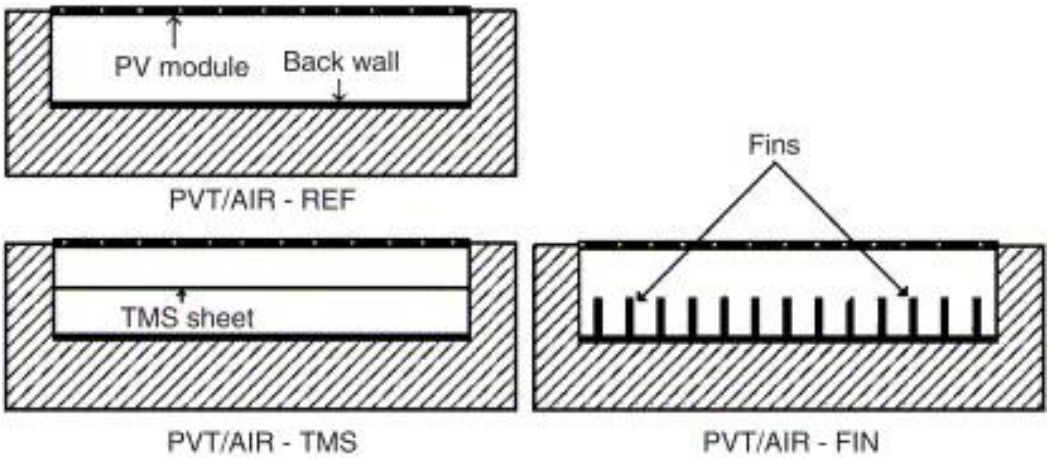

Figure 2–18: Cross section of PV/T air collector modeless, the flow direction is perpendicular to the page [95].

Hussain el al .[112] have tested three different designs of heat exchanger (air passage behind the PV/T panel) honeycomb, V-groove, and stainless steel wool had been tested to study their effectiveness in improving the overall performance of a photovoltaic/thermal (PV/T) air base solar collector. These heat exchangers were set horizontally into the channel located on the backside of the PV module. The laboratory test condition was under 828 W/m2 radiation, 0.02 kg/s to 0.13 kg/s mass flow rate. They found that at a mass flow rate of 0.11 kg/s, the best performance was the

honeycomb with thermal efficiency of efficiency of 87% and electrical efficiency of 7.13%. At the time the other two V grove and stainless steel PV/T systems had, thermal and electrical efficiencies of (71 %, 7.04 %) and (86 %, 6.88 %) respectively

Mojumder et al. [113] have conducted an experimental study to analyse an air-based single pass PV/T solar collector system with a number of rectangular thin fins . It was concluded that the BIPV/T system integrated with fins system has higher electrical and thermal efficiency, and the PV surface, collector back, the mass flow rate as well as the fin numbers considerably affected the rear surface and air temperature. Also concluded that the number of fins and the mass flow rate significantly affect the PV/T system's performance, as the PV efficiency raised by about 0.81% for the module with four fins at the mass flow rate of 0.14kg/s in comparison with the case of 0.02 kg/s air flow rate and a system without fins.

Farshchimonfared et al. [114] have conducted a study with the aim of optimizing the channel depth, the air mass flow rate per unit collector area and the air distribution duct diameter of the air based PV/T collector, considering the entire system performance. They concluded that with the fixed rate of temperature rise (10 °C) of the PV/T collector, with a specified area and Length/ Width ratio of the collector, the optimum depth will vary between 0.09 and 0.026 m. Ooshaksaraei et al. [115] studied the performance of four air-based photovoltaic / thermal collectors with bifacial solar cells (which has the ability to absorb solar radiation from both the rear and front sides) . They found that the collector with double path parallel flow gives the highest total efficiency between 51% to 67% in comparison with the other models (double-path counter flow, single-path returning flow, and single-path collectors) with total efficiencies of (47% to 62%, 42% to 56%, 28% to 49%) respectively. Yang et al [116] have set an experimental rig to investigate the thermal characteristics of a two inlet open loop air based BIPV/T system using solar simulators. The results showed that by using this system the thermal efficiency increase by 5% comparing to the conventional one inlet BIPV/T system because along the air flow path the convective heat transfer coefficient is higher nearby the inlet because of the entrance effect, so an extra inlet means more area, then higher convective heat transfer coefficient, consequently higher heat transfer between the PV and air.

Solanki et al [117] have run an indoor test as shown in **Figure 2–19**, for calculating the thermal and electrical deficiency of an air based PV/T system, they simulated it to compare the theoretical and experimental data. The thermal and electrical efficiency obtained were 42%and 8.2% respectively, the results are similar to the previous studies at outdoor conditions.

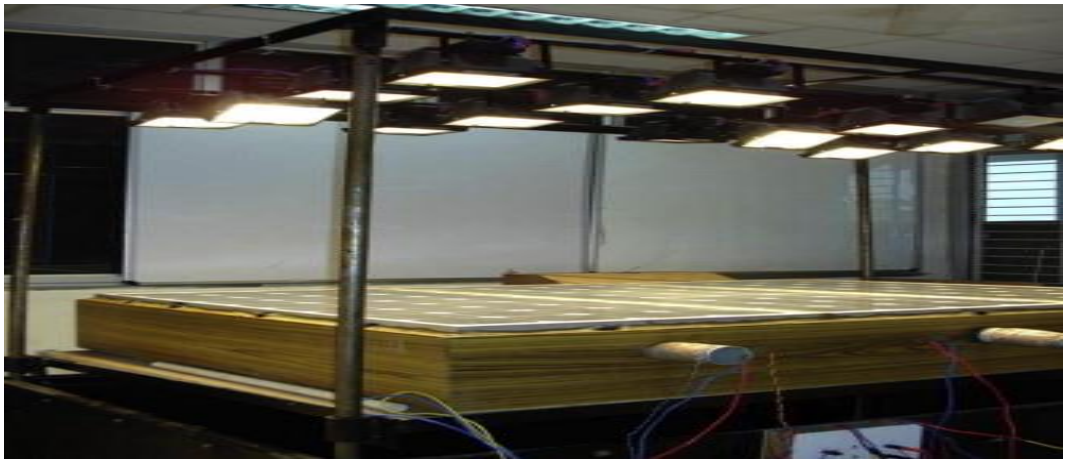

Figure 2–19: Experimental rig of air based PV/T [117]

Water-based PV/T: It can be divided into four types as sheet and tube PV/ T collectors, channel PVT collectors, free flow PVT collectors and two absorber PV - collectors. The simplest and more viable one is sheet and tube PV collector[96].

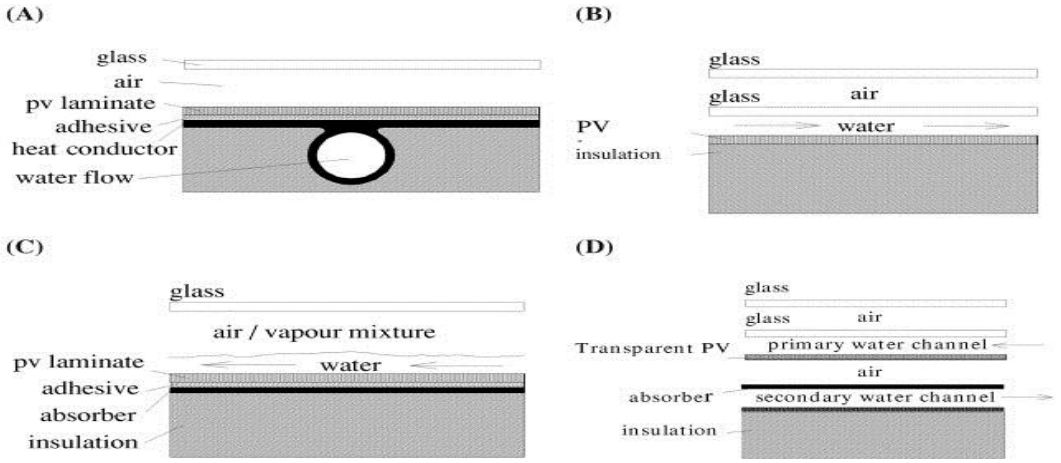

Figure 2–20: Different collector models: (A) sheet-and-tube PVT, (B) channel PVT, (C) free flow PVT, (D) two-absorber PVT (insulated type) [96]

The absorber is same as normal flat plate collector which is connected to a series of parallel tubes, or a serpentine pipe to the rear of the collector, usually the tube is made of copper due to the high conductivity. To get higher overall efficiency the collector

should be cooled down, this by forcing the water to circulate and absorb the heat from the panel. The exit hot water could be employed for heating or domestic use. Due to the higher thermal mass of water in comparison with air, it could remove more heat from the panel, consequently more effective cooling. The PV/thermal water cooling system has been developed by researchers to get over the demerits of the previous system[118] which improves both the solar thermal energy utilization and the solar electrical efficiency of the PV according to some engineering practice [119][120], but the big increase in water temperature during the cooling process could be one of the main barriers in front of improvement of the PV/thermal water systems. Water mass flow rate is one of the important factors of the efficiency of water base systems, as the system has the highest total energy efficiency in turbulent flow case [121].Generally for the typical water-based system the electrical efficiency is 9.5% and thermal efficiency is 50% [122].

Bahaidarah et al [123] have studied a water cooled hybrid PV system on theoretical and experimental bases in Dhahran and Saudi Arabia , they addressed that at the irradiance of 900 W/m2 the hybrid system with water cooling produce 750 W of overall electrical and thermal energy, but the output is 190 W electrical energy in case of just PV panel without cooling, so the hybrid PV/T system is nearly four times improved. Jarimi et al [124]have investigated a bi-fluid type PV/T module as illustrated in **Figure 2–21** they set an indoor rig for experiments and theoretical simulation using MATLAB, they used both air and water as a cooling medium , the results showed overall efficiencies (electrical and thermal) 58.10% and 62.31% for air and water-based systems respectively at the optimum flow rate.

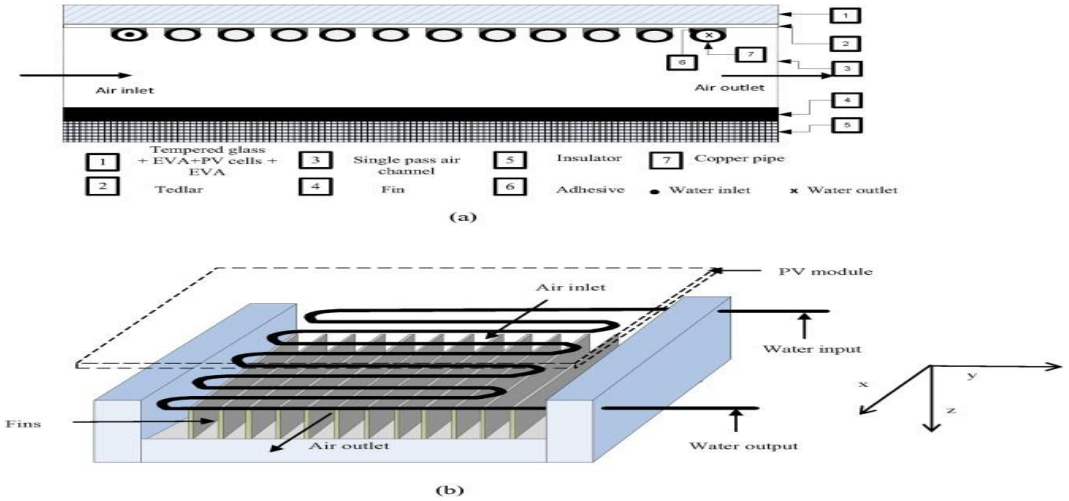

Figure 2–21: (a)Side view cross section, (b) front and top-view cross section of the designed bi-fluid PV/T solar collector [123]

Ji et al [125] studied the façade integrated photovoltaic/thermal system by computational thermal model of a residential house wall in Hong Kong, they concluded that the overall efficiencies were 48% and 43% for thin film and crystalline silicon PV respectively, a part of the improving efficiency by using the hybrid PV/T system, the PV façade could decrease the cooling load in the building as a result of reducing the sun heat absorption . He et al. [126] have conducted experiment study on PV/T system with natural circulation of water, so the system does not include circulation pump, in the result it saves electricity consumption also space by the pump. The outcome of the test was very positive, as the hot water could cover the requirements of domestic hot water, and the system could partially meet the need of industrial hot water

Refrigerant based PV/T : According to the weather and climate the type of cooling system is chosen, for cold weathers the PV system does not need cooling, because of the cold PV cells , but in hot weather sometimes the previous cooling systems (air and water-based) do not work appropriately, so the PV system needs a stronger cooling system . The refrigerant based PV/T is the best choice in this case, this cooling system is accompanied by a heat pump as a main part of the cooling system, this requires refrigerants for operation, the energy saving and economic aspect should be taken into consideration when choosing refrigerant based PV/T, because the operating expense is higher than the previous types. The coefficients of performance (COP) of a heat pump depends on the temperature of the delivered useful heat, the temperature of the energy

source, the working medium used, the characteristics of the heat pump system's parts and the most important one is the evaporator temperature. Combining of heat pump and solar system leads to improve the COP of the heat pump, improve the PV efficiency and displacing the fossil resource [107]. Ji et al [127] studied experimentally the performance of heat pump based PV/T, and the proved that the COP of the system could reach 10.4 with an average photovoltaic efficiency of 13.4%. Bakker et al. [128] showed that a 25m^2 uncovered roof PV/T with a heat pump cooling system, the PV/T system could supply one Dutch family all their heating demands and nearly all their electrical consumption. A typical refrigerant based PV/T system has approximately 65% thermal efficiency and 10% electrical efficiency [129].

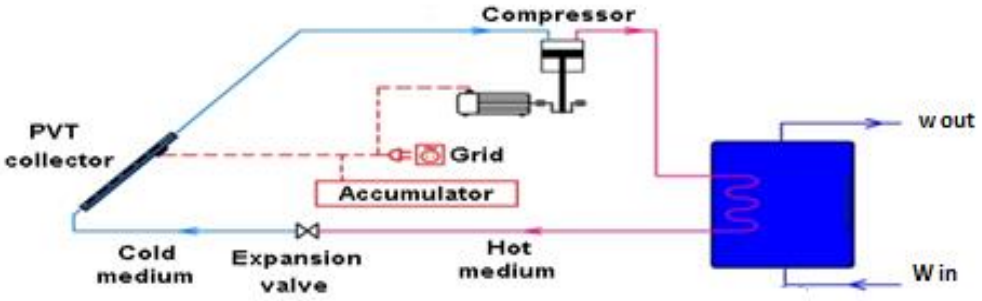

Figure 2–22: Hybrid system with heat pump [130]

Tsai [131] has modelled and validated a dynamic state of refrigerant based PV/T assisted heat pump water heating PVTA - HPWH system , he concluded that the rapid variation of weather condition has a slight negative consequence on the performance of the PVTA–HPWH system. Chen et al. [132] have conducted a numerical and experimental study on heat pipe PV/T heat pump system. They concluded that the rise of ambient temperature leads to the increase of thermal based coefficient of performance (COP_{th}), with an increase of 5 °C of ambient temperature the COP_{th} rise by 0.08, but general COP of the PV/T system decreases by 0.09. In addition, they found that the supply water temperature in condenser effects on the COP_{th} and overall COP of the PV/T system, if the supply water temperature rise by 5°C, both COPs decrease by 0.25

and 0.35 respectively. The effect of the backboard absorptivity on the systems COPs was investigated as well, they found that with an increase of 0.15 absorptivity of the backboard ,the COP_{th} increase by 0.03 but overall PV/T COP decrease by 0.03.

PCM-based PV/T: Due to the direct relation between the efficiency and cooling of PV systems and the disadvantages of the main conventional cooling mediums such as water and air. Phase change materials, phase change materials slurry and microencapsulated phase change materials are the most recent and effective solution for cooling the BIPV system due to the obvious advantages of them and mainly the high latent heat. These advantages made phase change materials a popular area of investigations, especially in the last decade. It is used in solar collectors as shown in **Figure 2–23**[133] ,when the heat produced from this system employed then it called PV/T system .

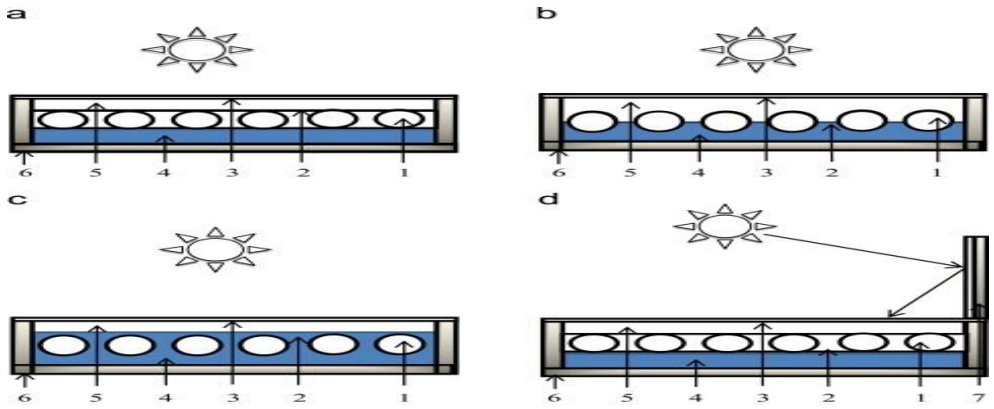

Figure 2–23: Diagram of PCM based flat plate solar collector (a) below tubes, (b) half perimeters of the tubes, (d) immersed tubes, (d) with reflector, (1) tubes, (2) absorber, (3) glass cover, (4) PCM, (5) air layer, (6) insulation, (7) reflector [132]

Phase change materials based hybrid PV/T technology is still in research and development phase, and limited in laboratories. Integrating PCM in PV systems is an effective way for limiting the temperature of the PV panels toward increasing the efficiency of the system, it could enhance it up to 5% [135] but it might not be economically viable if just used to improve PV conversion efficiency. So hybrid PV/T - PCM which is on its start stage could be a better choice , it employs the absorbed heat to be used in different services, this kind is accompanied by significant challenges in need to be faced [136]. Choosing PCM for a particular application and local weather condition is difficult, because of the absence of a slandered reference of PCMs and non-

investigated properties of most PCMs. **Table *2-5*** shows the properties of the desired PCM for photovoltaic thermal regulation[137].

Table 2-5: Properties of the desired PCM for photovoltaic thermal regulation[137]

	Requirement	Reason for requirement
Properties		
Thermal	High latent heat	Maximum heat absorption
	High heat capacity	Minimum sensible heating
	Good thermal conductivity	Efficient heat removal
	Reversible phase change	Diurnal response
	Fixed melting point	Consistent behaviour
Physical	Congruent melting	Minimum thermal gradient
	Low volume expansion	No overdesign
	High density	Low containment requirement
Kinetic	No super cooling	Easy to freeze
	Good crystallisation rate	Faster solidification
Chemical	Chemical stability	Long life
	Non-corrosive	Long container life
	Non-flammable	Comply building safety codes
	Non explosive	Environment friendly
	Non-toxic	
Economic	Abundant	Market competitiveness
	Cheap and cost effective	Economic viability and market penetration
Environmental	Recyclable/reusable	Ease to dispose of
	Odour free	Comfortable to apply in dwellin

Crystalline silicon cells seem to be the most economically feasible in PV-PCM systems , because the temperature rise has the most harmful effect on the PV system comprise crystalline silicon cells in comparison with the system comprising organic or thin film cells [138]. However the PCM is an attractive and relatively new coolant medium for

PV/T systems , but liquid as cooling medium permits a better utilization of the thermal energy and gives a homogenous temperature distribution of the Surface [139] .

Kant et al. [87] have conducted a heat transfer study of photovoltaic panel integrated with PCM to investigate heat transfer mechanisms between PV module and PCM . They concluded that the PV module integrated with PCM reduce the power loss. This because of the isothermal phase change nature of PCM during changing the phase, therefore it delays the increase of the panel temperature by absorbing the extra thermal energy of it. So the maximum power loss could reach 14% for the PV that not integrated with PCM, in case it could reach just 11% with PCM integrated PV. Su et al. [140] have simulated a computerized module to analyse the dynamic performance of photovoltaic / thermal solar collectors integrated with different thickness layers of 2,3,and 5cm PCMs. Electrical and thermal parameters such as outlet temperature of the air, solar cell temperature, electrical and thermal power, electrical and thermal efficiency are analysed to assess the dynamic performance of the system. In this study, the heat transfer pipes integrated with a PCM layer at several positions of the air pipes, as the working fluid is air and shown in **Figure 2–24**.

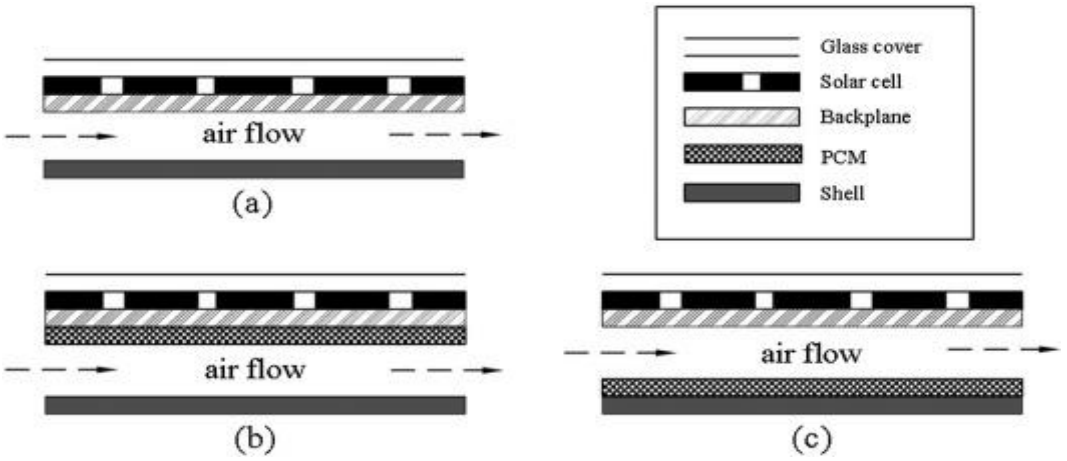

Figure 2–24 : The sectional view of the PV/T collector with PCM at different positions [140]

The results showed that the position of PCM layer in the photovoltaic/thermal collector has a significant influence on the act of the PV/T collector. Moreover, confirmed that the performance of the PV/T collector in upper integrated PCM style is the best among the group of different styles shown in **Figure 2–24**. The overall efficiency of the PV/T collector in upper PCM style Figure 2-24 (b) is the highest, and it is 10.7% higher than

the style with no PCM included Figure 2-24 (a). Finally, they concluded the thickness of 3 cm PCM for the optimum upper PCM integrated style shows the best thermal and electrical performance. Huang et al. [141] have numerically studied the thermal regulation for building integrated photovoltaics using PCMs, this study was validated depending on previous experimental studies on single flat aluminium plate system. , PV/PCM system without internal fins and PV/PCM system with internal fins. They concluded that a significant enhancement in the thermal performance attained by using the metal fins in the PCM container. The fins give a more uniform temperature distribution on the PV module. The phase change of PCM increases the thermal capacity of the system. Nevertheless, increased numbers of fins limit the movement of PCM in the liquid state. Elarga et al. [142] have developed a physical – mathematical model to simulate the dynamic thermal and electrical performance of PV integrated with PCM for double skin facades. The outcome of this study showed that including PCM in this system could significantly affect to reduce the cooling load indoor space. The monthly cooling load reduced in the range of (20% - 30%) unrelatedly to the climate. At last, the study advised that the melting temperature of the used PCM is the key point to ensure the effectiveness of the system including PCMs.

Hasan et al. [143] have installed three 65 watts PV /T collector in two different climates Dublin in Ireland (53.33°N, 6.24°W) and Vehari in Pakistan (30.03°N, 72.25°E) to compare the energy and cost saving in two different climates. One of the three PVs used as a reference, the other two had two different PCM in bags attached to the back of the PV, the PCMs were a eutectic mixture of capric-palmitic and salt hydrate. As a result, they concluded that this kind of PV/T-PCM is more viable economically in high solar radiation and temperature climates like Pakistan. Park et al. [144] have carried out an experimental and simulation study of PCM based PV system as shown in **Figure 2–25**, the experimental rig was set under south Korea weather condition, it showed a 5 ^{o}C decrease in PV temperature in comparison with a conventional PV which lead to increase 3% of overall PV efficiency.

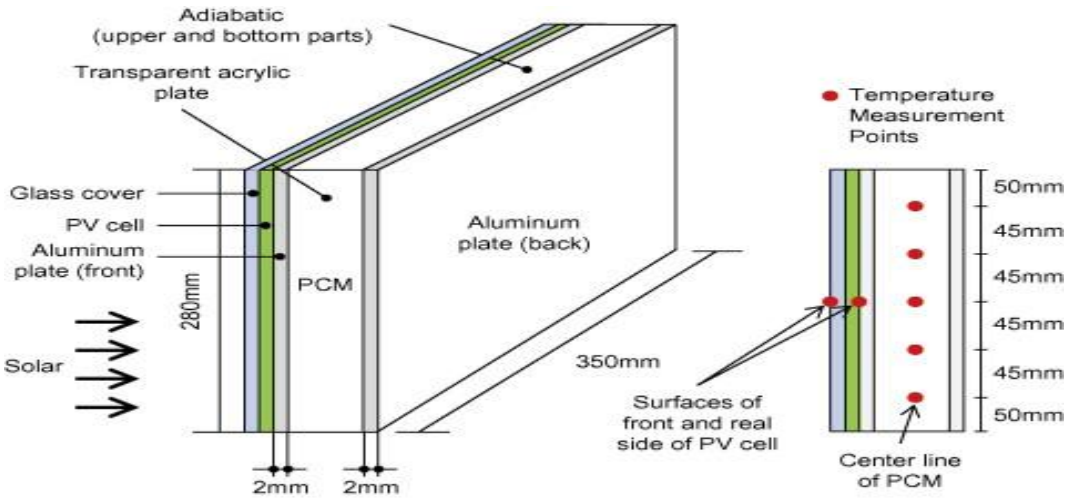

Figure 2–25: Schematic diagram of the PV/PCM module [144]

Browne et al. [145] have investigated the characterisation of a PV/T - PCM system, this system compared to the PV/T with the same water circulation for both systems. The concluded that the PV/T-PCM system increased the heat storage potential in comparison to the PV/T system with same simulation conditions, the heat delivered by the PV/T-PCM system was higher than the PV/T system by approximately 6°C. In higher temperature climate, the PV/T-PCM system increased the heat storage by 100% in comparison with PV/T system. Hassan et al. [146] have investigated the impact of building integrated photovoltaic PCM systems on building energy efficiency in a hot climate, Building integrated photovoltaics (BIPV) panel containing PCM , including the PCM in this system could decrease the temperature of the front and back of the PV panel by 12.3 °C and 22.6 °C respectively. Consequently, the PV electricity production of 7.2% at peak time and 5.5% for daily average. The presence of PCM in the system also helps to reduce the heat losses into ambient, thus storing 47.7% of incident irradiance as thermal energy in comparison to 0.36% for PV alone. It dropped the heat transmission to inside by 9.6% at peak and 7% average daytime, which means a drop of 5°C and 3.5 °C for peak time and average daytime respectively of indoor air temperature.

Ho et al[147] [148] have modelled a CFD numerical simulation to discover the effects of different MEPCM layer thicknesses and MEPCM melting points on the thermal and electrical performance of a building-integrated photovoltaic (BIPV) as shown in

Figure 2–26 by using a water saturated microencapsulated phase change material layer as a passive thermal management medium .

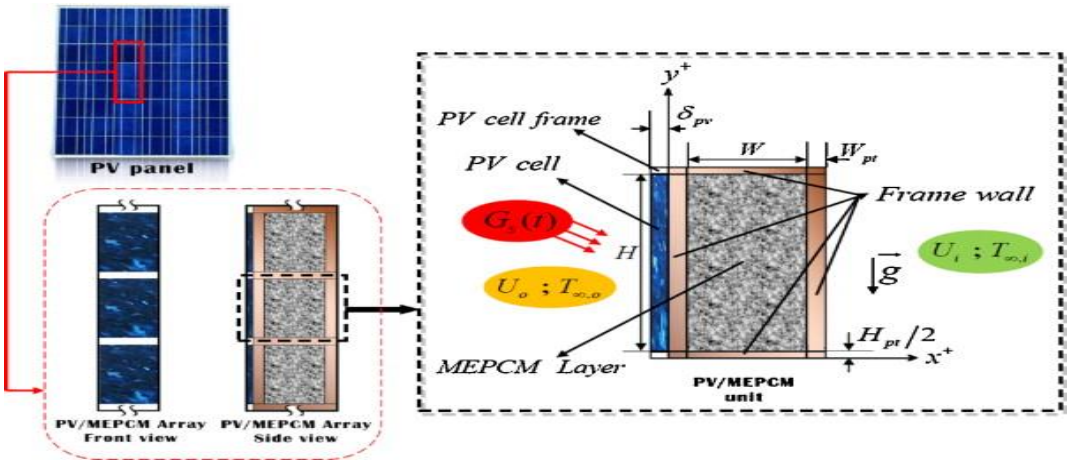

Figure 2–26: Schematic of heat transfer in a PV-MEPCM module and PV-MEPCM cell [147]

In the first study, the simulation carried out for a PV without PCM, and another two with different kind of PCMs their melting points were 30 and 32 ºC respectively, each PV with two thickness of 2 and 3 cm. The results showed that in winter the PV temperature without PCM reached 26.7 ºC with lowest average electrical efficiency of 19.84%. For summer time, the temperature rose to 38.5 ºC and lowest average electrical efficiency of 18.78%. For PV/MPCM system with 3cm layer thickness and 30 ºC the melting point of PCM, the performance of the system improved, at the peak sunshine hours of summer day the PV temperature reached 34.1 ºC, the single day electrical capacity was 231.439 kJ/m, which represents 2.013% extra electric capacity per day over the PV system without PCM.

Table 2-6: Overall performance of untreated PV cells versus PV/MEPCM cell [147]**.**

Summer	W (cm)	T_M (°C)	Tpv,max(°C)	ηpv,min(%)	ηpv,min.increase (%)	ηpv,day(%)	ηpv,day-increase (%)	Qpv,E,day(%)	Qpv,E,day-increase (%)
PV cell Without MEPCM	0	–	38.5	18.784	–	19.04	–	226.873	–
PV/MEPCM cell	2	32	35.3II	19.077II	1.56	19.328II	1.513	230.305II	1.513
	2	30	36.4II	18.971II	0.996	19.327II	1.507	230.316II	1.518
	3	30	34.1II	19.179II	2.103	19.422II	2.006	231.439 II	2.013

Note: ll refers to the second day data

In second case , Am=0.277 = (W /H) the ratio of the width to the height of the MPCM layer, and melting temperature of 26ºC , in summer and after one day of operation, more than half of the MPCM stay in the liquid phase, but in winter a middle part of the MPCM layer does not freeze. The result showed that there is an optimal Am between (0.277-1) for a better performance in the normal condition. After 10 hrs of operation half of MPCM layer with a melting point of 34 ºC do not melt, and all MPCM with a melting point of the 26ºC melt at the same condition.

Generally, the PV/T with air coolant has a very poor heat removal act due to its small thermal mass. The water type over the operation time, the system become less effective when the water temperature increase. Besides the effective cooling of the refrigerant-based type, it is difficult to handle, as depressurisation and pressurisation are needed along the system, a part of that there is a risk of the leakage of the refrigerant. In addition, the high cost of the heat pipe PV/T makes wide deployment unlikely. Finally, the MPCM-S based PV/T is not applicable yet, because it is just at the research and investigation stage.

There are no specific rules for using the correct PV/T system, because it is more dependent on the actual application, also the geographical location. The latter is important due to the intensive of the solar radiation. So the low solar radiation and ambient temperature locations, the air based PV/T is more appropriate and cheap for space heating which is required almost all the year, and at locations with high solar radiation. PV/T using water as a cooling medium is more applicable to get water preheating services, and by air heat extraction it could provide space heating in winter [149].

2.2.3 Summary of the Current PV/T Research

The established research about PV/T technology includes primary information about PVs and their materials, PV/T benefits over PV, and targeted to: i) describe the energy conversion and transfer in PV/T modules, ii) enhance the geometric and structural parameters of the PV/T systems to increase efficiency iii) identify the optimal system type, taking into consideration the cost of the system. Although lots of studies have been carried out in PV/T systems field, many technical barriers still exist in front of its developments, such as the higher temperature of the working fluid, inefficient heat removal value, leakage and freezing of the working fluid, as well as an unevenness of fluid distribution are exist . Air based PV/T technologies have the smallest heat removal value because of their low thermodynamic qualities. Water-based PV/T technologies face some barriers such as a non-stop increase in water temperature over the working time and freezing possibility in cold weather. Refrigerant based PV/T technologies are similarly not perfect type, as they have some practical problems with the great risk of the refrigerant leak, difficulty in pressure maintenance across the operation time, and uneven refrigerant distribution across multiple coils. PCM based PV/T technology has lately been recommended, it still in research and laboratory stage and require further investigations.

2.3 Potential opportunities for developing PV/T system

2.3.1 Decreasing the Thermal Resistance between PV units and Thermal absorbers

In PV/T fabrication process the thermal absorber is usually glued to the PV lamination, and a layer of Tedlar Polyester Tedlar (TPT) is used as a back sheet of the PV to improve the longevity of the panel [150], this causes a drop of the thermal efficiency of the PV/T , due to the non-conductive property of the TPT sheet then increase the thermal resistance between the absorber and the PV lamination. So a treated aluminium–alloy sheet could be a good alternative to the conventional TPT for solving this problem, it has higher thermal conductivity and solar absorptance of (144 W/m-K, 5%) in comparison with the conventional TPT (0.648 W/m-K, 2%), and lower solar transmittance of 0.2% in case it is 12.8% for TPT [151].

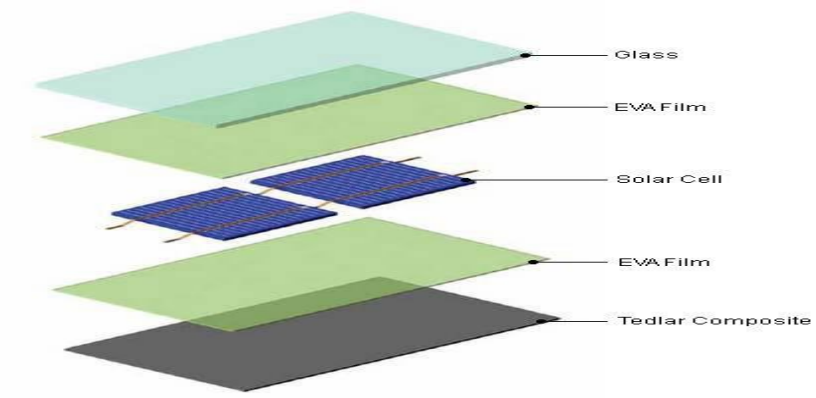

Figure 2–27: Solar panel layers: TPT layer as back sheet [151]

2.3.2 Developing a pack of Computer Simulation Model to assess the systems performance

Few types of research have been done to involve PCM in PV/T technology fields, but using MPCM-S is novel and is at the very early stage of investigations. Developing a steady state model of the heat transfer capacity of the thermal absorber with the heat balance of different system components is essential. Further simulations are needed for energy model of dynamic performance.

An assessment of PV/T under a real climate condition has not carried out yet, unlike the steady state this will retain the challenges as thermal adaptability and dynamic weather condition. So combining a theoretical predict with an experimental result could produce a logical output for both dynamic and steady state.

2.3.3 The Investigation of the System in Practical Buildings

The PV/T systems are practically available on buildings and projects, but still there are no enough researches and investigations about the performance of the systems under actual circumstances of the buildings. The result of this kind of studies reflects positively PV/T market.

2.4 Chapter Summery

An intensive review about PCM, MPCM and MPCM-S has been carried out including the practical application of PCM and MPCM in building energy generally and PV/T particularly. The results of the review simplified the understanding of PCM and PV/T technical developments and recognise the barriers and difficulties associated with their applications, toward the aim of combining them in a novel MPCM-S based PV/T system. In addition, the review resulted in finding the optimal slurry and its components for the research purpose, as limited phase change temperature range are available for solar applications. .

The best choice is the organic PCM (octodecane) with a melting point of 28 °C with polymer shell for encapsulation. The MPCMs have higher resistance to damage and are stronger when their diameters are less than 10 μm, but flocculation should be considered in very small diameters that could be prevented by adding less than 1 wt. percentage ionic surfactant. The size of MPCM particles was investigated, it found that the MPCM particle with thick shells exhibits less damage with forced circulation by the pump ,but thinner MPCM particle shell enhance the heat transfer more, and it is preferred in case of higher heat transfer requirements. The centrifugal pumps are the best kind for MPCM circulation, as they are able to pump the MPCM- for a long period without damage to the shells of the microcapsules. For preparing the MPCM-S, water is the best carrier fluid, because it is cheap and easy to handle.

Although numerous researches have been carried out in PV/T field, these systems still have many technical obstructions, for example the higher temperature of the working fluid, ineffective heat removal value, freezing and leakage of the working fluid, as well as an imbalance in liquid distribution.

Air based PV/T system is most popular PV/T and has been technologically advanced in the commercial sector. It can achieve up to 8% electrical and up to 39% thermal efficiency, which is mostly dependent on airflow temperature and speed. The key problem accompanied the air based PV/T systems lies in their poor heat removal value, due to the low heat conductivity and heat capacity.

Water-based PV/T system is a common technology as well, and it is widely applicable. It can reach up to 9.5% and 50% electrical and thermal efficiency respectively and it is mainly reliant on water flow rate and temperature, as well as water flow channel shape, size, and geometric. In comparison with air-based systems, it could increase the electrical efficiency of PV units and rise thermal energy employment. However, the possibility for improvement is restricted by characteristic technical problems like rising water temperature through operation time.

Refrigerant type PV/T system can increase the solar employment rate sufficiently over water and air based systems, hence it is likely to be more popular in future. It is generally work in combination with a heat pump. Its act is mainly reliant on the type of the refrigerant, its thermal and physical properties and the structural and geometric parameters of the refrigerant flow passages. This technology could reach up to (10%) electrical plus (65%) thermal efficiency. Such system characterises a significant enhancement in PV cooling system, nevertheless it faces several problems like an inequity in refrigerant distribution through the coils, pressure control difficulty during operation time, and potential of refrigerant leakage.

PCM-based PV/T is comparatively new technology especially MPCM-S based which still in very early research phase. Including PCM with the unique properties gives such a system a big chance of improving PV/T systems. The PCM based PV system could enhance the efficiency up to 5 %, but it might not be economically viable when it is used just to improve PV conversion efficiency. So hybrid PV/T - PCM is a better choice, which employs the absorbed heat to be used in different services, this kind is accompanied with significant challenges in need to be faced.

The review results aided to classify the technical obstructions existing in current PCM based PV/T system, establish a technical approach for the PV/T research, figure the research direction for the following chapters, and suggest new research opportunities.

CHAPTER 3: EXPERIMENTAL RIG DESIGN

3.1 System Description and working principle

The proposed MPCM-S based PV/T system comprises a PV collector, an electricity control unit, and a flat plate heat exchanger to cool down the slurry (this is the evaporator of a heat pump). The system includes the heat pump that consists of a compressor, evaporator (flat plate heat exchanger), expansion valve and a water tank with a coil inside to act as a condenser. As well as a pump for circulating the slurry, all these are illustrated in **Figure 3–1** .

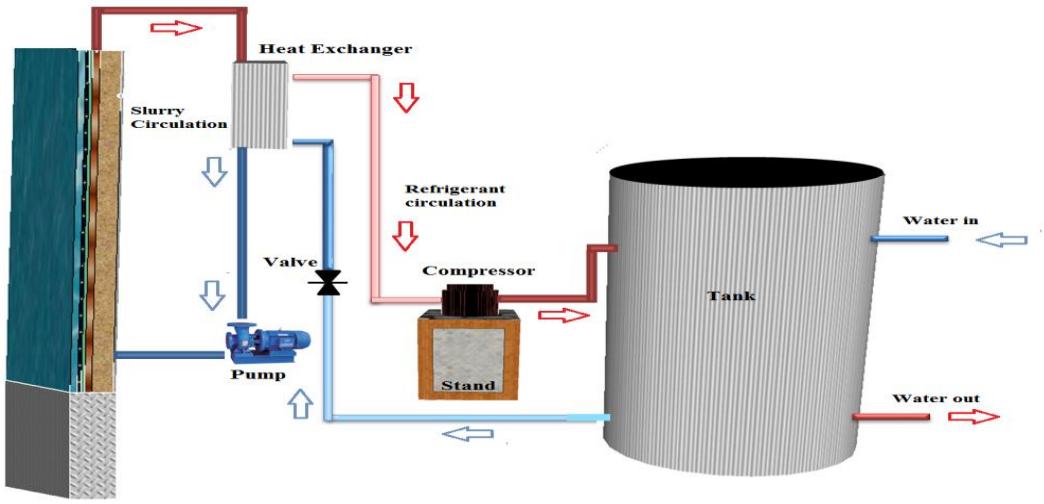

Figure 3–1: Diagram of the PV/T system s work principle.

In the PV/T module, a copper serpentine pipe installed underneath the PV layer as to extract the heat from the PV module as shown in **Figure 3–2**, and connected to the flat plate heat exchanger by flexible pipes, which returns to the absorbed pipe for the slurry circulation. When the slurry passes through the absorber pipe, it absorbs the heat from the PV; consequently, the PCM changes its phase from solid to liquid, and circulates back to the heat exchanger. The role of the heat exchangers is to cool down the slurry until the PCM returns to its solid phase and be ready to absorb more heat from the PV module.

The proposed PV/T module as shown in **Figure 3–2** contains a multilayer structure of:

1. Thermal glazing covers with high transmittance over 0.9.
2. Multi-structure PV lamination, including (the tempered glass, EVA sealant, PV cell, EVA sealant, and aluminium alloy sheet) in order.
3. Serpentine pipe made of copper due to the high thermal conductivity.
4. Insulation layer made of the mineral wool placed above the polystyrene board.
5. Lightweight polystyrene board as a back layer.

The module generates the DC current as a result of the solar irradiation, then via an inverter the DC current will be converted into AC current to be stored in a battery or supplied to the grid. In the meanwhile, the MPCM-S circulates through the absorber pipe as a cooling medium to reduce the module temperature, toward the main aim, which is higher electricity outcome.

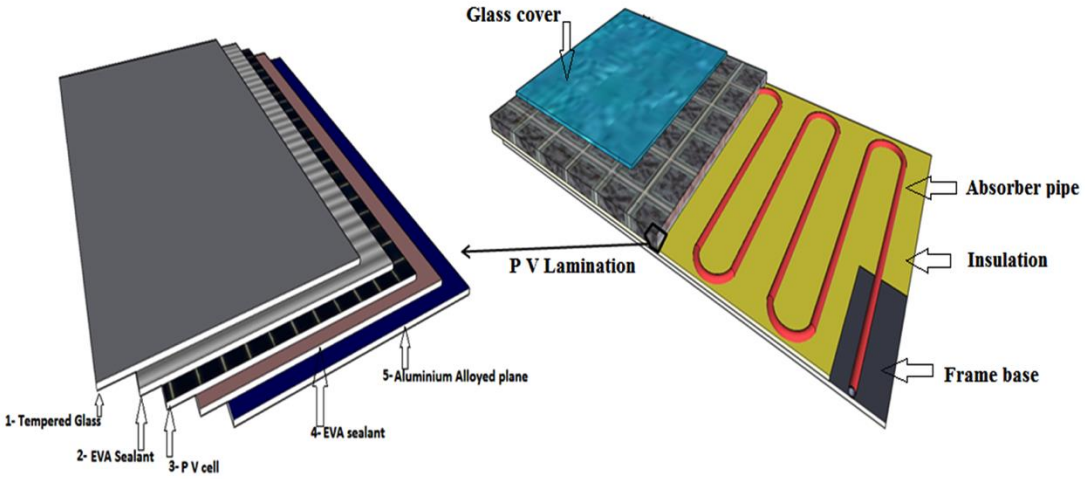

Figure 3–2: The PV/T module, and outline of PV lamination

In the heat pump cycle, the heat exchanger represents as the evaporator, and is the joint device between heat pump cycle and the slurry circulation cycle. The flat plate heat exchanger consists of a number of compressed thin plates, here two fluids (slurry from the PV module as the hot fluid and the refrigerant from the heat pump cycle as the cold fluid) pass through the heat exchanger, they interact but don't mix, because it's design allow the two different fluid to pass in alternate directions. For cooling purpose the

PCM in the slurry needs to change the phase from liquid to solid (to be ready for absorbing heat from the PV cells), this will be achieved when the liquid refrigerant in the heat exchanger absorbs the heat from the slurry and turns into vapour, then pass through the compressor to increase pressure and temperature, this heat will be transferred to the water tank through a coil placed in the water tank and represents the condenser in the heat pump. The hot water from the condenser could be employed for the domestic use. The refrigerant leaves the condenser as a high pressure and cold liquid, to reduce the pressure it needs to pass through the expansion valve, and return to the heat exchanger (evaporator) as a cold and low pressure liquid. Again the refrigerant absorbs the slurry heat from the heat exchanger for another heat pump cycle as mentioned.

The compressor is responsible for increasing the pressure of the refrigerant while it's passing through from the evaporator to the condenser, and it is responsible to deliver the refrigerant all over the heat pump. When the heat pump works in the PV/T system, the temperature of the evaporator and the condenser will be fixed, accordingly their pressure will fixed as well. When the temperature of the evaporator (heat exchanger) increases by receiving the solar radiation, automatically the driving speed of the compressor increases to deliver more refrigerant far more cooling down the PV panel.

Figure 3–3(a) shows the P-V (Pressure-Volume) diagram which defines the change in pressure and volume during a thermodynamic process. And T-S (Temperature – Entropy) diagram as shown in **Figure 3–3**(b) is a very common and useful tool to show the change in entropy (the degree of randomness and disorder in a system) and temperature during heat transfer process, for the ideal process the area under the (T-S) curve represents the heat transferred to the system during the process. Both diagrams show very clearly the heat pump cycle as a thermodynamic process.

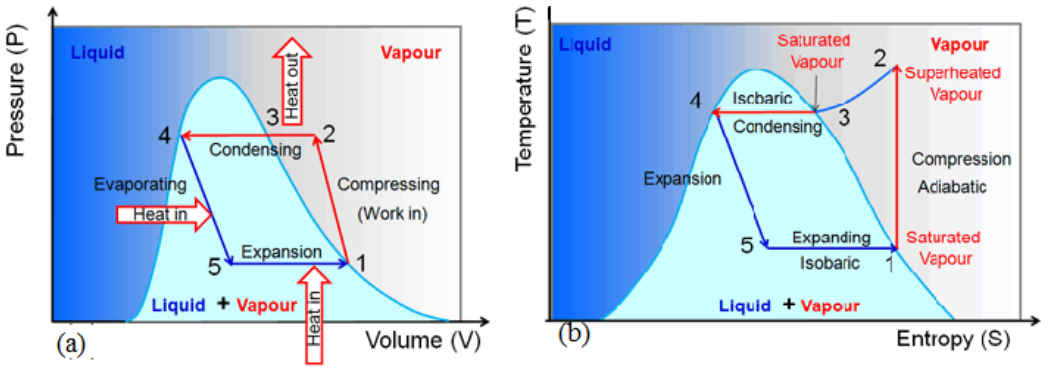

Figure 3–3: Heat pump refrigerant cycle (a) pressure-volume diagram, (b) temperature – entropy diagram [152]

3.2 Description of components

The proposed design is the start point of project preparation, which developed based on the fundamental knowledge and established experience by the researchers. These are subject to correction, modification and update.

3.2.1 PV/T Panel

Glazing cover: The glazing cover is an important part of the PV module that contributes to enhancing the outcome of a PV/T module, it is in charge of absorbing the solar irradiation and limiting the heat loss of the module. It could be single or double glazing cover. However, the double-glazing could protect the PV lamination better from any bad weather conditions and damages, it minimises the solar radiation input because of its low transmittance. However the double glazing cover has higher thermal efficiency than the single one, the latter has higher electrical efficiency, so the single glazing cover is more promising [153].

Al (Aluminium)-alloy-based PV Layer (PV lamination): The PV cells were applied on an Al-alloy base board, it consists of 72 cells in the (6x12) array, each cell size is (120x120x0.3) mm, it covers about 80% of the baseboard area which is (0.8x1.6) 1.28$m^{2.}$ Al-alloy has been chosen as a replacement of the conventional Tedlar–Polyester–Tedlar TPT baseboard, because of its higher thermal conductivity, higher solar absorptance and lower solar transmittance [151], as shown in **Table 3-1**.Apart from its main role as a base board of the PV cells, the coated Al alloy in this preliminary

design was employed as an electrical insulation and to protect the baseboard from corrosion during its operation life.

Table 3-1: Property difference between Al-alloy and TPT

	Al-alloy	***TPT***
Thermal conductivity	144 W/m.K	0.648W/m.K
Solar absorptance	5%	2%
Solar transmittance	0.2	12.8%

Serpentine pipe: A copper serpentine pipe of 9mm outer diameter and 7mm inner diameter was chosen to be fixed under the absorber plate. Copper pipe was chosen because of the high thermal conductivity. For PV and HVAC applications, the diameter of cooling pipes normally is in mm. it could be chosen according to the piping of the connected HVAC system which is around 4mm with a wall thickness of 1mm [56]. In the case of slurry circulation, it is advised to have larger diameter with a higher mass concentration of MPCM [19]. The pipe is fixed in grooves of the absorber plate for more contact area, therefore, more cooling. There are two main kinds of pipes in PV/T systems parallel and serpentine, the latter been chosen because the MPCM-S needs longer time in the pipe to achieve the phase change. The serpentine pipes are in parallel with 90 mm space (W) in between as shown in **Figure 3–4**.

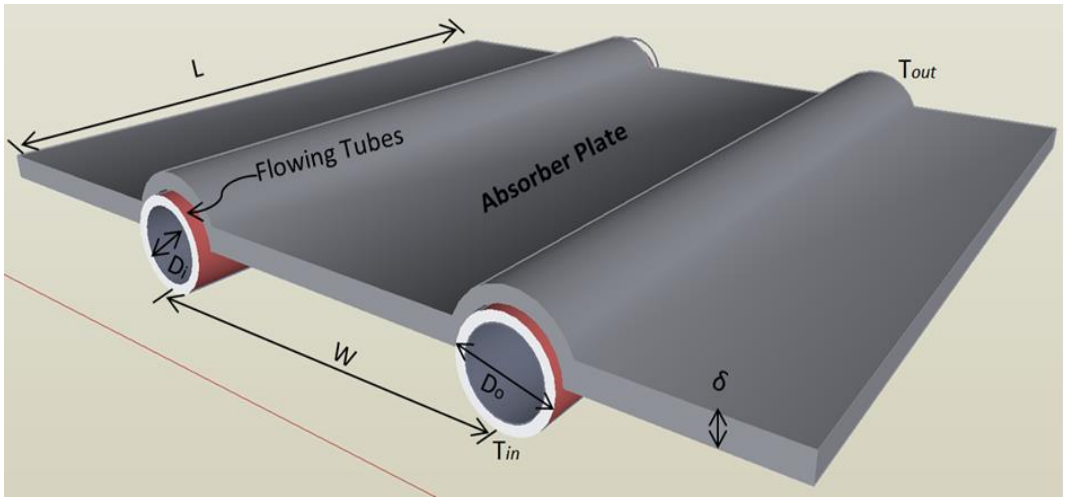

Figure 3–4: The schematic of absorber plate and serpentine pipe

Insulation material: Good insulation means the higher thermal efficiency of the PV/T by minimizing the heat loss, the most common insulation materials for this purpose are;

fiberglass, polystyrene and polyurethane. The most effective materials have higher thermal resistance (R) value in ($K.m.W^{-1}$). Fibre glass is widely used but it has lower R-value (3.1 $K.m.W^{-1}$) per inch than polystyrene and polyurethane [154]. Therefore, polystyrene and polyurethane are two good choices. **Table 3-2** shows the common insulating materials with their advantages and disadvantages.

Table 3-2: Popular insulating materials, "R" values, advantages and disadvantages [97]

Insulating material	**"R"($K.m.W^{-1}$) per inch (2.54 cm)**	**Advantages**	**Disadvantages**
Polyurethane, board	6.25	Very good R-value, can be used with fibreglass resins	Not always easily available, relatively expensive
Polyurethane, spray	7.0	Very good R-value, can be used with fibreglass resins, easy application with spray equipment	Not always easily available, expensive, requires special spray equipment
Polyurethane, poured (two-part chemical)	7.0	Very good R-value, can be used with fibreglass resins, relative ease of application	Not always easily available, expensive, requires very careful volume calculations
Polystyrene, sheets (smooth) Trade name "Styrofoam"	5.0	Readily available, low cost, reasonable R-value	Cannot be used with fibreglass resins unless protected, easily damaged
Polystyrene foamed in place and expanded moulded beads. Known as Isopor, Polypor, etc.	3.75 to 4.0	Reasonable R-values, lower cost than smooth surfaced sheets	Cannot be used with fibreglass resins unless protected, easily damaged

The actual PV/T module used for the experiments was as designed. The serpentine pipe connected to the heat pump and the circulating pump with flexible connection pipes of ½ inch, (15) T type thermocouples was set on the back of the Al – alloy baseboard as

shown in **Figure 3–5** to measure the PV panel temperature. The outer layer is a single clear glazing with high solar transmittance of 0.9 to allow transmission of the solar radiation, meanwhile to prevent extreme heat loss. The geometrical, thermal and physical parameters of the prototype module are detailed in **Table *3-3***. The panel generates DC current that later on converted to AC via inverter then will be or saved in a battery or transferred to the grid.

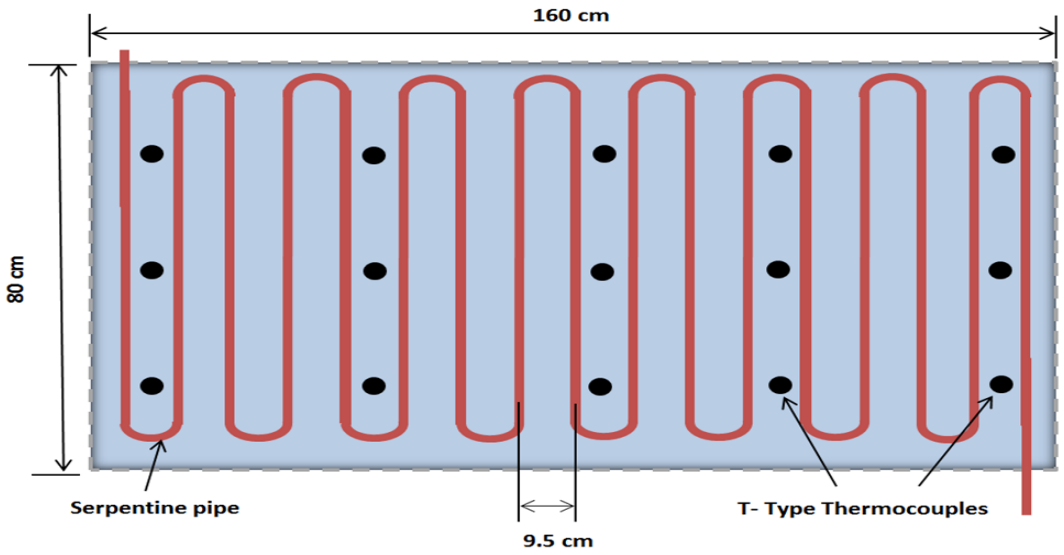

Figure 3–5: Schematic of the actual serpentine pipe of the module and the thermocouples positions.

Table 3-3: Physical, thermal and geometrical parameters of the module

Item	Value
PV/T module area, m^2	1.28
PV electricity net area, m^2	1.177
Absorb tube inner diameter, m	0.007
Absorb tube outer diameter, m	0.009
Tube spacing, m	0.095
Thickness of PV cell, mm	0.2
Thickness of tempered glass layer in lamination, mm	3.2
Thickness of EVA layer, mm	0.50
Thickness of bond, mm	10
Thickness of aluminium alloy plane, mm	1
Thickness of insulation, mm	40
Thickness of back plate, mm	10
Thermal condictivity	
Thermal conductivity of pipe (copper), $Wm^{-1}K^{-1}$	390
Thermal conductivity of PV cell, $Wm^{-1}K^{-1}$	84
Thermal conductibity of glass, $Wm^{-1}K^{-1}$	1.0
Thermal conductivity of EVA, $Wm^{-1}K^{-1}$	0.35
Thermal conductivity of bond, $Wm^{-1}K^{-1}$	1.15
Thermal conductivity of aluminium alloy, $Wm^{-1}K^{-1}$	230
Thermal conductivity of insulation, $Wm^{-1}K^{-1}$	0.045
Thermal conductivity of polystyrene board, $Wm^{-1}K^{-1}$	0.39
Others	
Cell's electrical efficiency at reference temperature (25°C), %	16.5
Temperature coefficient of PV cell power generation	0.0045
Module electricity output at rated condition, W	195

3.2.2 Heat pump

It delivers heat energy from the heat source to the destination called a heat sink, the heat is transferred by the refrigerant. The compact plate heat exchanger is widely used in

heating and cooling applications, it delivers a large heat transfer surface area per volume, so it is suitable for small rooms. It consisted of rectangular thin stainless steels, they compressed and welded together in a frame, they provide a parallel flow channel for alternating cold and hot fluid. Plate heat exchanger has higher thermal performance in comparison with tube heat exchangers [155] For the experimental purpose a 900W compressor and an environmentally friendly refrigerant R134a were preferred as a heat transfer fluid of the heat pump.

The actual heat pump used for the experiments was consists of a 1100W compressor, which was bigger than the proposed one, because it was already available in the laboratory, it was charged with the environmentally friendly R134a refrigerant as proposed with a flow rate of 0.012kg/s. A 200 L cylinder water tank (condenser) with a copper heat exchanger coil built up inside to absorb the refrigerant heat and transfer it to the water and to be utilized later, an expansion valve which is suitable for maximum working pressure of 52 bar and working temperature range of -50 to50 ºC, and a flat plate heat exchanger (evaporator), **Table 3-4** shows the parameters of the used flat plate heat exchanger. Heat-pump's evaporation and condensation temperatures are 15 and 70^{o}C respectively.

Table 3-4: Flat plate heat exchanger's parameters

Parameters	**Nomenclature**	**Value**	**Unit**
Heat exchanger plate thickness	δ_{hx}	0.00235	m
Heat exchanger plate height	H_{hx}	0.206	m
Heat exchanger plate cluster width	W_{hx}	0.076	m
Heat exchanger plate length	L_{hx}	0.055	m
Heat exchanger number of plates	N_{hx}	20	-
Heat exchanger operating temperature range	T_{hx}	-160 - 225	ºC
Heat exchanger operating pressure range	P_{hx}	0-3.24	MPa

3.2.3 MPCM-S:

The compound n-octadecane is desirable as a PCM for the core of the MPCM because it has latent heat of (241.2 J/g), which is higher than most PCMs, this PCM is encapsulated in a polymer shell. Also this PCM has an appropriate phase change temperature 28 ºC , which is suitable for the building energy applications [156]. Water was chosen as a carrier fluid for the MPCM particles to form the slurry, because water does not react with the coating and core material of the MPCM, is easy to handle, has a high thermal capacity itself, and is very cheap [11].

The actual used PCM was n-octodecane PCM as proposed, it was encapsulated in polymer shell, and it was in form of wet cake which contains 30% of water and 70% of microencapsulated phase change material, the properties of the product is shown in

Table 3-5. The morphology of the microencapsulated PCM was observed using a Scanning -Electron Microscope (SEM) instrument (JEOL JSM- 6400, Japan). **Figure 3–6** shows the images of the microcapsules for different instrument magnification. It is shown that the microcapsules have smooth and spherical surfaces. The diameters of microcapsules were measured by a particle characterization system (Malvern Instrument, Malvern Masterzer 2000). It was found that the microencapsulated PCM particles have the diameters ranging from 1 to 100 μm, with the average diameter of 18.2 μm, as shown in **Figure 3–6**.

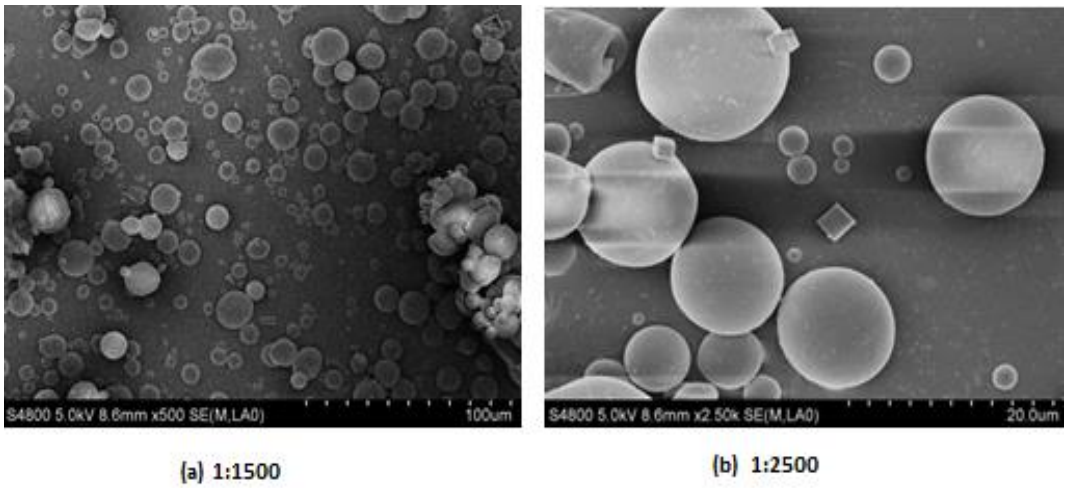

Figure 3–6: SEM images of MPCM particles for different magnification

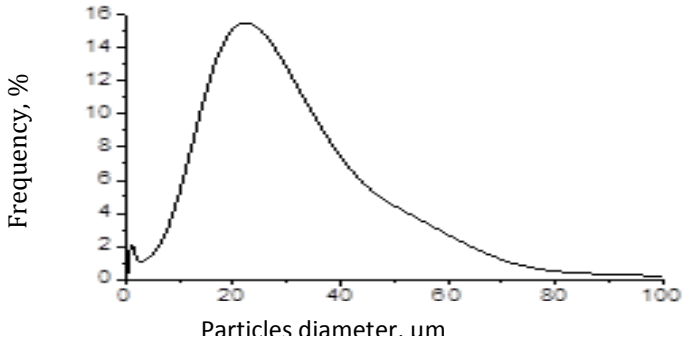

Figure 3–7: Diameter of the MPCM particles

Table 3-5:The MPCM 28 product displays the following general properties[157]

Typical properties	
Appearance	White to slightly off-white colour
Form	Wet cake (70% Solids, 30% Water)
Capsule composition	85-90% wt.% PCM 10-15 wt.% polymer shell
Core material	Paraffin (n-octodecane)
Particle size (mean)	17-20 micron
Melting point	28ºC (82ºF)
Heat of Fusion	180 - 195J/g
Thermal stability	Extremely stable – less than 1% leakage when heated to 250ºC
Thermal cycling	Multiple

The product needed in the test is MPCM-S and not wet cake, only wet cake was available in market, so the preparation process was carried out in the lab after lots of investigations and consultations from the chemistry department of Hull University and the professional employees in the Micro-teck labs (the supplier of the wet cake). The slurry contains MPCM, water and Gum guar modifier (thickener) to disperse the MPCM

particles throughout the bulk of the slurry as shown in **Figure 3–8**. Calculations have been done before preparation for the amount of each part of the slurry.

An example calculation is given for 10% MPCM-S. Following the same procedure 5%and 15% were prepared.

The preparation formula of 202 g of slurry with 10% concentration is as below:

Slurry = 180 g water + 20 g MPCM +2 g modifier

Wet cake = 70% MPCM+ 30% water

20 / 0.7 = 28.6 g wet cake

28.6 x 0.3 = 8.6 (water in 28.6 g of wet cake)

By deducting 8.6 from 180 g water

180 -8.6 = 171.4 g water for 200g slurry

So for 202 g slurry:

171.4 g water +28.6 g wet cake + 2 g modifier

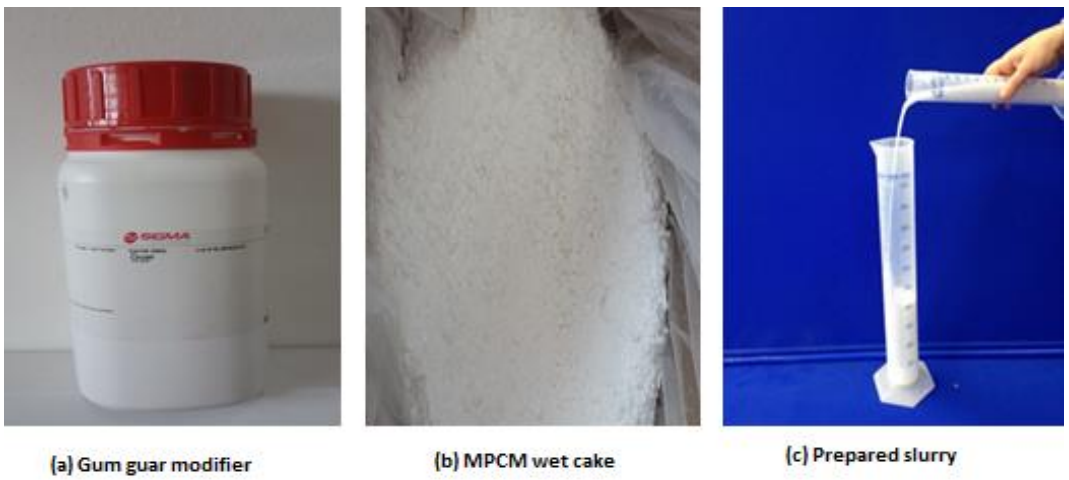

Figure 3–8: The prepared slurry and its components

The slurries with each concentration 5%.10%.15% and 20% have passed through some tests to confirm their important physical properties like suspension stability and ability to flow (Newtonian or Non- Newtonian), as shown in **Figure 3–9**.

Figure 3–9: The suspension stability test of the prepared slurry

Physica MCR 102 (Anton Paar) rheometer was used to find the viscosity of the slurry. Properties of the slurry as a bulk could be calculated depending on the properties of its components, by using the correlations [4-1] to [4-6] in section 4.1.

3.3 Experimental Instrumentation

For the purpose of laboratory measurement and apart from the main parts of the PV/T system, some measurement instruments were proposed to measure the main parameters of the test like temperature, pressure, flow rate and irradiation. The most important record of the test is the PV module temperature.

As proposed for measurements purpose 15 thermal detector were fixed on the baseboard of the PV cells as shown in **Figure 3–5** Some more thermal detectors were installed in different positions like the inlet and outlet of the heat exchanger from the heat pump side (to record the refrigerant temperature). Further three thermal detectors were installed for measuring inlet, outlet and inside water temperature of the water tank (condenser). Two of each (temperature probe, pressure transmitter, and flow sensor) were installed on the inlet and outlet pipes of the module. The probes have a sensor

steak that goes inside the pipes to be in direct touch with the slurry for accurate measurements of the inlet and outlet slurry temperature, which are key variables. The pressure transmitter measures inlet and outlet pressure of the slurry, for calculating the pressure drop when the slurry circulates through the serpentine pipe, and the turbine flow sensors measure the flow rate of the slurry through the module.

Two solar simulators of 4000W that represent the sun radiation were placed on a rack opposite of the PV module to direct the solar radiation perpendicularly on the module, their intense could be controlled to deliver the required radiation for the test, for measuring the intensity of the radiation a pyranometer was placed on the support frame of the module. Finally, all these measured data need to be collected, this has been done by an Agilent data logger with two - 20 channel Armature Multiplexers, meaning it has 40 points. This data logger has a two - way connection, one to the desktop computer and the other to the module by connecting wires from each sensor to one point of the mentioned 40 points. All these measurement instruments and their specifications are illustrated in **Table 3-6**.

Table 3-6: The main experimental instruments.

Instrument	Figure	Specifications	Quantity	Position
Solar simulator		Coated aluminium housing. Solar Constant 4000 - Radiation unit Inclusive 4000W lamp and UV-Filter(Atlas)	2	Opposite side of the module (facing it)
Pyranometer		LP02-TR Hukseflux thermal sensor (radiaition sensor)	1	On the bracket of the module
Thermocouples		T- type	15	On the baseboard of the PV lamination
Pressure transmitter		(Germs Sensors) 3100R0010G01B000,10bar, 0-5V	2	Inlet and outlet of the module
Temperature Probes		PT100 RTD probes 90/00543945. Jumo-UK.	2	Inlet and outlet pipes of the module
Flow sensor		Turbine type, 200psi Pressure, 0.5-5 (Germs Sensors)	2	Inlet and outlet pipes of the module
Data logger With 2 modules number 34901A,20 channel Armature Multiplexer		(Agilent technologies) Agilent - 34972A&2 A3901 terminal modules	1	Next to the computer ,connected to both computer and the PV system
Particle analyzer		Malvern Masterzer 2000 (Malvern Instrument)	1	-

Rheometer		Physica MCR 102 (Anton Paar	1	-

3.4 Chapter Summery

The system concept and its working principles are defined in this chapter, the heat pump and the MPCM-S as a cooling fluid. The distinction of the MPCM-S based PV/T- heat pump system could be concluded as following: ii) the refrigerant temperature would be upgraded using a compressor to transfer heat from the refrigerant to water in the tank; iii) the electricity required for compressor could be delivered from the electricity generated by the PV, if the system was designed for this purpose, therefore creating a low or zero carbon solar heating operation. Any shortage or surplus of the electricity power could be co-ordinated through grid or battery storage. This system could be installed either on a building facade or as free stand heat and power generation unit.

This chapter outlined the system structure and included the proposed design of the different system components such as (the flat-plate heat exchanger, glazing cover, PV layer, insulation materials and heat pump). Proposed design are subject to correction, modification and update, so the conceptual design of each parameter was followed by the actual design used in the rig for the experiments. In addition, the preparation of the slurry illustrated including all components and preparing process in detail. For the purpose of laboratory measurement, this chapter showed the experimental instrumentations and their specifications and positions in the real experimental rig. These data and information will be applied as the input figures for the modelling and optimisation for the experiments in following chapters.

CHAPTER 4: THEORETICAL ANALYSIS AND DEVELOPMENT OF STEADY STATE MODEL

A theoretical analysis and investigation were carried out in collaboration with a research team from Hull University. Then the research team developed a computerised steady-state model in MATLAB software to describe the performance of the PV/T-MPCM-S system under laboratory conditions, and it would enable to (i) determine the system performance with different variables, (ii) determine the optimal system configuration, and (iii) find a proper system design and best operational parameters. In addition, it is useful to predict the problems occur in the system and to find a way solving them.

4.1 Calculation and determination of the thermal and physical properties of the selected MPCM slurry

For any application of MPCM-S, the thermal and physical property of the bulk should be known, each application needs a slurry with different ratio of particle to carrier fluid, this apart of a particular thickness of the microcapsule shell and its ratio to the core material that is PCM. Any change of the above contents leads to change in a thermal and physical property of the bulk (slurry). The formulas used for calculating the specific heat and density of the microcapsules and the slurry were derived from mass and energy balance principle [158]:

$$\rho_{particle} = \left(\frac{d_{core}}{d_{particle}} \right)^3 \frac{\rho_{core}}{W_{core}} \tag{4-1}$$

$$Cp_{particle} = \frac{(W_{core} . C_{core} + W_{shell} . C_{shell}) \rho_{core} \rho_{shell}}{(W_{core} . \rho_{shell} + W_{shell} . \rho_{core}) \rho_{particle}} \tag{4-2}$$

$$Cp_{slurry} = W_{particle} . Cp_{particle} + W_{water} . Cp_{water} \tag{4-3}$$

The composite sphere approach was used for calculating the thermal conductivity of micro capsules [159]:

$$\frac{1}{K_{particle}\, d_{particle}} = \frac{1}{K_{core}\, d_{core}} + \frac{d_{particle} - d_{core}}{k_{shell}\, d_{particle}\, d_{core}} \tag{4-4}$$

The Maxwell's relation was used to find the thermal conductivity of the MPCM-S [43]:

$$K_{slurry} = \frac{2K_{water} + K_{particle} + 2W_{particle}\left(K_{particle} - K_{water}\right)}{2K_{water} + K_{particle} - W_{particle}\left(K_{particle} - K_{water}\right)} \tag{4-5}$$

The following equation was used to calculate the slurry viscosity at a certain temperature[160]:

$$\frac{\mu_{slurry}}{\mu_{water}} = \left(1 - \phi - A_{\phi}\phi^{2}\right)^{-2.5} \tag{4-6}$$

Where; ø is the particle volumetric concentration of the slurry. Aø = 3.7, is the constant that depends on the shape, size and type of the particle.

4.2 Fluid Theory and the Mathematical Formulas representing the System

The solar energy transfer and conversion for the system at steady state occurs in four stages as shown in **Figure 4–1** : i) part of the solar radiation is absorbed, while the rest is dissipated into the air, ii) the absorbed part is converted into electricity by the PV cells, iii) the remaining part of the absorbed thermal energy is transferred to the slurry via the copper serpentine pipe, and iv) prompting the transported heat by the slurry using heat pump.

Some assumptions were made as below, to simplify the energy model development:

- The system operates under a quasi-steady condition.
- Heat losses through all the insulation layers of the module are ignored.
- Heat losses through the serpentine pipe are negligible.
- The transmittance of the EVA layers is 100%.
- The electrical losses of the solar cells and PV module are negligible.

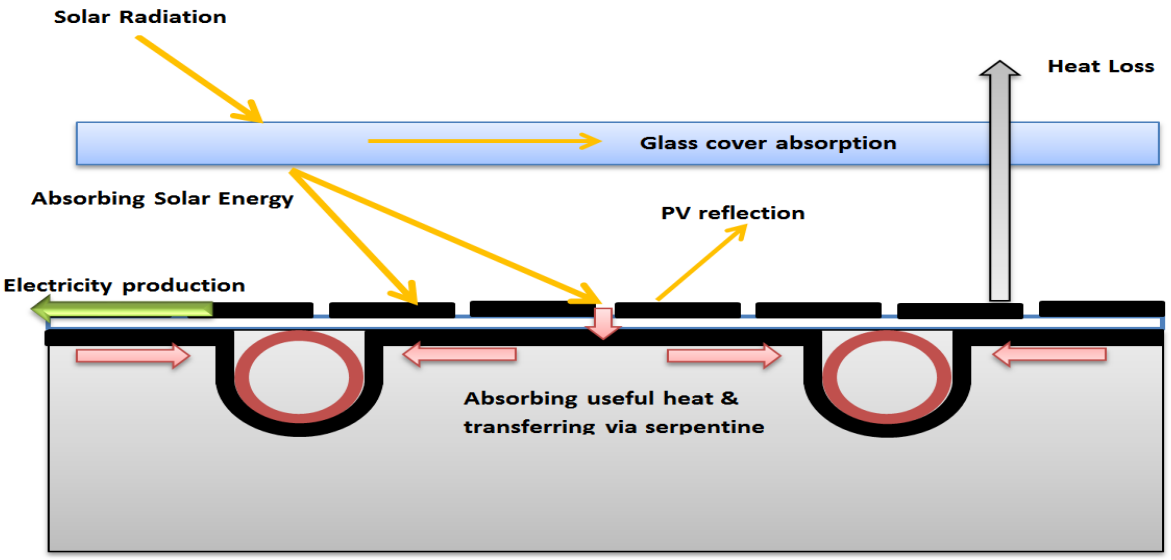

Figure 4–1: Schematic of the solar energy conversion and transfer processes

4.2.1 Absorbed Solar Radiation

Once the solar radiation strikes the PV module, the absorbed radiation will convert into electricity by the PV cells, a small amount of the absorbed heat will dissipate into surroundings that is due to conductive/conduction heat transfer and diffusion of the radiation, the rest of the heat will convert into the useful heat that will be employed later.

The absorbed energy is the energy delivered to the module and it is a function of the transmittance of the glazing cover, the solar radiation striking the module and the absorptance of the PV surfaces [99][161]

$$Q_{abs} = \tau c^{Nc} \tau_{g,pv} \left[\alpha_p \beta_p + \alpha_b (1 - \beta_p)\right] A_m I \qquad (4 - 7)$$

Where; τc : the visual transmittances of cover plate , τg, pv: the visual transmittances of glazing layer of PV lamination, Nc: the number of cover plates, αabs , αb: are the absorption ratios of the PV layer and its baseboard, βp : the packing factor of PV layer, Am : the collector area of the module in m^2.

4.2.2 Heat loss

An amount of the absorbed energy will be dissipated into the surrounding, that is due to the temperature difference between the top cover of the module and the surrounding air, the heat loss from the back and the edges of the module is considered to be zero, because they assumed as a super insulated area. For steady state condition and single cover module, the heat loss from the top cover will pass through two stages , in the first stage the heat transfer from the PV absorber to the glazing cover, and the second stage is the heat transfer from the glazing cover to the surrounding air [99]. **Figure 4–2** shows the stages of the heat transfer which placed in series.

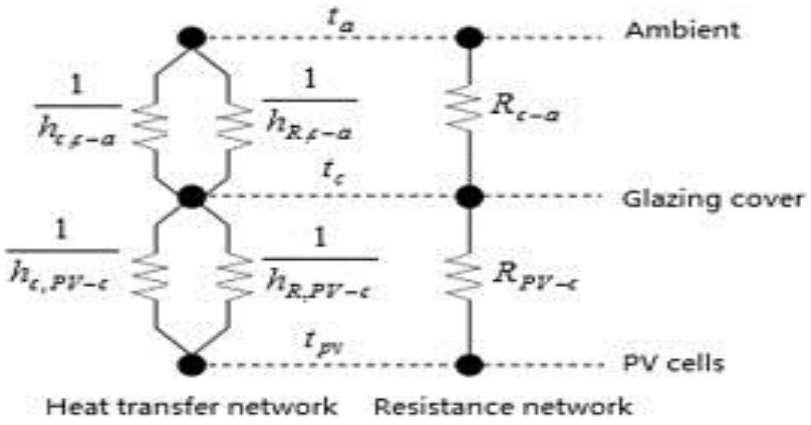

Figure 4–2: Heat loss network of a typical single glazed covering PV/T unit [161]

The heat loss from the top cover could be written as [161]:

$$Q_L = U_L A\left(T_{pv} - T_a\right) \tag{4- 8}$$

Where; Q_L: total heat loss (W), U_L: overall heat transfer coefficient (W/m^2-K), T_{pv}: average temperatures of PV absorber, T_a: ambient air temperature (K)

U_L is the overall heat transfer coefficient and could be expressed as [161]:

$$U_L = \left(\frac{1}{h_{c,pv-c} + h_{R,pv-c}} + \frac{1}{h_{c,c-a} + h_{R,c-a}} \right)^{-1} \tag{4- 9}$$

Where; *hc,pv-c* , *hc,c-a*: are convective heat transfer coefficients (W/m^2-K) of PV absorber (pv)to the top cover (c), and convective heat transfer coefficients (W/m^2-K) of top cover to the air (a) respectively, h_R*,pv-c*, h_R*,pv-c* : are radiative heat transfer coefficients (W/m^2-K)of of PV absorber (pv)to the top cover (c), and radiative heat transfer coefficients (W/m^2-K) of top cover to the air(a) respectively.

a-Heat Transfer coefficient from the PV absorber to the Glazing Cover

The exist of the air between the absorber and the glazing cover, transfers the heat by convection, so the coefficient of the convective heat transfer could be expressed as below[162]:

$$h_{c,pv-c} = \frac{K_{a,pv}}{\delta_{a,pv}}\left\{1 + 1.446\left(1 - \frac{1708}{Ra_{a,pv}\cos\theta}\right)^{+}\left[1 - \frac{1708\ \sin(1.8\theta)^{1.6}}{Ra_{a,pv}\cos\theta}\right] + \left[\left(\frac{Ra_{a,pv}\cos\theta}{5830}\right)^{0.333} - 1\right]^{+}\right\} \quad (4\text{-}10)$$

Where: Ka,pv : thermal conductivity of air gap at the average temperature of PV layer and cover surface (W/m-k), δa,pv : PV layer to glazing cover distance (m)
θ : the collector angle between the bracket with plus means zero (positive values only)
Raa,pv : Rayleigh number of the air gap at PV layer and cover surface.

The Rayleigh number is expressed as:

$$Ra_{a,pv} = \frac{g(T_{pv} - T_c)\delta_{a,pv}^3}{v_{a,pv}^2 T_{a,m}}\Pr_{a,pv} \quad (4\text{-}11)$$

Where: g : gravity acceleration (m/s^2) , ν_a: kinematic viscosity of air at the PV and inner cover surface (m2/s) $Pr_{a,pv}$: Prandtl number of the air gap at PV layer and inner cover surface, it is independent of temperature (its value is 0.7), $T_{a,m}$: average air temperature of PV layer and inner cover surface.

The average air temperature could be written as below:

$$T_{a,m} = (T_{pv} + T_c)/2 \quad (4\text{-}12)$$

Where: T_{pv}: average temperature of PV layer (K), Tc: average temperature of the inner cover surface (K).

The radiation heat transfer coefficient is given by[99] :

$$h_{R,pv-c} = \frac{\sigma\left(T_{pv} + T_c\right)\left(T_{pv}^{2} + T_c^{2}\right)}{\left(1/\varepsilon_{pv}\right) + \left(1/\varepsilon_c\right) - 1} \qquad (4-13)$$

Where :T_c : average temperature of external cover surface (K), ε_{pv} , ε_c : are infrared emissivity of the PV layer and glass cover surface respectively, σ : Stefan–Boltzman constant ($5.6679\times10^{-8}W/m^2\text{-}K^4$)

b- Heat Transfer from the glazing cover to the Surrounding Air

The convective heat transfer coefficient of an exposed surface to the air , could be calculated depending on Klein equation[163] :

$$h_{c,c-a} = \frac{8.6V^{0.6}}{L^{0.4}} \qquad (4\text{-}14)$$

Where: V: wind speed (m/s), L: is the characteristic length of the collector (m).

The minimum convective coefficient for a surface that exposed to the air is considered as 5W/m, so if the Klein equation gives a result less than 5W/m, then it should be replaced by 5W/m.

The radiation heat transfer coefficient includes the sky temperature(T_{sky})as the reference of the radiation temperature, but due to the little effect of the sky temperature on the results, it usually replaced by the air temperature, so [162] :

$$h_{R,c-a} = \varepsilon_c\sigma\left(T_c + T_a\right)\left(T_c^{2} + T_a^{2}\right) \qquad (4\text{-}15)$$

4.2.3 Electricity Production from the Absorbed Energy

There is a strong relation between the electrical efficiency of the PV module and its back surface temperature that could be expressed as below [164]:

$$\eta_e = \eta_r \left[1 - \beta_{pv} \left(T_{pv} - T_r\right)\right] \quad (4\text{-}16)$$

Where: η_r : is the reference efficiency at standard conditions (R = 1000 W/m2 and T_r=25 °C) and β_{pv} : is the temperature coefficient of pv (K^{-1}).

The electricity output could be calculated as below:

$$Q_e = \eta_e \beta_{pv}\, \tau_c\, \tau_{g,pv}\, \alpha_{pv}\, IA \quad (4\text{-}17)$$

4.2.4 The heat Yield

For the steady state condition, the absorbed energy is divided into three parts; thermal energy (Q_{th}), electrical energy (Q_e) and heat loss (Q_L), so the thermal energy could represent as below:

$$Q_{th} = Q_{abs} - Q_L - Q_e \quad (4\text{-}18)$$

The sheet-tube configuration in Figure 4–**4** is considered to perform the heat analysis .The heat absorbed by the fin will be directed to the serpentine pipe along its width direction, and then the heat flow travels through the cross-sectional fin area. This one-dimensional heat transfer process starts from the fin end (x = 0) to finish at the fin base [x = (W/Np-Dp)/2]. The heat flow process using the finite element approach is shown in Figure 4–**3**, dx indicates to the step length of the numerical calculation.

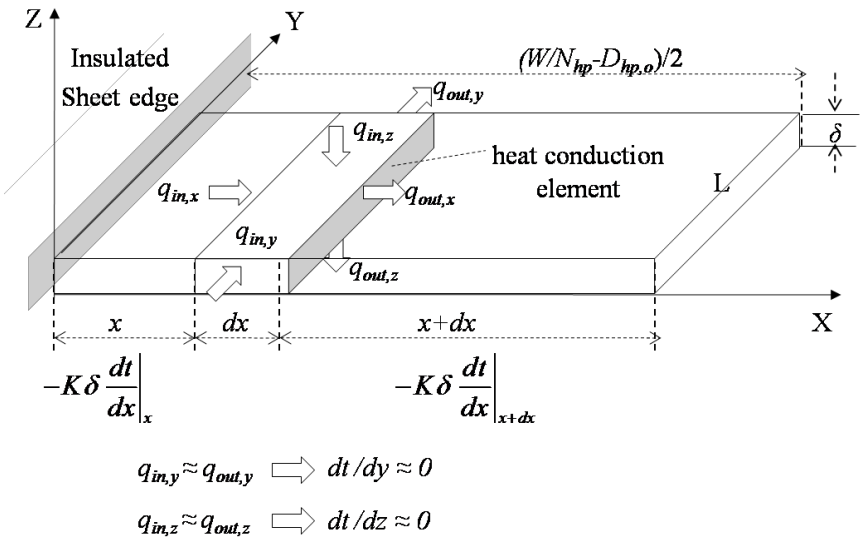

Figure 4–3: The heat flow at the segment length (dx) on the fin sheet

The following energy conversion equation can be applied to analyse the finite element per unit width:

$$\left(S - U_L'\left(T - T_a\right)\right)\Delta x + \left(-K\delta\frac{dT}{dx}\right)_x - \left(-K\delta\frac{dT}{dx}\right)_{x+\Delta x} = 0 \qquad (4\text{-}19)$$

where, S= $q_{abs} - q_{e,}$ (q_{abs} and $q_{e)}$ are the absorbed solar energy and electricity rate per unit length of the module (W/m^2); k and δ are the thermal conductivity in (W/m-K) and thickness (m) of the fin sheet, and $U_{L'}$ is the overall heat transfer coefficient.

The useful heat has been calculated using the Hottel–Whillier model, the heat flux in flow direction is not considered owing to the even heat input. According to the Hottel–Whillier equation, the useful energy is the energy absorbed minus the heat loss, this in case of flat plate thermal collector:

$$Q_u = LW F'\left[Qabs - U_L'\left(t_{f-}t_a\right)\right] \quad (4\text{- }20)$$

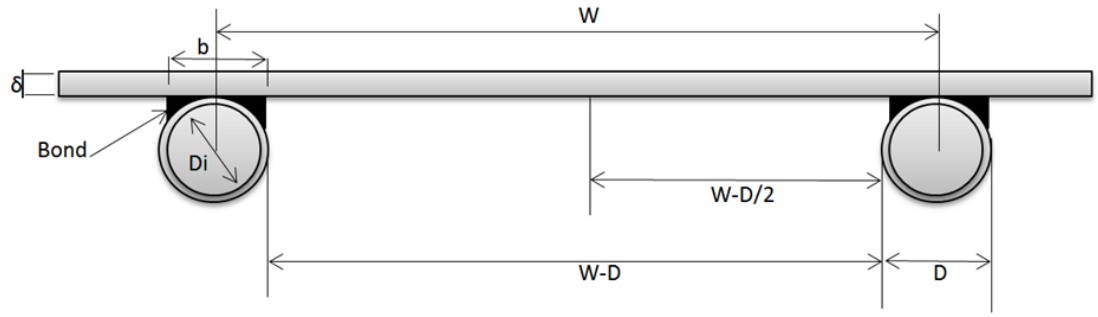

Figure 4–4: Schematic diagram of flat plate sheet and tube configuration.

The Hottel–Whillier equation for a combined PV/T module [165]:

$$Q_u = LW F'\left[S - U_L'\left(t_f - t_a\right)\right] \quad (4\text{-}21)$$

Where, t_f is the fluid temperature

The overall heat transfer coefficient to involve T $_{fin}$:

$$U_L' = \frac{T_{pv} - T_a}{T_{fin} - T_a} U_L \quad (4\text{-}22)$$

The collector thermal efficiency factor F` represents the ratio of the system's actual useful heat gain to the overall converted solar heat at a certain working fluid temperature. It is expressed as :

$$F' = \frac{1/U_L'}{\frac{W}{N_p}\left\{\frac{1}{U_L'\left[(W/N_p - D_{p,o})F + D_{p,o}\right]} + \frac{1}{C_b} + \frac{1}{\pi D_{p,i} h_c}\right\}} \quad (4\text{-}23)$$

Where; C_b; is the bond conductance, and F is the standard fin efficiency and is expressed as below:

$$F = \frac{\tanh\left[m(W/N_p - D_{p,o})/2\right]}{m(W/N_p - D_{p,o})/2} \quad (4\text{-}24)$$

In addition, the variable, m, is expressed as:

$$m = \sqrt{\frac{U_L'}{K_f \delta_f}} \quad (4\text{-}25)$$

The convection heat transfer coefficient of the working fluid in the heat absorber can be expressed as below:

$$h_c = \frac{Nu_f K_f}{D_{p,i}} \quad (4\text{-}26)$$

Where; Nu_f is the Nusselt number.

For the MPCM-S based turbulent flow, the Nusselt number is calculated using the following equation [59]

$$Nu_f = 4.8527 \times 10^{-4} \, \mathrm{Re}_m^{0.7733} \, \mathrm{Pr}_m^{2.7941} \, Ste^{0.3159} \times \left(\frac{L_1 + L_2}{D}\right)^{-0.333} \left(\frac{\mu_m}{\mu_w}\right)^{-2.4349} \quad (4\text{-}27)$$

The Nusselt number for MPCM-S based laminar flow is expressed as:

$$Nu_f = 0.8148 \times 10^{-4} \, \mathrm{Re}_m^{0.4593} \, \mathrm{Pr}_m^{0.4836} \, Ste^{0.1277} \times \left(\frac{L_1 + L_2}{D}\right)^{0.3059} \quad (4\text{-}28)$$

Where, μ_m is the average dynamic viscosity of the slurry in the phase change region, and μ_w is the average dynamic viscosity of water-based on the inner tube wall temperature.

The Nusselt number for water-based turbulent flow, Nu_f can be calculated using the following equation [163]:

$$Nu_f = 0.023\,\mathrm{Re}_f^{0.8}\,\mathrm{Pr}_f^{0.4} \tag{4-29}$$

In addition, for the water-based laminar flow, Nu_f can obtain by the following formula [30]:

$$Nu_f = 4.364 + \frac{0.086\left(RePr\,\frac{D}{L}\right)^{1.33}}{1 + Pr\left(Re\,\frac{D}{L}\right)^{0.83}} \tag{4- 30}$$

The heat obtained by the passing fluid is given by:

$$Q_f = \dot{m} C_p (t_{outlet} - t_{inlet}) \tag{4-31 }$$

4.2.5 Upgrading the Heat using the Heat Pump

If the system operates in conjunction with a heat pump, heat pump energy consumption and upgrading the heat should be clarified. When the refrigerant absorbs the heat from the slurry in the heat exchanger, then this refrigerant vapour upgrades its heat by passing through the compressor, then leaves as a high temperature refrigerant vapour, finally will condense and release the heat in the water tank which represents the condenser of the heat pump. The heat absorbed by the refrigerant in the heat exchanger is expressed as:

$$Q_u = Q_{e,t} = mr\, A_{cr}\, (H_1 - H_4) \tag{4-32}$$

Where, *H1* and H_4 are the thermal enthalpies of the refrigerant (kJ/kg) at point 1and 4 in **Figure 3–3**; and A_{cr} is the cross section area of the refrigerant tube (m^2).

The compressor operation is assumed as isentropic condition, and the output heat of the heat pump is calculated as:

$Qc,t = mr\ Acr\ (H_2-H_3)$ (4-33)

Where, H2 and H_3 are the thermal enthalpies of the refrigerant (kJ/kg) at points 2 and 3.

The consumed electricity of the heat pump could be calculated as:

$Q_{c,e} = mr\ A_{cr}\ (H_2-H_1)$ (4-34)

Where, H_2 and H_1 are the thermal enthalpies of the refrigerant (kJ/kg) at points 2 and 1.

4.2.6 Pressure drop and pump's power consumption

The pressure drop (head loss) need to be investigated to ensure the correct performance of the system. If it goes over the pressure driving the flow (passive or active), then it will result in the stop of the flow. There is pressure drop due to friction losses as well as dynamic losses during flow rate across pipes, they are caused by changes in velocity or direction (commonly at the fittings). The pressure drop of the serpentine pipe is calculated by the following formula:

$$\Delta p = \left(\lambda \frac{L}{D_i} + \sum \xi \right) \cdot \frac{\rho \mathrm{v}^2}{2} \quad (4\text{-}35)$$

Where the friction factor of the copper tube, λ is defined as:

$\lambda = 64 / \mathrm{Re} \qquad \mathrm{Re} \leq 2300$

Or

$\lambda = 0.0025\ \mathrm{Re}^{1/3} \qquad 2300 < \mathrm{Re} \leq 4000$

Or

$\lambda = 0.3184 / \mathrm{Re}^{0.25} \qquad \mathrm{Re} > 4000$

The power consumption of the pump could be calculated by the next formula:

$$Q_p = \frac{\Delta p \dot{m}}{\eta_p} \tag{4-36}$$

4.2.7 Efficiencies calculations:

The electrical efficiency is defined as:

$$\eta_e = \frac{Q_e}{AI} \tag{4-37}$$

The useful heat received by the absorber will finally be transferred to the heat received by the coolant fluid, i.e., water or MPCM-S, which is represented by Q_u. The thermal efficiency is calculated using the following formula:

$$\eta_{th} = \frac{Q_{th}}{AI} = \frac{Q_u}{AI} \tag{4-38}$$

The module's overall solar efficiency η_o would be the sum of both electrical and thermal efficiencies, defined as:

$$\eta_o = \eta_e + \eta_{th} \tag{4-39}$$

Taking into account the energy consumed by a pump, that is for overcoming the flow resistance of the slurry (or water) through the serpentine pipe, the module's net efficiency, η_{net}, can be calculated by:

$$\eta_{net} = \frac{Q_e + Q_{th} - Q_p}{AI} \tag{4-40}$$

If the system is in conjunction with a heat pump, the electricity consumed by the heat pump should be add to the circulating pumps electricity consumption.

4.3 The Algorithm of the Computer Model and Operation

The previously listed equations represent the heat transfer process used for the system modelling and operational predictions. The algorithm used in the model is as follow:

I. Enter the weather data and PV/T module's geometrical and operational parameters, including the solar radiation, ambient temperature, wind speed, PV/T module's size & area, absorbing tube's size & length, layer thickness, optical & thermal properties of associated materials, and the thermal and physical parameters of the working fluid including the inlet temperature and flow rate etc. Then calculate absorbed solar energy Q_{abs} using Eq. (4-7).

II. Assuming a start-up PV cell temperature t_{pv} and determining the electricity yield, heat loss, and heat gain of the PV/T module:

- Heat balance in relation to the glazing cover is analysed by Eq. (4-8), which results in a solution to the heat loss, Q_{L}.
- Heat balance in relation to the PV cells is analysed using Eqs. (4-17) and (4-18), which results in determination of the converted solar electricity Q_{e} and heat Q_{th}.

III. Assuming the outlet temperature of the slurry, and calculating the heat transfer rate from the PV cells to the slurry:

- Assuming the outlet temperature of the slurry, calculate its relevant thermal and physical properties at the mean temperature condition, and then calculate the heat obtained by the fluid across the absorbing pipe using Eq. (4-31), which results in determination of the useful heat gain Q_f.
- Heat transfer from the PV cells to the slurry is analysed using Eq. (4-21), which results in determination of the useful heat gainQ_u.
- If $|(Q_{\mathrm{f}} - Q_{\mathrm{u}})|/Q_{\mathrm{u}}$ is greater than 0.1% (error allowance), then updating the outlet temperature of the slurry and returning to step (III) for re-calculation until the requirement for the error allowance is met.

IV. If $|(Q_{\mathrm{th}} - Q_{\mathrm{u}})|/Q_{\mathrm{u}}$ is greater than 0.1% (error allowance), then update t_{pv} by 0.01℃ or -0.01℃ and return to step (II) for re-calculation; repeat until $|(Q_{\mathrm{th}} - Q_{\mathrm{u}})|/Q_{\mathrm{u}}$ is equal or less than 0.1%.

V. Calculate the module's energy efficiencies using Eqs. (4-36) to (4-40).

VI. Completion of the iteration when the time is running out at the end of operation and export of the simulation results.

VII. Program termination.

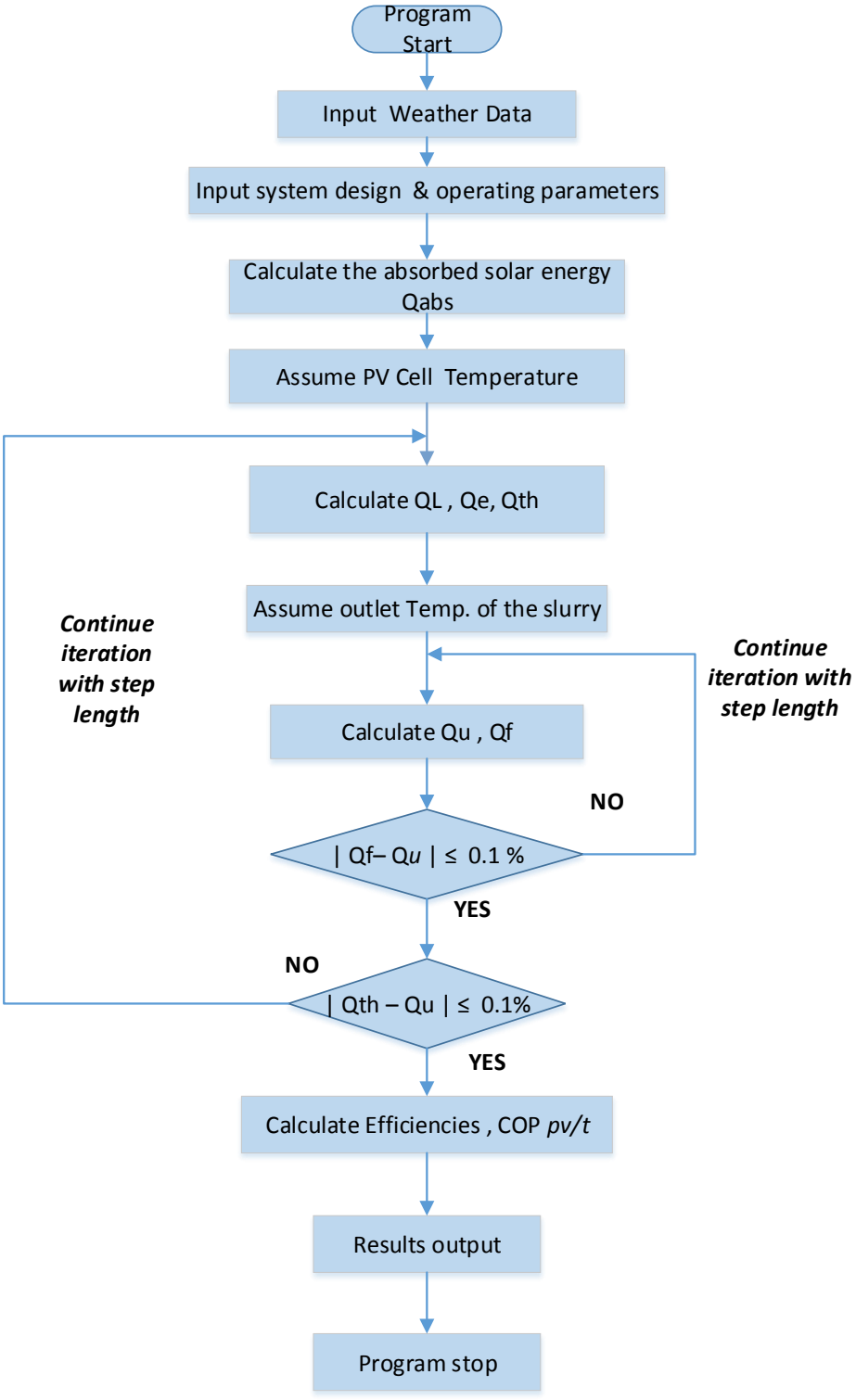

Figure 4–5: Algorithm flowchart of the computer model and operation

4.4 Validation of the computational model

The computer model was validated using the experimental data from reference [153], so the physical, geometrical, thermal parameters and working fluid (water) of the published system were used for running the computer model , as detailed in **Table 4-1**.

Table 4-1: Physical, thermal and geometrical parameters of the published BIPV module [153]

Symbol	Description	Value	Remarks
A	PV/T module effective area	0.873 m^2(675*1293 mm)	
$f_{pv}A$	PV electricity net area	0.65 m^2	
D_i	Absorb tube inner diameter	0.008 m	
D_o	Absorb tube outer diameter	0.010 m	
W	Tube spacing	0.095 m	
K_{abs}	Absorber conductivity(copper)	390 W m^{-1} K^{-1}	
K_{pv}	PV cell conductivity	84 W m^{-1} K^{-1}	
$K_{g,pv}$	Glass conductivity	1.0 W m^{-1} K^{-1}	
K_{eva}	EVA conductivity	0.35 W m^{-1} K^{-1}	
K_b	Bond conductivity	1.15 W m^{-1} K^{-1}	
δ_{abs}	Thickness of the absorber	0.20 mm	
δ_{pv}	Thickness of PV cell	0.35 mm	
$\delta_{g,pv}$	Thickness of glass layer in lamination	3.2 mm	
δ_{eva}	Thickness of EVA layer	0.50 mm	
δ_b	Thickness of bond	0.01 m	
η_{rt}	Electrical efficiency at reference temperature	12.14%	
β_{PV}	Temperature coefficient of PV cell power generation	0.0045 $°C^{-1}$	

I	Irradiance	800 W m^{-1}	
V	Wind speed	1 m/s	3 m/s,5 m/s,7 m/s
t_a	Ambient temperature	20 °C	15, 17.5, 22.5, 25 ° C
t_{inlet}	Inlet temperature of the tube	20 °C	

Figure 4–6 shows the comparison between the published and simulated data of the BIPV systems electrical and thermal efficiency when changing the water inlet temperature from 15 to 25 °C, the comparison shows a very good agreement between the published and simulated outputs.

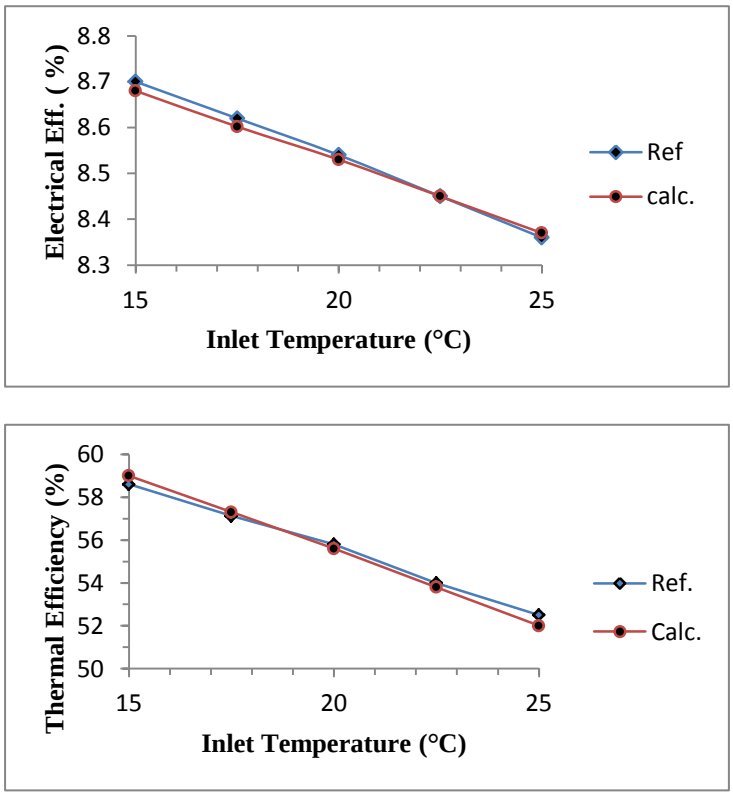

Figure 4–6: Comparison between the published and simulated data Inlet temperature – Electrical.& Thermal Efficiency correlations

Figure 4–7 also shows a good agreement between published and simulated outputs. The figure illustrates the comparison between the published and simulated data of the BIPV systems electrical and thermal efficiency with changing the wind speed from 1-7 m/s.

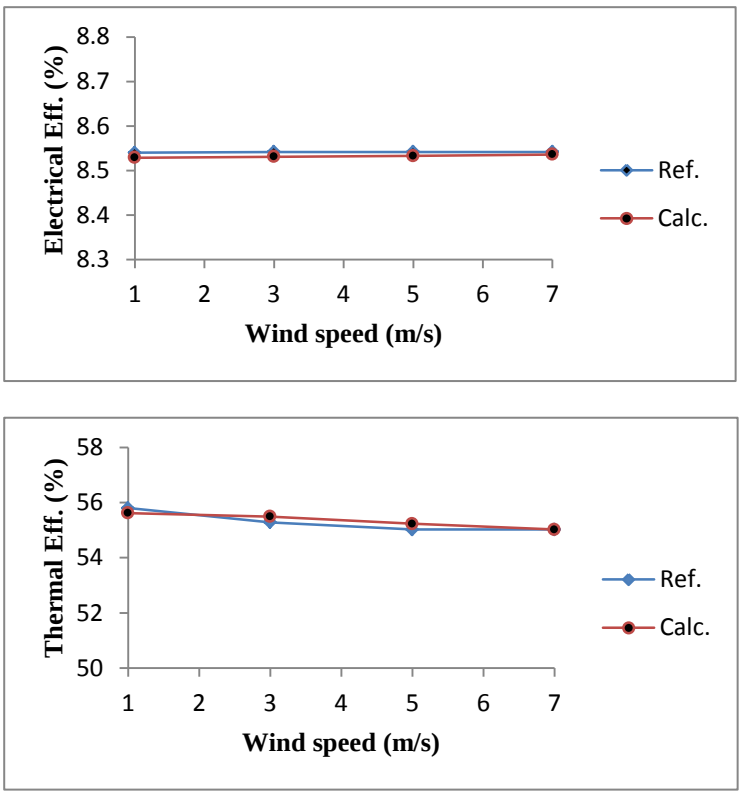

Figure 4–7:Comparison between published and simulated data
Wind speed - Electrical &Thermal Efficiency correlations

However, a slightly big difference appears in **Figure 4–8**, which shows the comparison between the published and simulated data of the BIPV systems with different ambient temperature, the biggest deviation, is on both electrical and thermal correlation at ambient temperature of 25 ºC. In electrical-ambient temperature correlation, the mean error is 0.14%, but the maximum error is 0.32%, which is at 25 ºC. In the thermal efficiency /ambient temperature comparison, the maximum error of 0.91% occurred at the same point 25 ºC, and mean error was 0.41%.

In spite of the deviation shown in **Figure 4–8** at 25 ºC, which is acceptable in PV/T engineering point of view, generally both data from the published paper and the module simulation showed a very good agreement, this indicates that the computer module

could successfully predict the operational performance of the module with satisfactory accuracy.

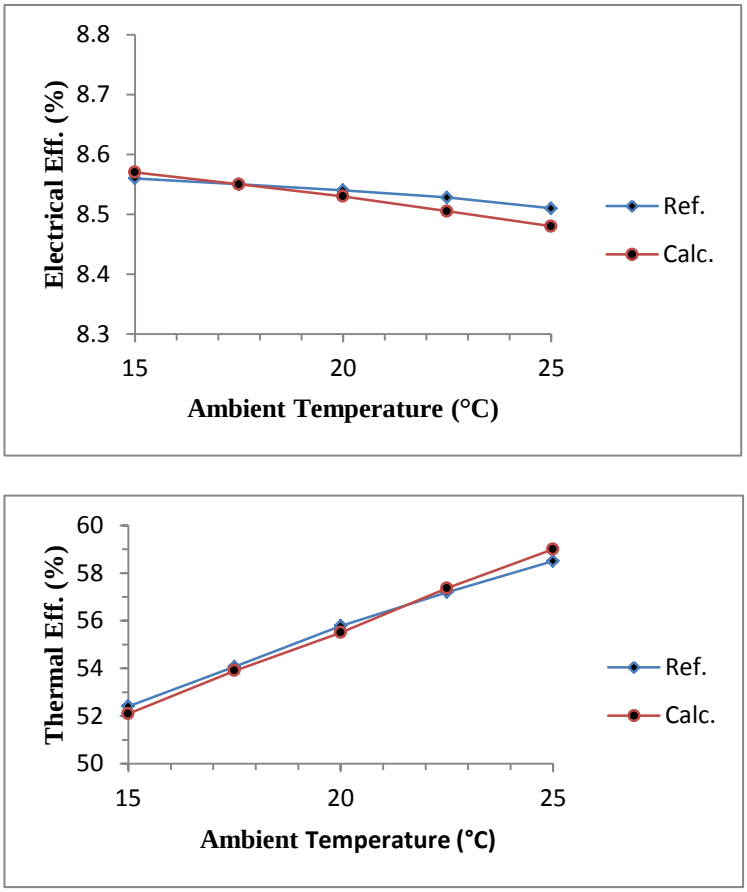

Figure 4–8:Comparison between published and simulated data Ambient temperature – Electrical & Thermal Efficiency correlations

4.5 Model Operation with MPCM-S and Result Discussion

The computer model was used to predict the performance of the PV/T module with MPCM-s as cooling fluid, toward the target of finding the problems associated with its operation in all aspects such as fluid flow, heat transfer and power generation. Also to validate the conceptual design of the rig to produce best electrical and thermal outputs. For that purpose, the influence of the main effective factors on the systems operation such as mass fraction of MPCM in the slurry, fluid flow state, and the serpentine pipe diameter should be investigated.

4.5.1 Effect of the MPCM mass fraction

The simulation was conducted with variable concentration of MPCM (0 %, 5%, 10%, 15%, and 20%). The following parameters were fixed: radiation 1000W/m^2, ambient temperature 20 ºC, wind speed 1 m/s and mass flow rate of 0.02kg/s. The **Figure 4–9** to **Figure 4–15** show the influence of MPCM mass fraction on the dynamic viscosity, PV temperature, serpentine piping's pressure drop, and the module's electrical, thermal, overall and net efficiencies.

Figure 4–9 and **Figure 4–10** show the direct effect of the MPCM mass concentration on the flow state of the slurry under a steady mass flow rate of 0.02kg/s. In **Figure 4–9** with increasing the mass concentration the dynamic viscosity is growing, especially after 10% it grows sharper, that led to the suppression of the desirable turbulent flow as illustrated in **Figure 4–10**, because with increasing the mass fraction the Reynolds number is falling, particularly when the concentration is more than 10% the slurry does not reach the turbulent flow condition, then lose the heat transfer enhancement advantage by the phase change. Therefore, the slurry with concentration up to 10% is more beneficial than greater concentration, because it is still in turbulent flow condition.

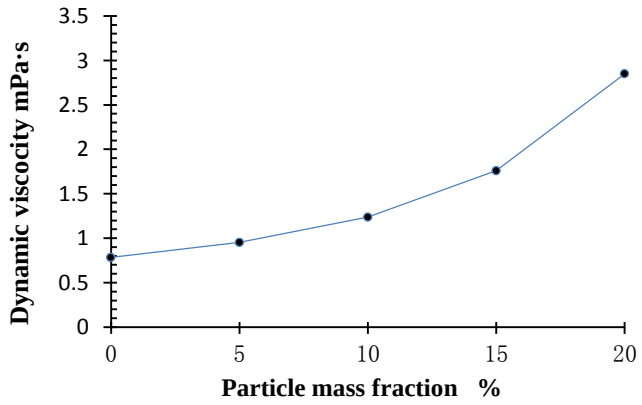

Figure 4–9: The dynamic viscosity - Particle mass fraction correlation

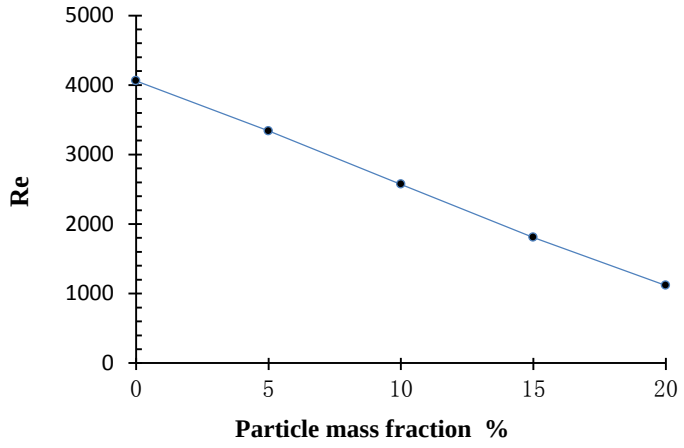

Figure 4–10: Reynolds number -Particle mass fraction correlation

The impact of the concentration on the PV temperature is shown in **Figure 4–11** as well, as known that the turbulent flow leads to a reduction in PV cell's temperature, due to the enhanced heat transfer capability that leads to higher heat absorption from the PV cells, and the slurry with a concentration exceeded 10% hardly reaches turbulent flow, consequently the cooling act gets weaker, leading to higher PV temperature with high concentration.

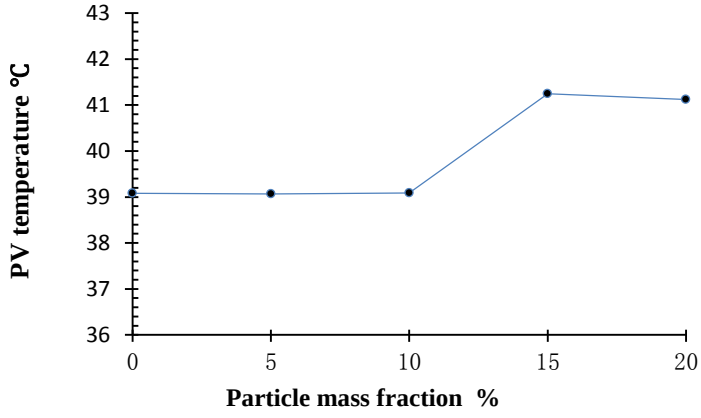

Figure 4–11: PV Temperature-particle mass fraction correlation

The reduction of heat transfer capability with concentration over 10% causes a reduction in electrical, thermal and overall efficiencies as illustrated in **Figure 4–12** ,

Figure 4–13 and **Figure 4–14** respectively. This reduction in the efficiencies is due to increasing the PV temperature for the slurry with concentration over 10%.

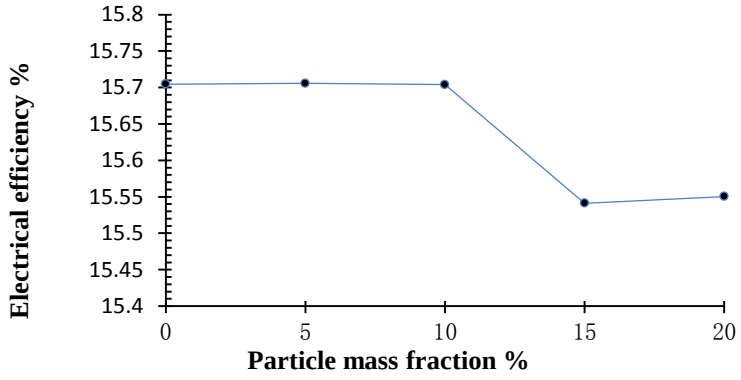

Figure 4–12: Electrical Efficiency -Particle mass fraction correlation

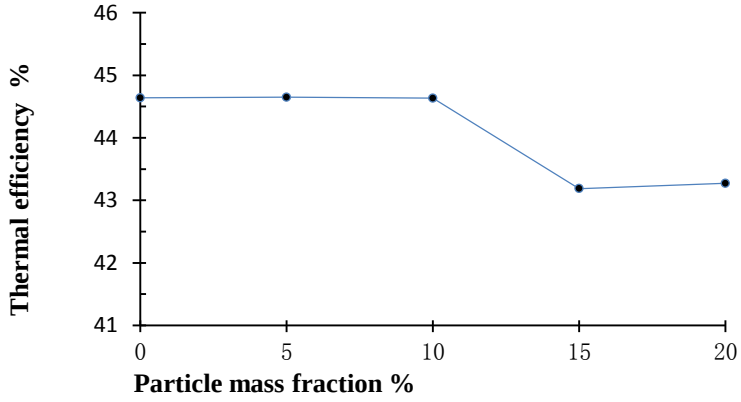

Figure 4–13: Thermal efficiency- Particle mass fraction correlation

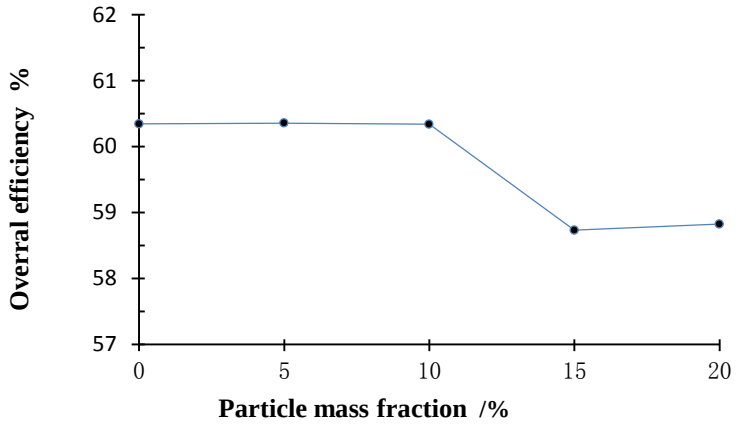

Figure 4–14: Overall efficiency- Particle mass fraction correlation

So generally, net efficiency reaches its highest level when the mass concentration is 10% and decreased with higher concentrations as shown in **Figure 4–15**. In case of fixed flowrate, higher concentrations do not reach turbulent flow state, then cause a higher-pressure drop, consequently reduce the net efficiency of the system, and this proves that the slurry over 10% is not viable.

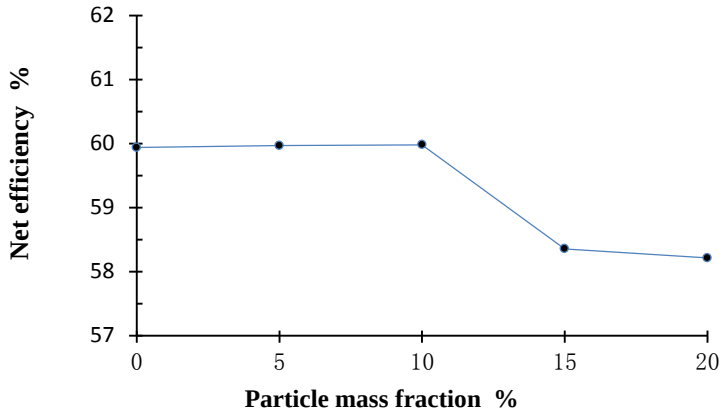

Figure 4–15: Net efficiency- Particle mass fraction correlation

4.5.2 Effect of the Reynolds number

The simulation was run with a number of fixed parameters such as radiation 1000W/m2, ambient temperature 20 ºC, fluid inlet temperature at 25℃, and wind speed 1 m/s. It was conducted with Reynolds numbers of 1800, 2600 and 3350 to analyse the output of changing the flow condition on the system operation. **Figure 4–16** to **Figure 4–21** show the influence of Reynolds number and MPCM mass concentration on the PV cell temperature, serpentine pipe pressure drop, and the electrical, thermal, overall and net efficiencies.

Figure 4–16 shows the decrease in the PV cell temperature with increasing both mass concentration and Reynolds number, at concentration 5% the PV temperature is 40 ºC with Reynolds number of 3350 (turbulent flow state), but it increases to 46 ºC with Reynolds number of 1800 (laminar flow state). That means the Reynolds number has a major effect on the performance of the system.

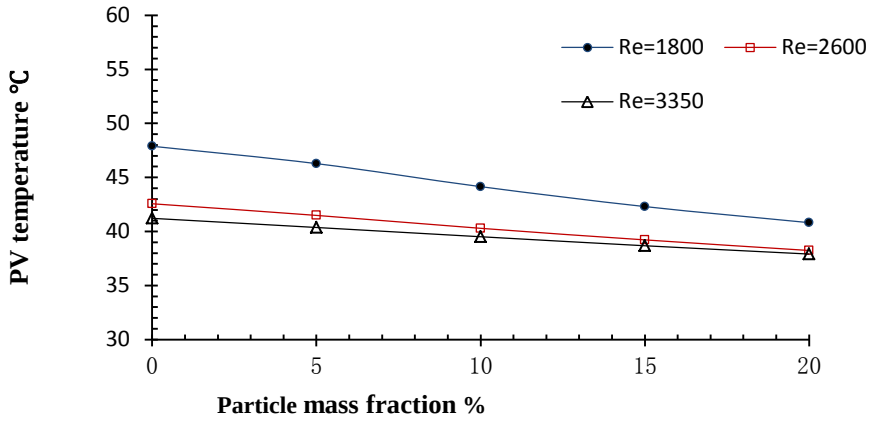

Figure 4–16: Impact of MPCM mass fraction and Reynolds number on PV temperature

The pressure drop trended upward with increasing the mass concentration and Reynolds number as shown in **Figure 4–17**. In case of 15% concentration and upward the pressure drop increase very sharply which put a limitation of the MPCM concentration percentage in the slurry that should not exceed 15% in any case. When the concentration is 5% the pressure drop increase with increasing Reynolds number, but this rate rise more with increasing the MPCM concentration of 10% and upward.

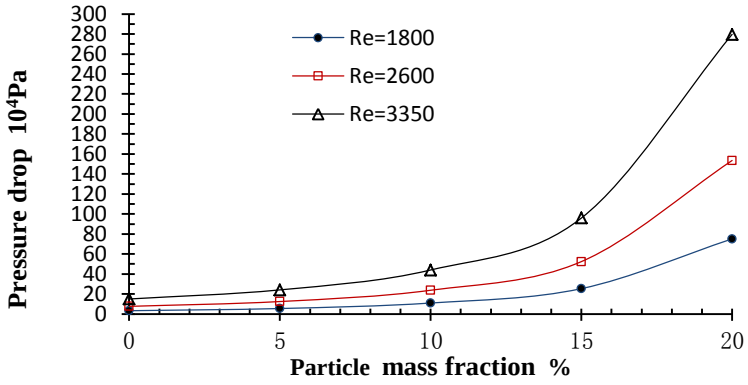

Figure 4–17: Impact of MPCM mass fraction and Reynolds number on Pressure drop

The electrical, thermal and overall efficiencies grew as shown in **Figure 4–18** to **Figure 4–20 .** The figures show that the enhancement of the efficiencies from Reynolds number of 1800 to 2600 is very high in comparison with the enhancement between

Reynolds number 2600 to 3350, especially at 5% and 10% concentration. **Figure 4–18** illustrates that in case of 5 % concentration, the electrical efficiency jumps from 15.1 % to 15.5% for Reynolds number from 1800 to 2600 respectively, but it slightly increase from 15.5% to 15.6 % from Reynolds number of 2600 to 3350. Therefor the outputs of Reynolds number 2600 and 3350 are very close and higher than the laminar flow state with Reynolds number of 1800.

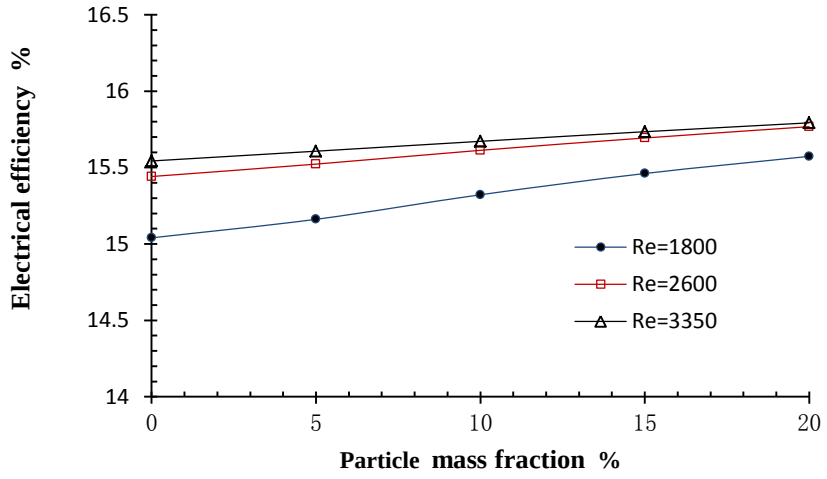

Figure 4–18: Impact of MPCM mass fraction and Reynolds number on Electrical efficiency

Figure 4–19 shows that the thermal efficiency rise with increasing Reynolds number, the enhancement decrease with higher particle mass fraction, thermal efficiency at 10% is 41.2%, and then it rises to 43.8 at Reynolds number of 2600, but it increases slightly to 44.3 with Reynolds number of 3350.

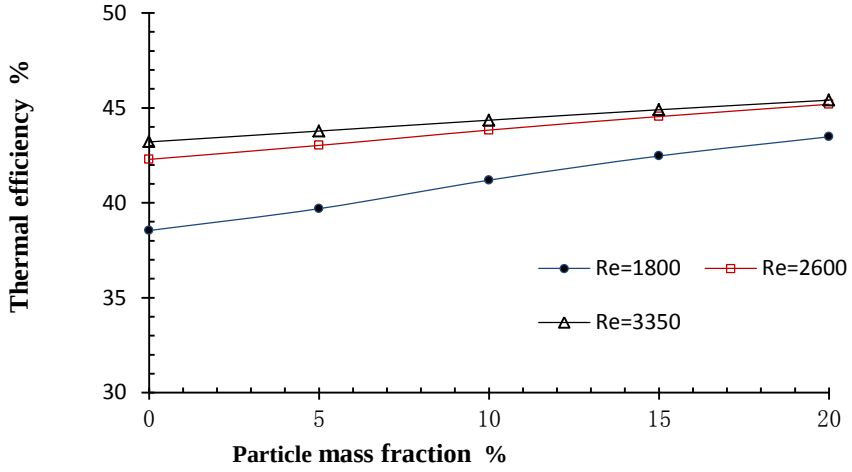

Figure 4–19: Impact of MPCM mass fraction and Reynolds number on Thermal efficiency

Overall efficiency consists of electrical and thermal efficiency, so it grows with higher Reynolds number and mass concentration as shown in **Figure 4–20**, and the enhancement of the efficiency is minor with the change from Reynolds number 2600 to 3350.

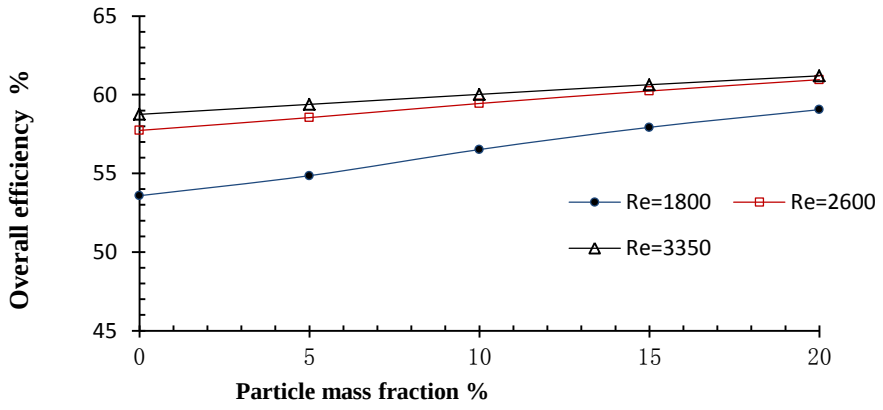

Figure 4–20: Impact of MPCM mass fraction and Reynolds number on Overall efficiency

Finally, the net efficiency for all three Reynolds number curves initially increased with raising the mass concentration, and then the sharp decline started afterward 15% concentration as illustrated in **Figure 4–21**. The best operational case is the one with highest net efficiency, this occurs at Reynolds number of 2600 and MPCM mass concentration of 10%, it achieves highest net efficiency of 58.9%, and electrical,

thermal, and overall efficiencies of 15.6%, 43.8% and 59.4% respectively. The second best operational condition is at concentration of 5% and Reynolds number of 3350 that achieves the net efficiency of 58.8%. Both cases are very similar, they both could be considered as the best operational condition, and choosing one of them depends on the application conditions.

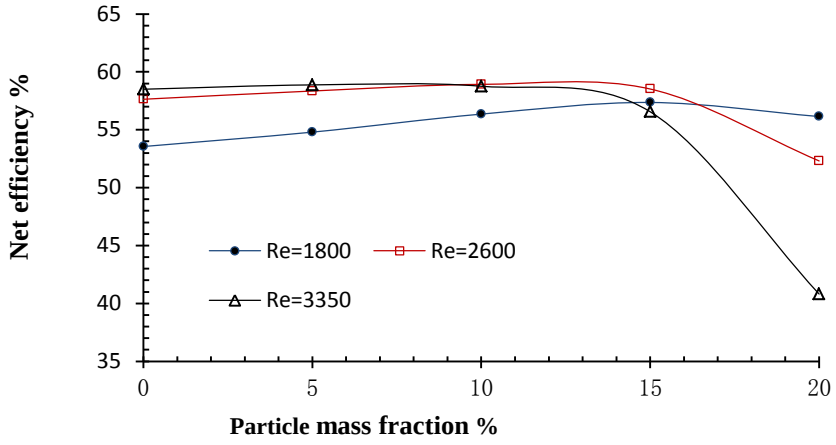

Figure 4–21: Impact of MPCM mass fraction and Reynolds number on Net efficiency

4.5.3 Effect of the serpentine piping size

The simulation was run with a number of fixed parameters such as radiation 1000W/m2, ambient temperature 20 ºC, fluid inlet temperature at 25℃, wind speed 1 m/s, and Reynolds number of 3350. It was conducted with concentration of (0-20) % and three different internal diameters of the serpentine pipe (6, 7, and 8) mm. **Figure 4–22** to **Figure 4–27** explain the impact of changing the MPCM mass fraction and the serpentine pipe diameter on the PV cells temperature, serpentine pipe pressure drop, and (electrical, thermal, overall and net) efficiencies.

Figure 4–22 shows that for all three different diameters, the PV cell temperature decrease with increasing the MPCM mass concentration and showed that increasing diameter enhance the cooling of the PV cell. In case of 10% MPCM mass concentration PV temperature of 6mm, 7mm, and 8mm pipe diameter are 41°C, 39.5 °C and 38°C respectively.

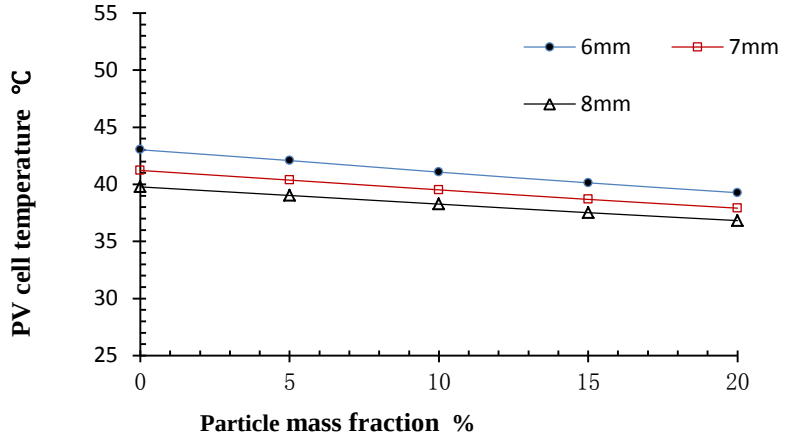

Figure 4–22: Impact of MPCM mass fraction and internal diameter of the pipe on PV cell temperature

Figure 4–23 illustrates the growing of the pressure drop with increasing the MPCM mass concentration for all three different diameter cases, at the same time if they compared, the biggest diameter (8 mm) shows the lowest pressure drop along all points. The lowest pressure drop of $165227*10^4$ Pa occurs at 8mm with slurry 5% MPCM concentration, this pressure drop increase with minimizing the pipe diameter, it is $241014*10^{4\ Pa}$ and $369523*10^4$ Pa for 7mm and 6mm diameters respectively.

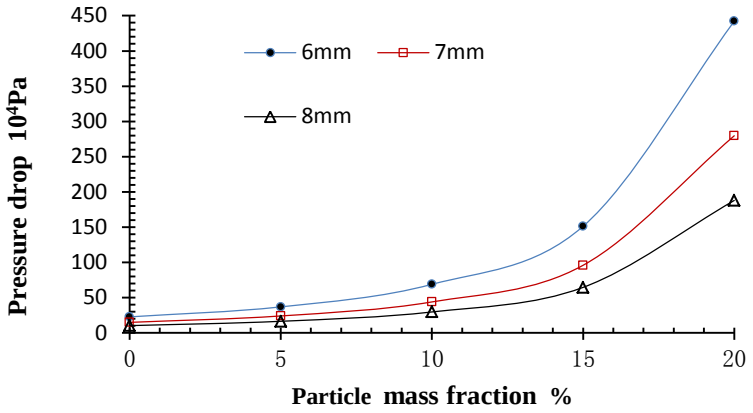

Figure 4–23: Impact of MPCM mass fraction and internal diameter of the pipe on pressure drop

Figure 4–24 to **Figure 4–26,** the electrical, thermal and overall efficiency increase as the concentration grows, so the output of the biggest diameter (8 mm) represents the highest efficiencies. In case of 10% particle concentration slurry and 8 mm pipe diameter, the electrical, thermal and overall efficiencies are 15.7%, 45.2% and 60.9% respectively.

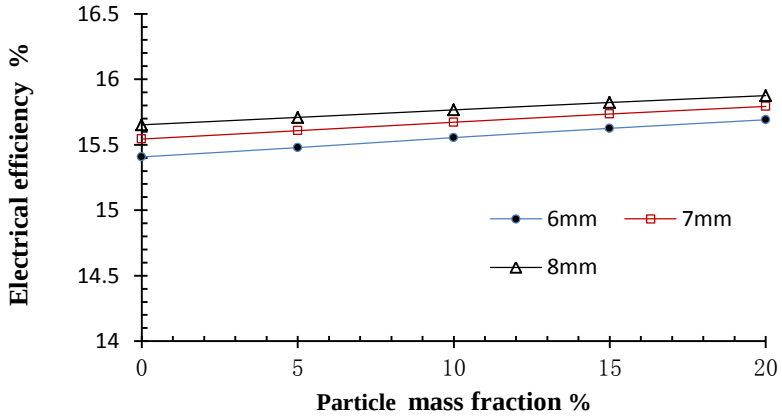

Figure 4–24: Impact of MPCM mass fraction and internal diameter of the pipe on electrical efficiency

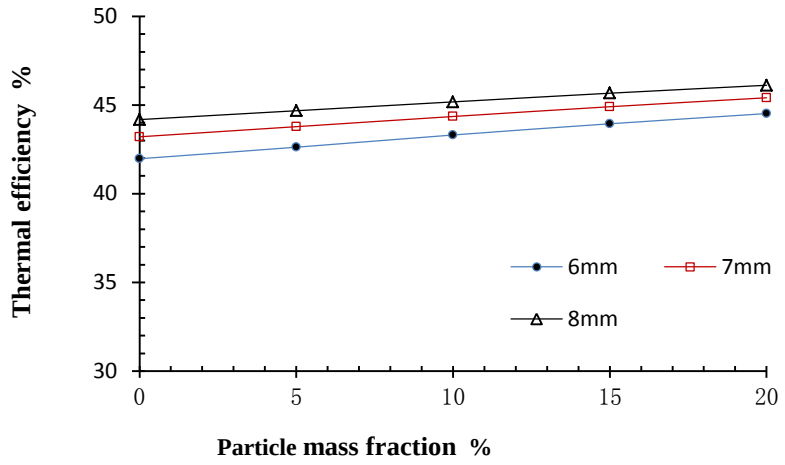

Figure 4–25: Impact of MPCM mass fraction and internal diameter of the pipe on thermal efficiency

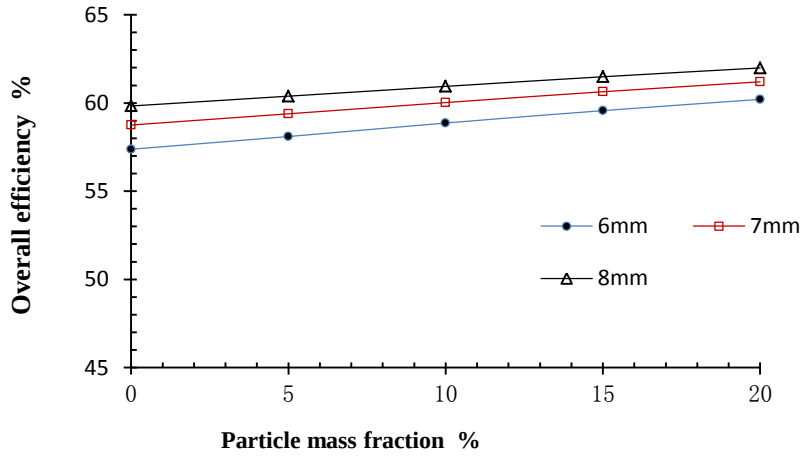

Figure 4–26: Impact of MPCM mass fraction and Internal diameter of the pipe overall efficiency

The larger diameter represents a better cooling at the same MPCM concentration case, which leads to higher electrical, thermal, overall and net efficiency. The net efficiency at the beginning grew with the increase in the MPCM concentration as shown in **Figure 4–27**, and after the mass concentration of 15%, the net efficiency decreased sharply because, at the same mass flowrate or Reynolds number, rising concentration means more electrical consumption consequently lower net efficiency.

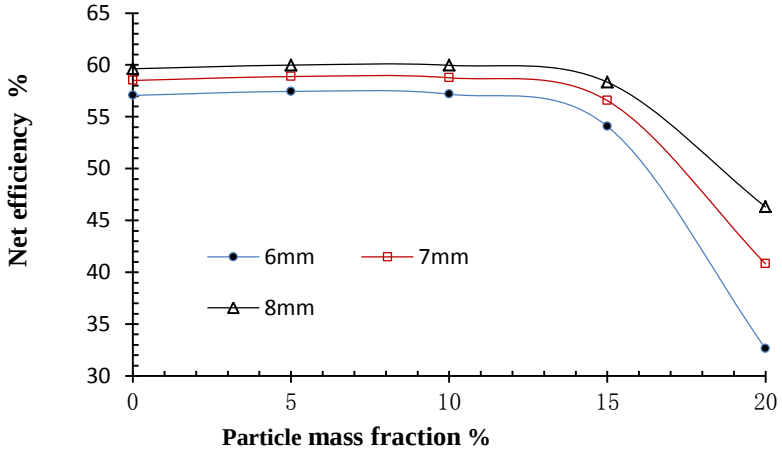

Figure 4–27: Impact of MPCM mass fraction and Internal diameter of the pipe on net efficiency

4.6 Chapter Summery

This chapter addressed the simulation model development and operation that is aimed to analyse the power generation, heat transfer and fluid flow problems occurring in various parts of the system, including PV/T module, heat exchanger and PCM. The validation of the simulation model was conducted using the experimental data of a previous study. The computerized module was run under specific operational conditions with concentrations of MPCM (0 %, 5%, 10%, 15%, and 20%) to test its influence on the performance of the system. The result showed the direct effect of the MPCM concentration on the flow condition of the slurry. The increase of the viscosity obstructs the slurry to reach the turbulent state of the concentration over 10% that means it stays in laminar flow state and then loses the heat transfer enhancement advantage by the phase change. Therefore, the slurry with concentration up to 10% is more beneficial than greater concentration. In addition, the increase of the concentration over 10% causes a sudden pressure drop in the serpentine pipe, which increases the input electricity demand for the circulation pump.

To verify the impact of the flow state on the performance of the system, the computerised module conducted under a specific operation condition with three different Reynolds number values of 1800, 2600 and 3350. The results showed that with increasing both MPCM concentration in the slurry and Reynolds number together, the PV module temperature decreases, and electrical, thermal and overall efficiency increase, but also the pressure

drop increase, which puts a limitation on the MPCM concentration percentage in the slurry. The best operational case with the highest net efficiency occurs at Reynolds number of 2600 and MPCM mass concentration of 10%, it achieves highest net efficiency of 58.9%, and electrical, thermal and overall efficiency in this case are 15.6%, 43.8%, 59.4% respectively.

For finding the optimum diameter for the serpentine pipe the simulation was run under a specific condition with three different internal pipe diameters of 6, 7 and 8 mm. The impact of changing the MPCM percentage and pipe diameter on PV cells temperature, serpentine pipe pressure drop, and electrical and thermal efficiencies were investigated. It concluded that increasing diameter enhanced the cooling of the PV cell, as a result the electrical, thermal and overall efficiencies increase as the concentration grows, so the biggest diameter gives the highest efficiencies. The smallest pressure drop occurs at the biggest diameter, as would be expected. Therefore, the diameter of 8mm represents the better output of the system performance, but the cost of larger diameter should be taken into consideration, as the financial part is the key point of any project.

CHAPTER 5: EXPERIMENTAL PERFORMANCE UNDER LABORATORY CONDITIONS

5.1 The experimental rig set up and test procedure

5.1.1 System assembly and connections

The system consists of two circulation cycles, MPCM –S cycle and refrigerant cycle (heat pump) as shown in **Figure 5–1** . In the refrigerant cycle, the heat pump employed an 1100 W-rated oversized compressor charged with environmentally friendly R134a refrigerant, the compressor was oversized because the heat pump was already available in the laboratory, and it should be considered later in system energy and COP calculations. A 200 litters cylinder water tank with built-in copper heat exchanging coils acts as the condenser and hot water storage for the heat pump cycle. Several insulation materials including polystyrene board for exchanger and the foam polyurethane for piping were used to reduce the heat loss of the system components. Some measurement sensors like thermocouples and flow meters were placed in the heat pump cycle and were connected to the data logger by some connection wires. All the instruments and sensors used in the experiment are outlined in **Table 3-6** and pictures of the rig are shown in **Figure 5–2**.

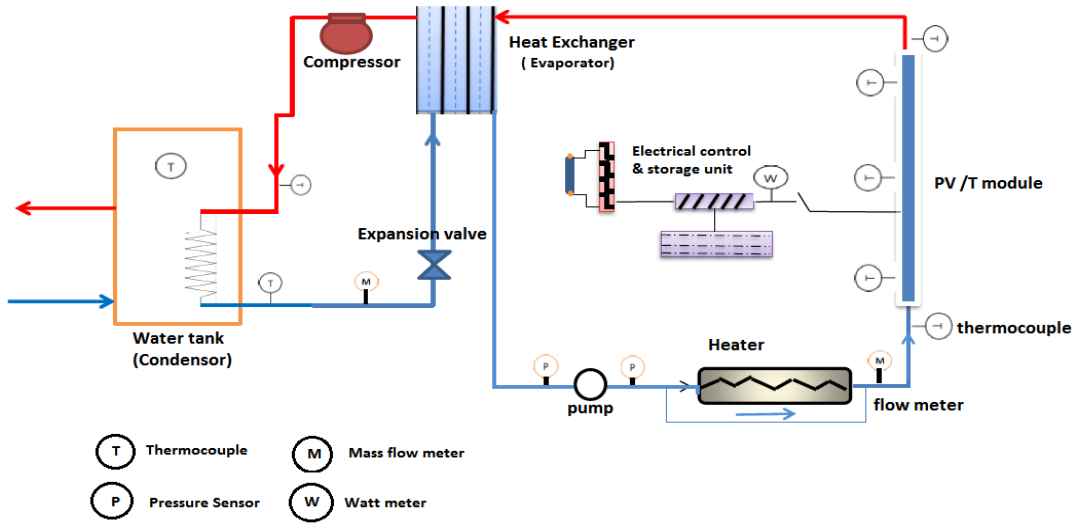

Figure 5–1: The experiment rig

The MPCM-S circulating cycle consists of a PV/T module (0.8m x1.6m) was fixed on a vertical frame, with 15 T type thermocouples placed on the back of the baseboard and connected to the data logger board by some connection wires. A water pump was placed in this part of the system for circulating the slurry, 13 mm flexible pipe was used for the connections in between the parts of this cycle. A re-heater was used for the regulation of the inlet temperature of the slurry. The electrical control and storage unit was placed next to the PV module to control the electrical output, convert DC to AC and store it in the battery. The slurry and refrigerant circuits are thermally connected by a flat plate heat exchanger that cools down the MPCM-S and represents the evaporator of the heat pump.

Some more sensors were located in the system, like two pressure transmitters were located on the outlet and inlet of the module for measuring the pressure drop in the system, two turbine type flow meters were placed on the inlet and outlet of the module, a wattmeter to measure the electrical outcome and a pyranometer (radiation sensor) was placed on the bracket of the module to measure the intensity of the radiation from the simulators. These entire sensors were connected to the data logger block, each by a specific kind of wire, connection function and electrical circuit. Because the experiments were running under the laboratory condition, so two 4000 W simulator as shown in **Figure 5–2** were placed on two iron and vertically movable shelves which were opposite of the module, generating and directing a vertical radiation onto the module. For controlling the intensity of the radiation for the experiments, an electrical control board was used. Finally, for data collection a data logger was used to collect data from sensors and transfer them to a computer.

The MPCM-S is a very important part that gives the novelty to the system, and was prepared in the laboratory as mentioned in detail in chapter 3. For measuring the properties of the slurry used, a rheometer was used to measure the viscosity of different MPCM concentration slurries (5%, 10%, and 15%) and a particle analyser was used to measure the particles diameter.

Connecting the sensors to the system and the data logger consumed lots of time, because each of them had a specific kind of wire, connection function and electrical circuit, thus frequently contacting the manufacturer of the sensors was required to set it

to give the proper outcome. Two data loggers have been operated with two different software, the first was available in the laboratory, it worked at the beginning with some sensors but later it has been changed because it was not very accurate and its board did not have enough points for all the sensors.

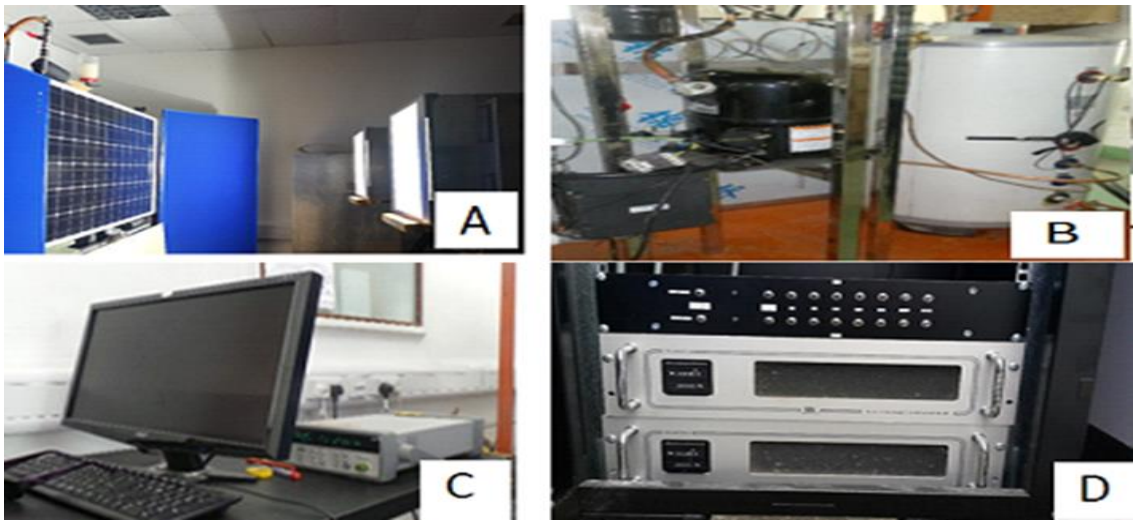

Figure 5–2: Experimental Rigs Components. (A) PV/T module facing two simulators, (B) Compressor and condenser, (C) Data logger, (D) Irradiation control board

5.1.2 The experimental procedure

The experiments were carried out in a laboratory of Hull University from (10 June - 12 July) 2014 in collaboration with a research team. Tests were run under steady state condition, which is more difficult than the dynamic condition tests because several parameters need to be unchanged. At each experiment, most parameters should be fixed while testing the impact of a particular changeable parameter. Three set of tests was carried out as listed in **Table 5-1**, the main parameters measured during the test were temperature, solar irradiation, pressure, power and flow rate by several sensors located in the system. To get useful data the system should be at steady state condition at least for 15 minutes. Each test took hours to achieve a steady state condition. The attained data were recorded via the data logger at 10 seconds intervals.

These three sets of experiments were run after a few months of testing the rig and its outputs, meaning before the mentioned three set of tests, the system ran for over a month with different parameters. But these three set of tests were run to examine the

effect of the solar radiation, MPCM-S flow condition which depends on Reynolds number, and the MPCM-S concentration as illustrated in **Table 5-1**

Table 5-1: Three sets of experimental operational parameters

	I, W/m^2	***Re***	***W, %***	***T_a, ℃***	***T_i, ℃***
Test 1	(500 – 900) ±5	2910	10	29.5 (±1)	24.75 (±0.5)
Test 2	600	1508 - 3496	10	29.5 (±1)	24.75 (±0.5)
Test 3	700	3000	0 - 15	29.5 (±1)	24.75 (±0.5)

Many operational and technical difficulties were faced during testing the rig. To achieve steady state, the experiments took longer time than the dynamic outdoor tests, also more monitoring was required. The oversized compressor caused a big problem, because the cooling output of the heat pump was higher than needed, thus the slurry at the inlet to the module reached very low temperatures, sometimes as low as 15 ºC. This was not acceptable for the cooling medium of the module (MPCM-S), the temperature should be a few degrees lower than its melting point (28ºC), to guarantee melting while passing through the serpentine pipe. For this reason, serpentine pipe has been chosen not the parallel pipes. After few ideas to maintain the inlet temperature, a pre-heater has been used to regulate the inlet temperature of the slurry.

The turbine type flow meter caused major problems during the tests, especially with 10% and 15% MPCM concentration slurry, due to the blockage of the little turbine inside the flow meter by clotting the microcapsules between the fins, this was shown on the computer when the flow rate was zero while the rig was working. To solve this, the reverse flow rate for few seconds was used, but it was interrupting the constancy of the tests, consequently consuming more time.

5.2 Experimental results

The experiments were run in the laboratory of Hull University in corporation with a research team to investigate the real performance of the energy system that was

predicted by developing a computer simulation module. The data and information provided by running the test is more reliable than the predicted once, and the latter could be validated depending on the results from the experiments. Some more calculation and analyses were done and added to the big data sheets from the tests, to calculate the efficiencies and the uncertainty of the experimental data. The thermal efficiency expressed as:

$$\eta_{th} = \frac{Q_{th}}{IA} \tag{5-1}$$

The electrical efficiency is defined as:

$$\eta_{e} = \frac{Q_{e}}{IA} \tag{5-2}$$

Then the net efficiency could be calculated as the sum of the thermal and electrical efficiency, with consideration of the power used for running the pump:

$$\eta_{net} = \eta_{e} + \eta_{th} - \frac{Q_{pump}}{IA} \tag{5-3}$$

To find the uncertainty of the experimental data, the standard deviation need to be calculated by:

$$S_{e=} \sqrt{\frac{1}{n}\sum_{i=1}^{n}\left(x_{e,i} - \bar{x}_{e}\right)^{2}} \tag{5-4}$$

Where; n: the number of experiments implemented; xe is the experimental and value, respectively; $\overline{xe}$: the arithmetic mean experimental value. Se: the standard deviation of the groups of testing results during each testing mode.

Then the uncertainty is expressed as:

$$U = \frac{S_e}{\bar{x}_e} \tag{5-5}$$

Figure 5–3 to **Figure 5–17** illustrate impact of the radiation (I), the slurry flow state (Re) and the MPCM concentration in the slurry (MPCM%) on the performance of the PV/T system, these records delivered by running three sets of test as shown in **Table 5-1.**

(a)Impact of solar radiation: By varying the solar radiation from 500 to 900 W/m^2, with remaining other parameters such as (Re 2910, MPCM concentration 10%, slurry inlet temperature 24.5 °C, and ambient temperature 29.5°C), the Test 1 was run to indicate the impact of the intense of the solar radiation on the performance of the PV/T module and its main parameters like (electrical and thermal output, backplane temperature, pressure drop, and net efficiency of the module).

Figure 5–3 and **Figure 5–4** showed that the electrical and thermal outputs of the system increases with higher radiation from 500 W/m^2 to 900 W/m^2, which led to a significant increase in the electrical output from 91.6 - 157.0 W and in its heat output from 448.5-743.3 W. The uncertainty is in an acceptable rate, which does not exceed 3.9%.

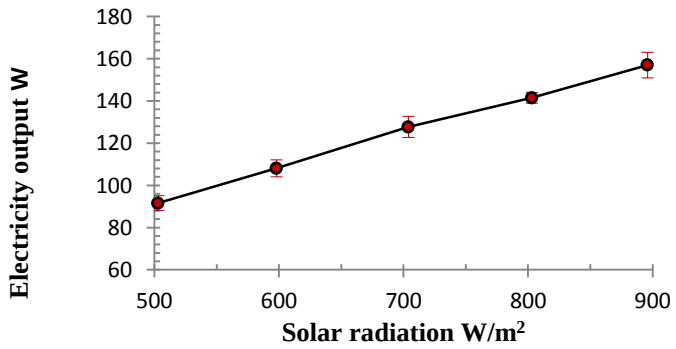

Figure 5–3: Impact of solar radiation on electrical output, %, Umax= 3.9%, $\bar{U} = 3.4\%$

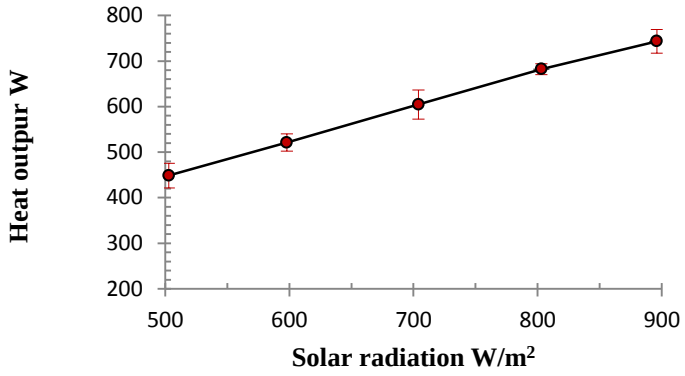

Figure 5–4: Impact of solar radiation on heat output, Umax= 6%, $\bar{U} = 4\%$

Meanwhile, the growth of the PV cell temperature with the same radiation change rate (500-900 W/m^2) is about 5 ºC, which is small for that high change rate of radiation, this because of the phase change materials impact that enhance the heat transfer performance of the cooling medium as shown in **Figure 5–5**.The maximum uncertainty is 3.3%.

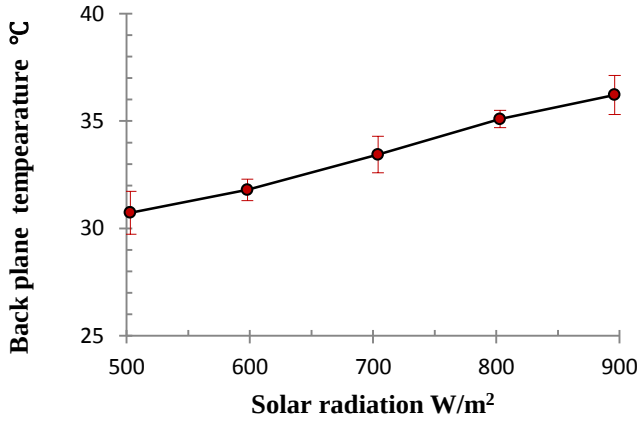

Figure 5–5: Impact of solar radiation on backplane temperature, Umax= 3.3%, $\bar{U} = 2.2\%$

The impact of growing the radiation on the pressure drop of the slurry flow in the serpentine pipe is illustrated in **Figure 5–6**, the pressure drop decreased with increasing the radiation, which indicates to lower viscosity with higher temperature, so decreasing the flow resistance of the slurry. The downward trend of the pressure drop is sharper

with the radiation between 500-600 W/m^2. The maximum uncertainty is 11.4%, it is relatively high,

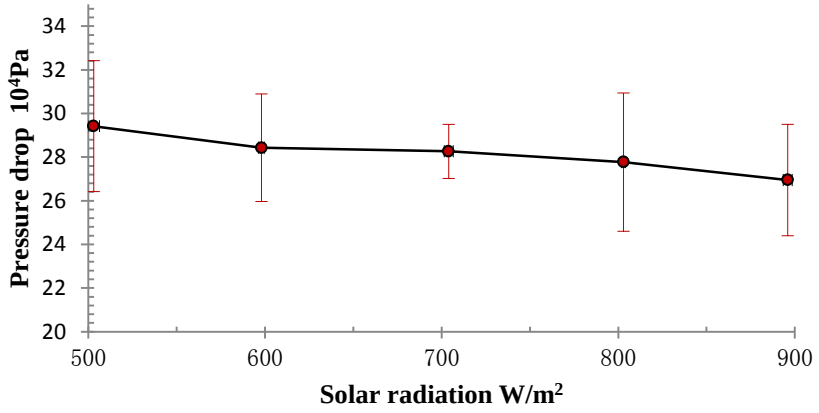

Figure 5–6: Impact of solar radiation on pressure drop, Umax= 11.4%, $\bar{U} = 8.8\%$

The net efficiency decreased smoothly from 83.9-78.5% with increasing radiation from 500-900W/ m^2 as shown in **Figure 5–7**. Rising the solar radiation result in an increase in temperature and a decrease in efficiency. The graph shows the highest maximum uncertainty of 12.4%.

For all tests the mean uncertainty Ratio ($\bar{U}$) and maximum uncertainty ratio (Umax) were calculated to check the experimental data. **Figure 5–3** to **Figure 5–7** showed that the mean uncertainty Ratio ($\bar{U}$) were in the range of 2.2 - 10.6%, and the maximum uncertainty ratio (Umax) were in the range of 3.3–12.4%. In some cases the uncertainty is high, it possibly caused by a number of fluctuated parameters including air temperature, electrical voltage imposed on the compressor and pump, the slurry flow rate, as well as set-up of the sensors and thermocouples. The uncertainty depends on the number of experimental implementation as well.

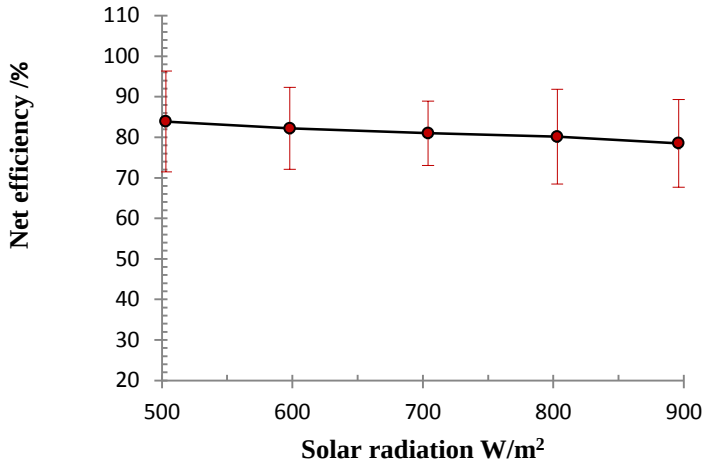

Figure 5–7: Impact of solar radiation on net efficiency, Umax= 12.4%, $\bar{U} = 10.6\%$

(b)Impact of the slurry flow condition (Reynolds number): By changing the Reynolds number which represents the flow state of the slurry from 1508 to 3496 with remaining other parameters such as (MPCM concentration 10%, Radiation 600W/$m^{2,}$ slurry inlet temperature 24.5 °C, and ambient temperature 29.5°C). Test 2 was run to indicate the impact of the change of the flow condition on the performance of the PV/T module and its main parameters like (electrical and thermal output, backplane temperature, pressure drop, and net efficiency of the module).

The impact of the Reynolds number on the electrical and thermal output was investigated, and as shown in **Figure 5–8** and **Figure 5–9**, with increasing the Reynolds number from 1508 to 3496, both electrical and thermal output were grown from (103-109 W) and (460 - 528 W) respectively, this indicates to the enhanced heat transfer with trending toward turbulent flow condition. The maximum uncertainty are in the acceptable rate of 3.3% and 4.7% in figures of electricity and thermal relation with Reynolds number respectively.

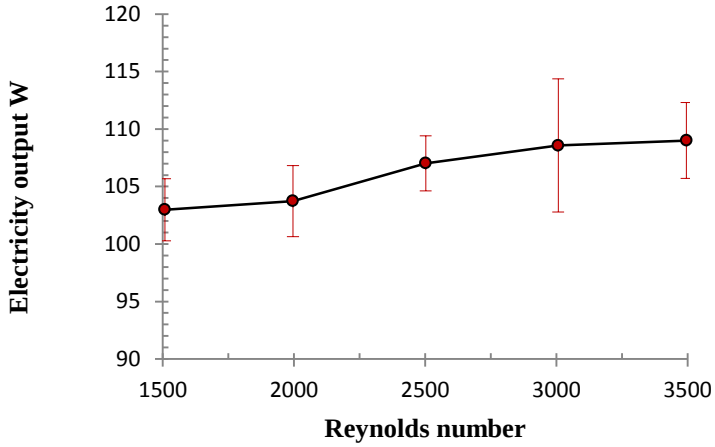

Figure 5–8: Impact of Reynolds number on electrical output, U max= 3.3%, $\bar{U} = 2.8\%$

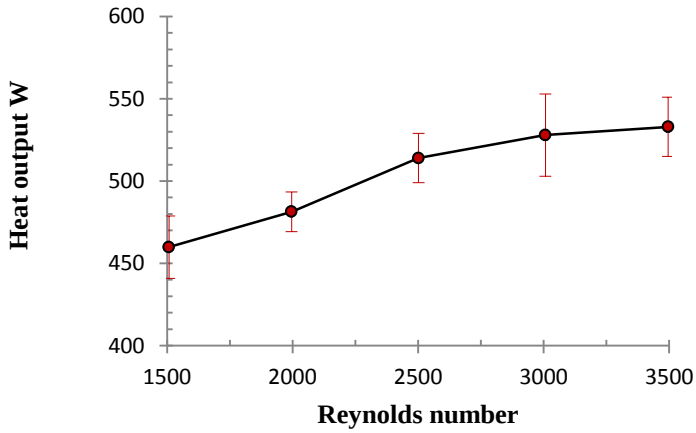

Figure 5–9: Impact of Reynolds number on heat output, U max= 4.7%, $\bar{U} = 3.5\%$

The growth of the Reynolds number reflected on the backplane temperature as illustrated in **Figure 5–10**, it led to more cooling effectiveness, as the backplane temperature trend is downward with increasing the Reynolds number. As the backplane temperature is 37°C when the Reynolds number is 1500(laminar flow state), then decreased to 32 °C with Reynolds number of 3500 (turbulent flow state). Maximum uncertainty is 4.5%.

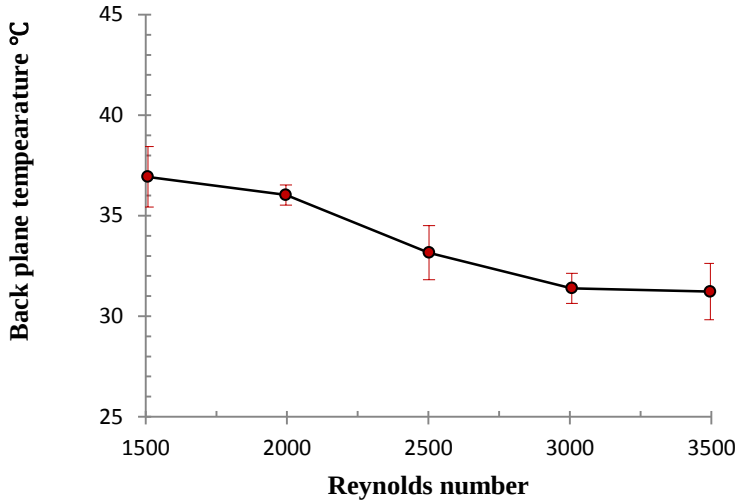

Figure 5–10: Impact of Reynolds number on backplane temperature, U max= 4.5%, $\bar{U} = 3.3\%$

The pressure drop increased with growing the Reynolds number, and the growth getting sharper with increasing the Reynolds number after the value of 2000 as shown in **Figure 5–11**. In case of Reynolds number 1500 the pressure drop is 80906 * 10^4 Pa and it increase to 445193 * 10^4 Pa. The maximum uncertainty is 11.9%.

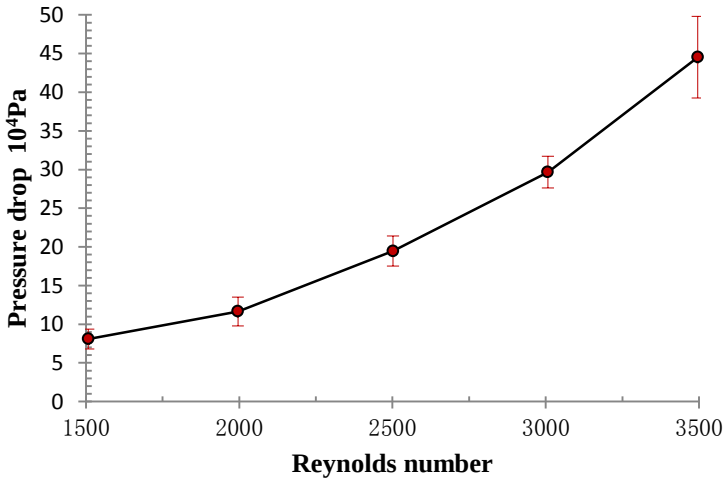

Figure 5–11: Impact of Reynolds number on Pressure drop, U max= 11.9%, $\bar{U} = 8.2\%$

As the cooling of the PV cells was enhanced with increasing the Reynold number, so it is expected that the PV/T module get higher net efficiency when the Reynolds number growing, this was proved in **Figure 5–12**. However, the net efficiency growth stopped at the Reynolds number of 3000 with a value of 81.6% and trended slightly downward to reach 81.3% at Reynolds number of 3500. This happened when the Reynolds number grew to a certain level around 3000, a sudden flow growth occurred in the serpentine pipe, which led to an apparent flow resistance, consequently the power consumption for the pump raised, that led to decreasing the net efficiency after the Reynolds number of 3000.The Maximum uncertainty is relatively high 12.7%.

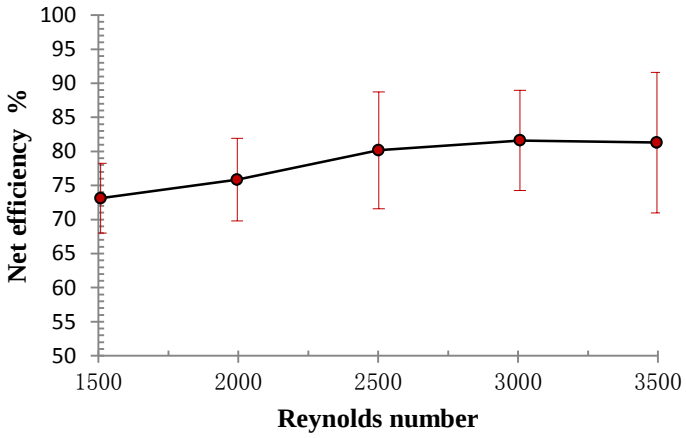

Figure 5–12: Impact of Reynolds number on net efficiency, U max= 12.7%, $\bar{U} = 9.6\%$

Besides the performance of the PV/T system, **Figure 5–8** to **Figure 5–12** also illustrated the maximum and average uncertainty, they showed that the mean uncertainty Ratio ($\bar{U}$) were in the range of 2.8-9.6 % and the maximum uncertainty ratio (U max) were in the range of 3.3- 12.7%. In some cases, the maximum uncertainty is in an acceptable range. However in few cases, it exceeds 10%, it could be a result of difference of the reading due to the varied parameters or uncertainty in measurement, as well as the number of the experimental implementations.

(c)Impact of the MPCM concentration

By changing the MPCM concentration of the slurry from (0-15%) with remaining other parameters such as (Reynolds number 3000, Radiation 700W/$m^{2,}$ slurry inlet temperature 24.5 °C, and ambient temperature 29.5°C), the Test 3 was run to indicate the impact of the MPCM concentration on the performance of the PV/T module and its main parameters like (electrical and thermal output, backplane temperature, pressure drop, and net efficiency of the module).

Figure 5–13 and **Figure 5–14** show that with increasing the MPCM concentration, both electrical and heat output increased, with a very slight increase from concentration 10% to 15%, which indicates to the minor positive effect of the slurry over 10% concentration of MPCM. Maximum uncertainty is a good rate of 2% and 5.4% for both mentioned figures respectively.

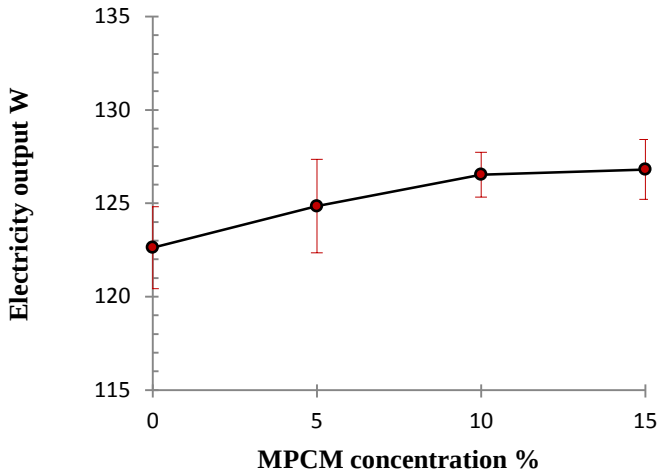

Figure 5–13: Electrical output as a function of MPCM concentration, U max = 2.0%, $\bar{U}$ =1.5%.

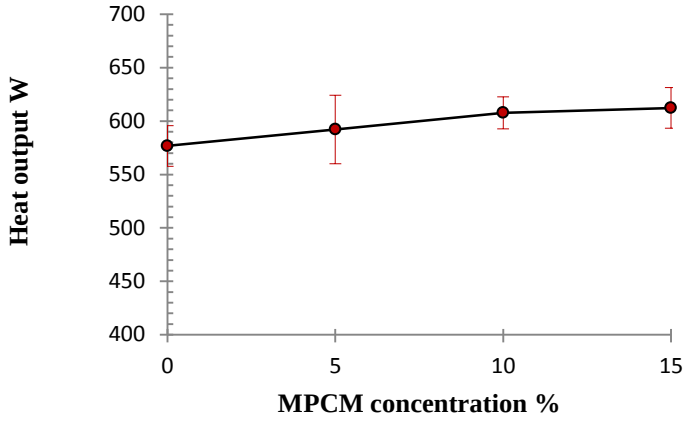

Figure 5–14: Heat output as a function of MPCM concentration, U max= 5.4%, $\bar{U} = 3.6\%$

Figure 5–15 illustrates that when the MPCM concentration grew, the backplane temperature decreased, again with slightly decrease in temperature with the concentration of 10 to 15%. The temperature decreased because of the enhancement of heat transfer with increasing the MPCM rate in the slurry, and then this improvement slows down with the concentration of over 10%. The maximum uncertainty is 4.8%.

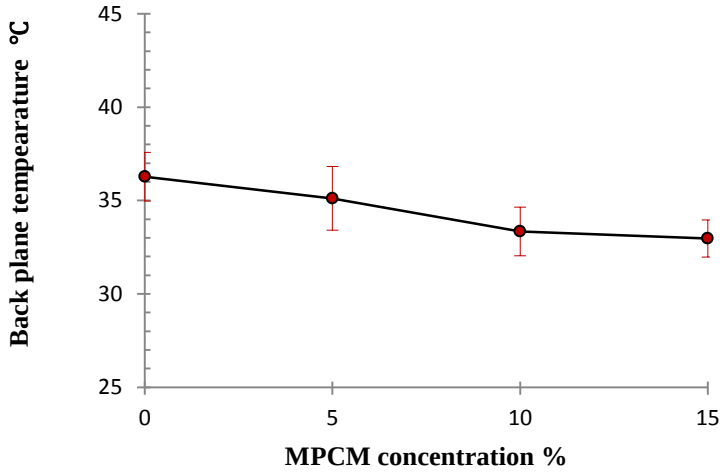

Figure 5–15: Backplane temperature as a function of MPCM concentration, U max= 4.8%, $\bar{U} = 3.8\%$

The pressure drop of the slurry flow in the serpentine pipe raised with growing the MPCM concentration as seen in **Figure 5–16**, but it increased very rapidly from the concentration 10 -15 % as it jumped from 29.6 x 10^{4}Pa to 81.4 x 10^{4}Pa respectively.

The high viscosity of the slurry over 10% led to the high rate of pressure drop. This rapid increase in the pressure drop causes a struggle of the slurry flow, and then it diminishes the benefit of increasing the MPCM concentration. The maximum uncertainty is high 11.6%.

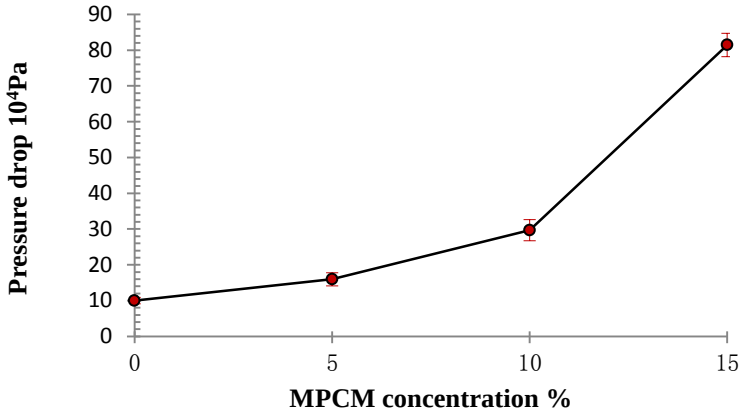

Figure 5–16: Pressure drop as a function of MPCM concentration%, U max= 11.6%, $\bar{U} = 8.6\%$.

Figure 5–17 illustrates the increase in net efficiency with increasing the MPCM concentration and it reached the highest value of 80.8% with the concentration of 10%, later that it trended downward to reach 78.18 when the concentration is 15 %. However, the highest net efficiency is at 10% concentration, but it has a good value of 79.58% at 5% concentration, with a slight difference of 1.2%.

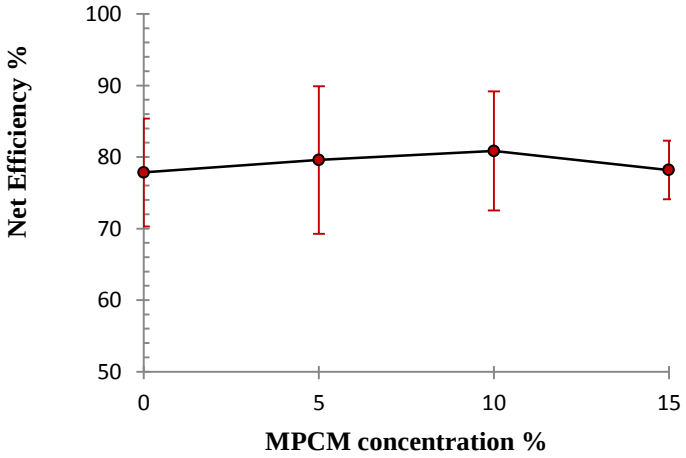

Figure 5–17: Net Efficiency as a function of MPCM concentration, U max= 13%, $\bar{U} = 7.6\%$

By investigating **Figure 5–13** to **Figure 5–17**, it could summarize that the 10% is the perfect concentration with the best output. The figures also show the maximum and average uncertainty, the mean uncertainty Ratio ($\bar{U}$) were in the range of 1.5-8.6% and the maximum uncertainty ratio (U max) were in the range of 2 – 13 %. The uncertainty over 10% is relatively high, due to some parameters such as uncertainty in measurement and the number of the experimental implementations.

5.3 Comparison with Simulation

To enable a comparison between the simulation (MPCM-S as a cooling fluid) and experimental results, the computer model was validated and run at the same conditions of the experimental tests. Then several sets of results were created to be compared with the experimental results in section **5.2** , this to investigate the accuracy of the simulation model as well as the root mean square percentage error (RMSPE) to identify the discrepancy between the simulation and experimental results.

The computer simulation should be run under the same operational condition of the experimental tests. For calculating this disagreement between the simulated and measured data from the tests, the root mean square percentage error (RMSPE) were applied by [166] :

$$RMSPE = \sqrt{\frac{\sum_{i=1}^{n}\left[100 \times \left(x_{e,i} - x_{s,i}\right)\right]^2}{n}} \quad (5\text{-}6)$$

Where; xs is the simulation value

Figure 5–18 to **Figure 5–32** show the simulated result curves accompanying the experimental one under conditions of three sets of test shown in **Table 5-1**.

The root mean square percentage deviation (RMSPE) was generally within the range (1.1 to 6.1%), but most of them were under 4%, this difference probably because of measurement incorrectness or theoretical assumptions. The uncertainty of the experimental output was already investigated and showed that they are acceptable for the engineering application of PV/T field. The investigations have been done for the validation of the MPCM-S based simulation model, again it showed that it is able to predict the energy performance of the slurry based PV/T system with acceptable accuracy.

(a)Impact of the Radiation: Under Test 1 conditions illustrated in **Table 5-1**, the computerized simulation was run to find the root mean square percentage deviation (RMSPE).**Figure 5–18** shows that the highest deviation between experimental and simulation outputs is at the radiation is 800 W/m^{2,} and the RMSPE is in an acceptable rate of 1.8%.

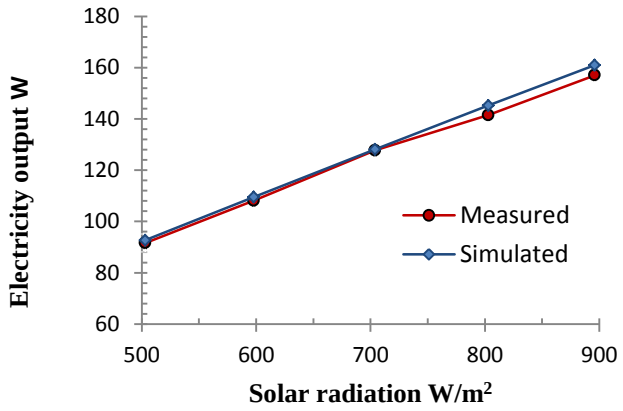

Figure 5–18: Impact of solar radiation on electricity output, RMSPE=1.8%

Figure 5–19 illustrates that with increasing the solar radiation, the heat output increase for both simulation and experiment, and the deviation increase to reach the maximum at highest radiation of 900 W/m^2, the RMSPE is 3.5%.

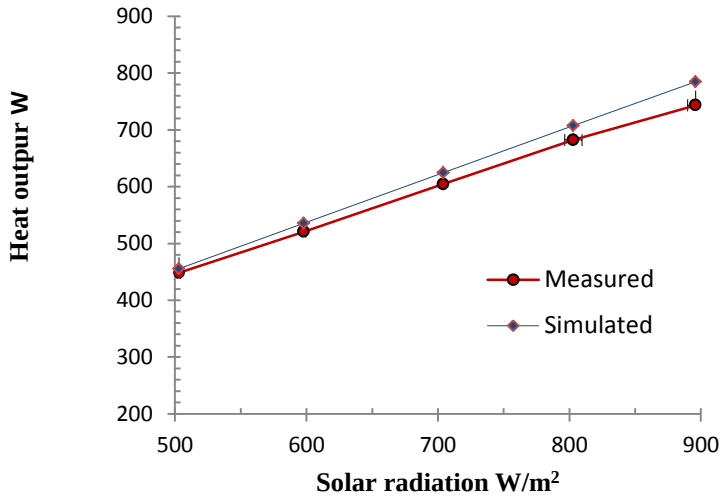

Figure 5–19: Impact of solar radiation on heat output RMSPE=3.5%

Both simulation and experiment output for the back board temperature grow with increasing the solar radiation, as it absorbs more heat, the deviation between both curves fluctuated in small range and reach the highest with the radiation of 900 W/m^2 as shown in **Figure 5–20**, RMSPE is relatively very low (1.1%), because there is a good agreement between the curves.

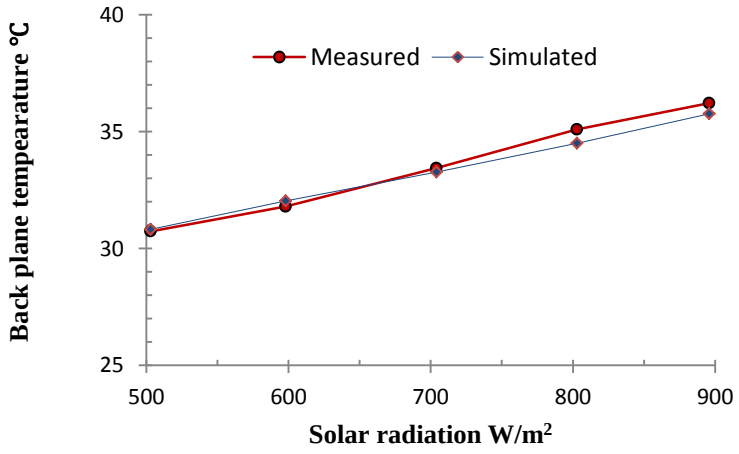

Figure 5–20: Impact of solar radiation on backplane temperature, RMSPE=1.1%

The pressure drop falls with increasing the radiation in both curves as shown in **Figure 5–21**, as the viscosity decrease leading to lessening the flow resistant of the slurry. The deviation is relatively high with radiation of 500 W/m^2 and decreases with radiation of 600 W/m^2, the RMSPE is 6.1%, it is the highest among the comparison outputs between the simulation and experiments, and this high deviation is due to the measurement errors and theoretical assumptions. Despite the high RMSPE, it is still in acceptable range for PV/T applications.

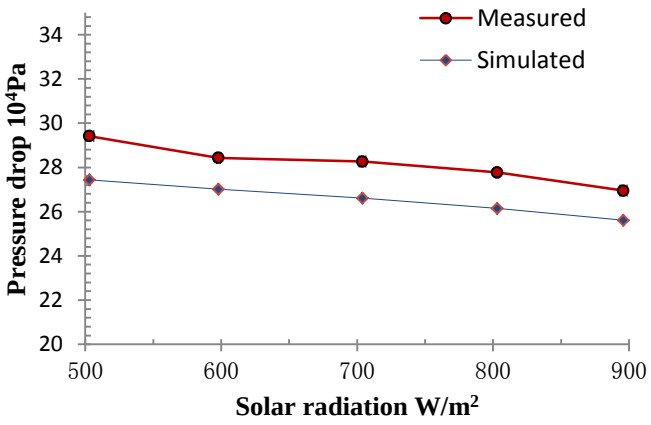

Figure 5–21: Impact of solar radiation on pressure drop, RMSPE=6.1%.

The net efficiency decreases with increasing the radiation for both simulation and experiment curves as illustrated in **Figure 5–22**, it falls smoothly in both curves, and the deviation increase with growing radiation until reaches the highest at the radiation of 900 W/m^2. The RMSPE is 3.2%, it is acceptable for PV/T application.

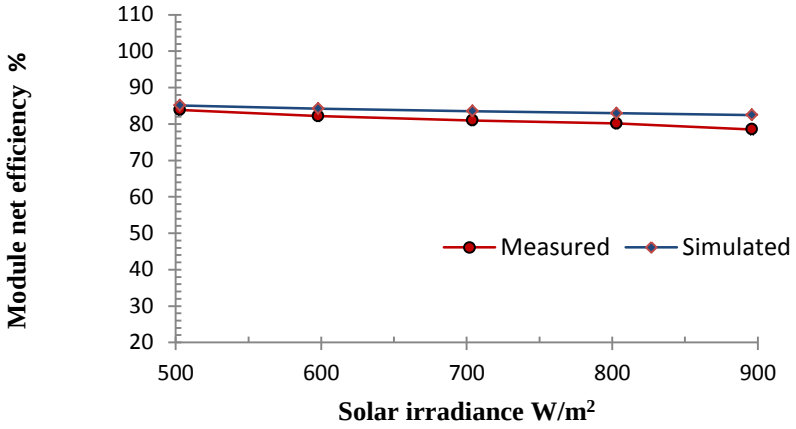

Figure 5–22: Impact of solar radiation on net efficiency, RMSPE=3.2%,

(b) Impact of slurry flow condition: : Under Test 2 conditions as detailed in **Table 5-1**, the computerized simulation was run to find the root mean square percentage deviation (RMSPE). The electricity and heat output increased with growing the Reynolds number for both simulation and experiment curves as shown in **Figure 5–23**, and

Figure 5–24 respectively, the deviation between two curves are higher with low Reynolds number, and reduced toward higher Reynolds number. The RMSPE are 2.4%, 3.7% for electricity and heat output figures respectively.

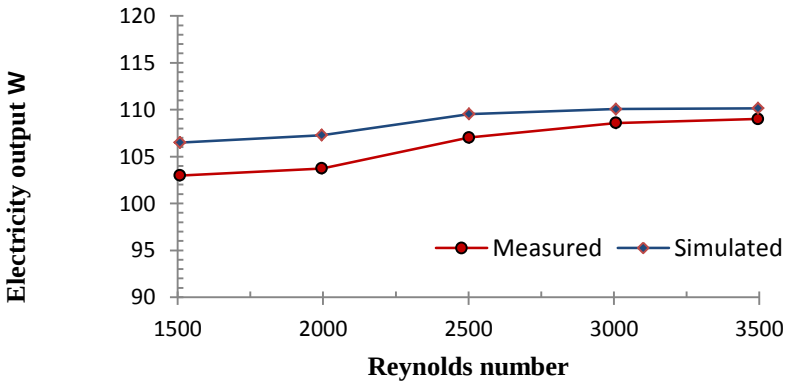

Figure 5–23: Impact of Reynolds number on electricity output, RMSPE=2.4%

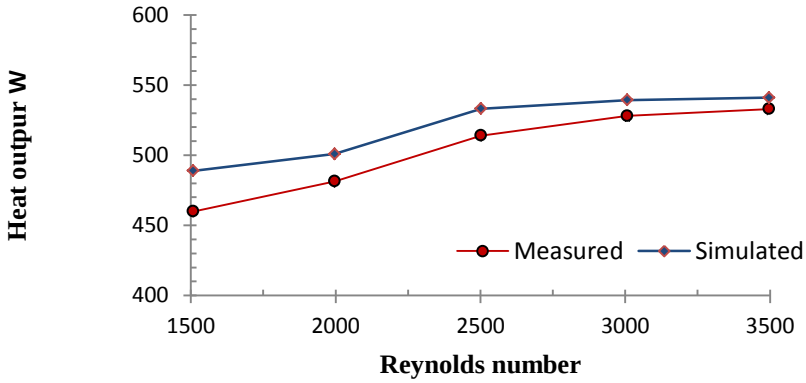

Figure 5–24: Impact of Reynolds number on heat output, RMSPE=3.7%

Increasing Reynolds number enhance the heat transfer of the slurry that leads to a fall in back board temperature for both simulation and experiment outputs as illustrated in **Figure 5–25**. The highest deviation is at Reynolds number of 1500 and decrease with rising the Reynolds number, RMSPE is 2.5%.

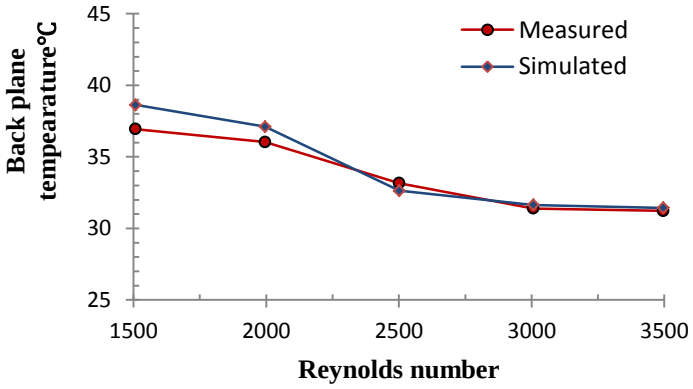

Figure 5–25: Impact of Reynolds number on backplane temperature, RMSPE=2.5%.

The pressure drop increase with growing the Reynolds number as shown in **Figure 5–26**.The RMSPE is 5%.

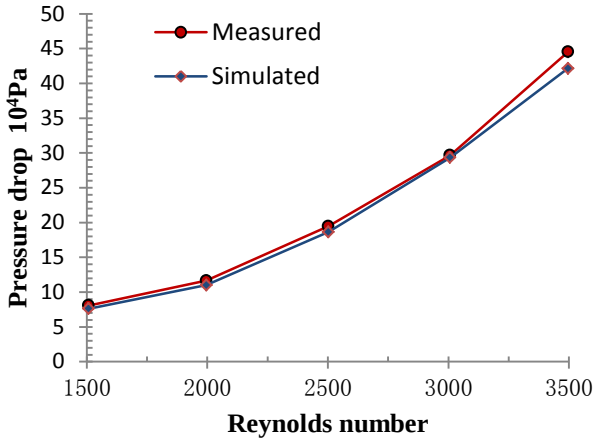

Figure 5–26: Impact of Reynolds number on pressure drop, RMSPE=5.0%

Net efficiency increase with rising the Reynolds number of both simulation and experiment as shown in **Figure 5–27** .The deviation decrease with rising the Reynolds number, it is maximum at Reynolds number of 1500. The RMSPE is 3.6%.

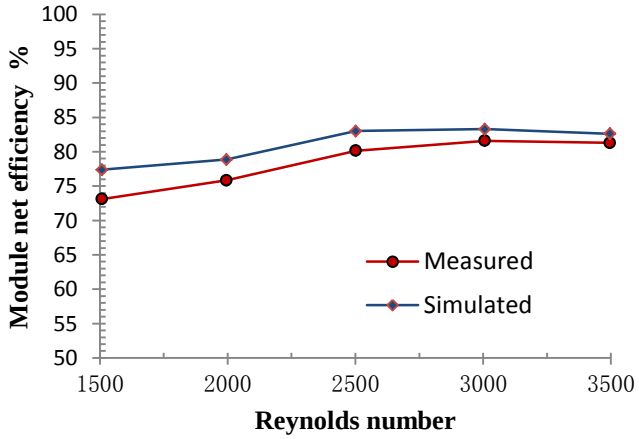

Figure 5–27: Impact of Reynolds number on net efficiency, RMSPE=3.6%

(c) Impact of MPCM concentration: Under Test 3 conditions as detailed in **Table 5-1**, the computerized simulation was run to find the root mean square percentage deviation (RMSPE).

Figure 5–28 and **Figure 5–29** show the relation between mass concentrations of MPCM with electrical and heat outputs respectively. The figures include both experiment and simulation outputs, the deviation between these outputs are higher with low concentration in both figures, and decrease with higher concentrations to reach the minimum with the concentration of 15%. The RMSPE are 1.6% and 3.3% for **Figure 5–28** and **Figure 5–29** respectively.

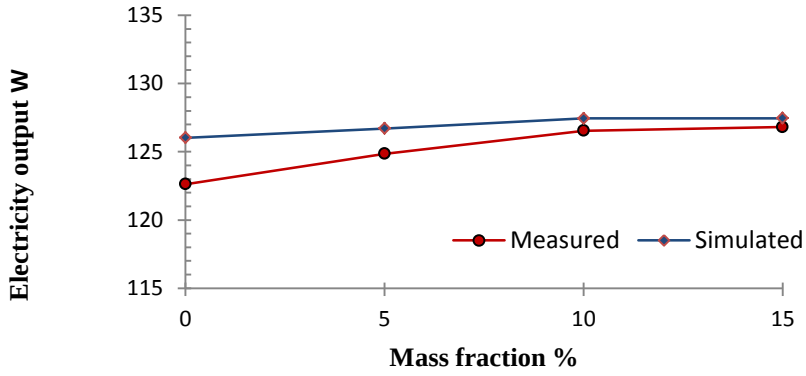

Figure 5–28: Impact of MPCM mass fraction on electricity output, RMSPE=1.6%

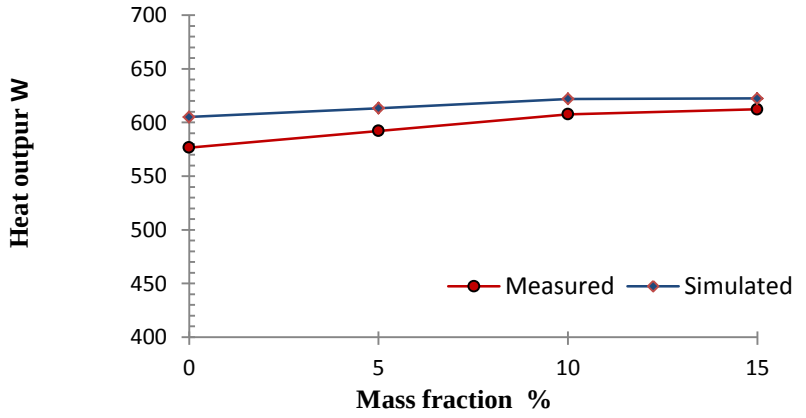

Figure 5–29: Impact of MPCM mass fraction on heat output, RMSPE=3.3%.

Figure 5–30 illustrates that the backplane temperature falls with higher mass concentration of MPCM in the slurry for both experiment and simulation outputs. The highest deviation occurs at 5% .The RMSPE is 1.9%.

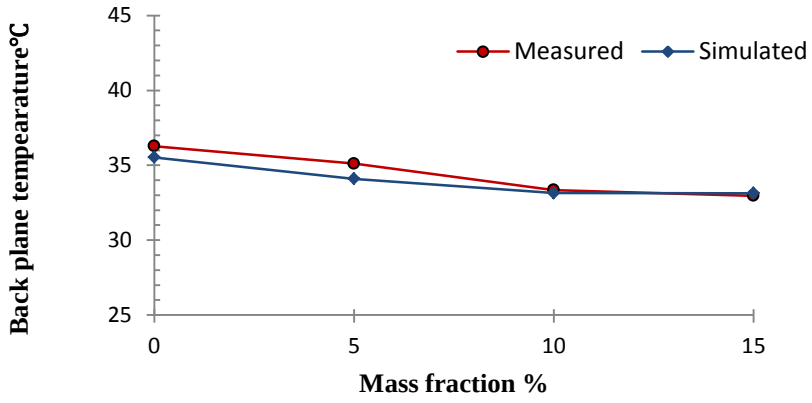

Figure 5–30: Impact of MPCM mass fraction on backplane temperature, RMSPE=1.9%

The pressure drop increase when the slurry contains a higher percentage of MPCM, due to the high viscosity with high concentration as shown in **Figure 5–31**. The deviation between the experiment and simulation results reaches the highest at concentration of 15%. The RMSPE is relatively high (5.7%).

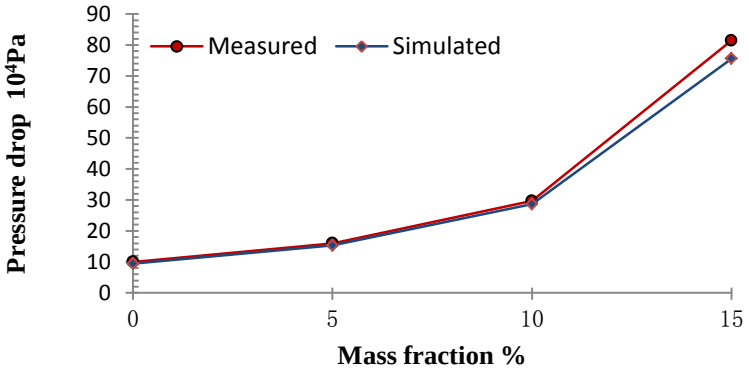

Figure 5–31: Pressure drop as a function of MPCM mass fraction, RMSPE=5.7%

The net efficiency increases up to 10% then falls toward 15% as shown in **Figure 5–32** due to the high viscosity over 10% slurry that needs more electricity for pumping the slurry. The deviation between the simulation and experiment outputs reduce with higher concentration, as it reaches the minimum at 15%. The RMSPE is 3.1%.

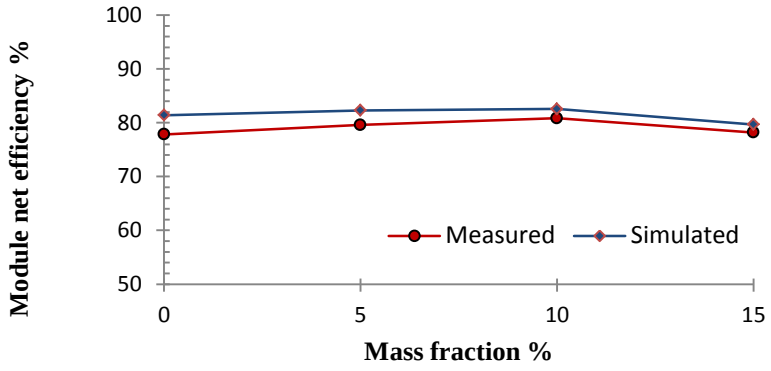

Figure 5–32: Impact of MPCM mass fraction on net efficiency, RMSPE=3.1%

5.4 Performance of the overall PV/T based heat and power system

The system (10% MPCM – S as cooling fluid) could meet the hot water criterion of 45°C [167] with high radiation and air temperature, then employed as useful hot water. The initial tank water was around 19°C in the morning. By the end of the day, in case of intensive radiation from 900 to 1000 W/m^{2}and ambient temperatures from 25 to 30°C, the water temperature could reach 55°C. In case of low radiation, the water could not reach the hot water criterion of 45°C. So in poor radiation and low temperature climates, an auxiliary heating device such as a gas boiler or electric heater should be accompanied to upgrade the water temperature to minimum of 45°C.

For further evaluation of the overall performance of the slurry based PV/T system, a test was run under the selected operational conditions of 10% MPCM concentration ,3000 Reynold number and 600W/m^2 solar radiation. The electrical and heat output were 108 and 520 W respectively, the associated electrical and thermal efficiency were 14.1 and 68.8%, and both together form the overall efficiency of 82.9%, **Table 5-2** shows the operational parameters and the outputs of the PV/T system. The heat output of the PV/T system was calculated by a correlation containing the temperature difference between the inlet and outlet of the water tank with the water flow rate. The power consumption for operating the PV/T system includes the slurry flow rate pump and the heat pump (the compressor), this power was needed to obtain the coefficient of the performance (COP) of the PV/T system. The output of the system is a sum of heat and electricity. If it is assumed that the heat resource is coal, then for converting the electricity output into

the equivalent thermal output produced by a coal fired power plant, it needs to be divided over (0.38) [122]. So the COP of the PV/T system was calculated by using the following correlation:

$$COP_{PV/T} = \frac{Q_{HP,th} + Q_e / 0.38}{Q_{HP,e} + Q_p} \quad (5\text{-}7)$$

Where $Q_{HP,th}$ is the thermal energy output from the system, Q_e is the electricity output from the system, $Q_{HP,e}$ is the electricity power used for operating the heat pump and Q_p is the electricity used for operating the slurry circulation pump .

The slurry pump and the compressor of the heat pump were both oversized, so it caused the production of an inadequate electrical output of the PV module (108 W), which was lower than the electrical amount of (138 W) that consumed for the operation of the system. Despite the unfitting operational condition, the system still attained the overall COP sys of (5.9), it is almost twice that of the solar assisted heat pump systems ISAHP [168].

Table 5-2: Operational conditions and outputs of PV/T system test.

Items	Value
Ambient temperature, t_a	29.45
Solar radiation, I, W/m^2	600
Pressure drop, Δp, Pa	290406
Volume flow rate, V, L/min	1.31
Inlet temperature, t_i, ºC	24.4
Outlet temperature, t_o ºC	28.3
Backplane temperature, t_b ºC	31.9
The pump electrical power consumption, Q_p, W	9.8
The compressor electrical power consumption, Q_{comp}, W	128.9
The module electrical efficiency, ηe, %	14.1%
The module thermal efficiency, ηth, %	68.8%

The system coefficient of performance, $COP_{PV/T}$	5.9

5.5 Chapter Summery

In this chapter, three sets of steady state test carried out under laboratory condition to illustrate the influence of the radiation (I), the slurry flow state (Re) and the MPCM concentration in the slurry (MPCM%) on the performance of the PV/T system. The first test showed that with increasing the radiation from 500 W/m^2 to 900 W/m^2: (a) The electrical output increased significantly from 91.6 - 157.0 W and the heat output from 448.5- 743.3 W, at the same time the growth of the PV cell temperature with the same radiation change rate is about 5 ºC, which is small for that high change rate of radiation. (b) The pressure drop decreased, which indicates to lower viscosity with higher temperature, therefore decreasing the flow resistance of the slurry. The downward trend of the pressure drop is sharper with the radiation between 500-600 W/m^2. (c) Finally he net efficiency decreased smoothly from 83.9-78.5.

The second test carried out with Reynolds numbers of 1508, 2600 and 3496 with remaining the other parameters unchanged. By increasing the Reynolds number; (a) both electrical and thermal outputs were grown from (103-109 W) and (460 - 528 W) respectively, this indicates to the enhanced heat transfer with trending toward turbulent flow condition. (b) The growth of the Reynolds number reflected on the backplane temperature, it led to more cooling effectiveness, as the backplane temperature trend is downward with increasing the Reynolds number. (c) The pressure drop increased and it rises sharper with increasing the Reynolds number. (d) The net efficiency rises, but the rise stopped at the Reynolds number of 3000 with a value of 81.6% and trended slightly downward to reach 81.3%. This happened when a sudden flow growth occurred in the serpentine pipe which led to an apparent flow resistance, consequently the power consumption for the pump raised, that led to decreasing the net efficiency after the Reynolds number of 3000.

The third test was carried out by changing the MPCM concentration of the slurry from (0-15%) with remaining other parameters unchanged, it showed that with increasing the MPCM concentration: (a)both electrical and heat output increased, with very slight

increase from concentration 10% to 15%, which indicates to the minor positive effect of the slurry with over 10% concentration of MPCM. (b) The backplane temperature decreased, again with slightly decrease in temperature with concentration of 10 to 15%. (c)The pressure drop of the slurry flow in the serpentine pipe increased, but it increased very rapidly from concentration 10 -15 %, as it jumped from 29.6 x 10^4Pa -81.4 x 10^4Pa respectively. This rapid increase in the pressure drop causes a struggle of the slurry flow, and then it diminishes the benefit of increasing the MPCM concentration after 10%. (d) The net efficiency increased and reached the highest value of 80.8% with the concentration of 10%, later it trended downward to reach 78.18 when the concentration is 15 %. So it is proved that 10% is the perfect concentration with the best output. The mean uncertainty Ratio for all the tests ($\overline{U}$) were in the acceptable range (1.5-10.6%) and the maximum uncertainty ratio (*Umax*) were in an acceptable range (2 – 13 %).

To compare simulation output to the experimental results, the computer model was validated and run at the same conditions of the experiments to investigate the accuracy of the simulated module, as well as calculating the root mean square percentage error (RMSPE) to identify the discrepancy between the simulation and experimental results, it was under 4 % for all tests, this variance probably because of measurement incorrectness or theoretical assumptions.

The system with 10% MPCM – S as cooling fluid could meet the hot water criterion of 45°C with high radiation and air temperature, then could be employed as useful hot water. With high radiation of (900 to 1000 W/m^2) and the ambient temperature as high as 25 to 30°C, the water temperature could reach 55°C. However, in low radiation and ambient temperature case, a support heating device could be used to heat up to 45°C.

If the system runs with 10% MPCM concentration slurry, 3000 Reynold number and 600W/m^2 solar radiation, it supplies the electrical and heat output of 108 and 520 W respectively, the associated electrical and thermal efficiency of 14.1 and 68.8%, and the overall efficiency of 82.9%, and finally (COP) of the PV/T system of (5.9).

CHAPTER 6: ECONOMIC AND ENVIRONMENTAL ANALYSES OF THE SYSTEM

To analyse the environmental influence on the new MPCM-S based PV/T system within Europes weather, two different climates were chosen for testing the systems application. Then investigating the environmental and economic impact associated with different weather applications. Stockholm (59.32° N, 18.06°E) and Madrid (40.41° N, 3.70° W) were chosen as one of the coldest and one of the warmest capitals in the Europe [169], and representing the northern and southern Europe respectively. The ambient temperature, solar radiation and wind speed are the main factors affecting on the systems operation to find the dynamic electrical and thermal outputs. These investigations based on annual average electrical and heat outputs, by using the computerized simulation from chapter 4, for MPCM-S based system 10 % MPCM concentration slurry was used.

Figure 6–1: Both cities (Madrid and Stockholm) position in Europe [170]

6.1 Weather data and annual thermal and electricity yields

6.1.1 Weather Data

Weather data for a typical design year relevant to different locations of the EU countries were extracted from the energy-plus database. Assuming that the energy system is installed on buildings locating in Stockholm and Madrid. By changing the radiation, ambient temperature and wind speed on hourly basis, the computerized simulation from chapter 4 was run for one year data to find the annual average electrical and heat outputs The hourly solar irradiance and ambient temperature from 06:00 AM to 6:00 PM from the Energy Plus weather files were used on a typical day for each month of the year. Madrid's weather is mostly warm, the temperature and radiation record the highest in July, the lowest temperature could reach is around 2 °C during the daytime in January. **Figure 6–2** derived from the energy-plus database shows the weather data of Madrid including the air temperature and radiation [1].

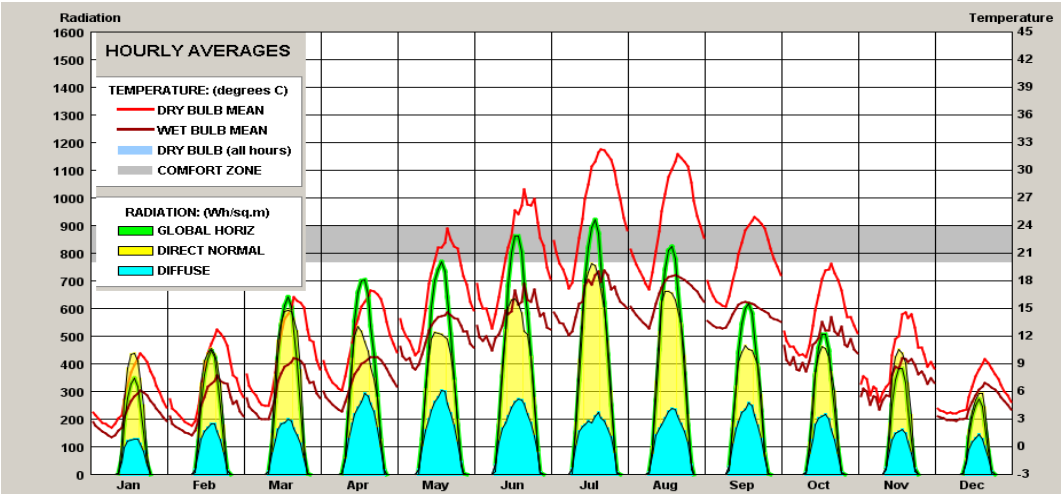

Figure 6–2: Weather data (Madrid)

The weather in Stockholm is cold with low radiation in comparison with Madrid, the highest temperature record is in July that is about 20°C, but the highest radiation is in May. The cold weather could drop the daytime temperature as low as - 4°C in January. **Figure 6–3** from the Energy-plus database shows the weather data of Stockholm including the air temperature and radiation. **Figure 6–4** shows the monthly mean wind speed in Madrid and Stockholm, generally the wind speed in Stockholm is higher than

Madrid, both cities have the highest wind speed in January, they are (3.1 m/s, 4.4m/s) for Madrid and Stockholm respectively.

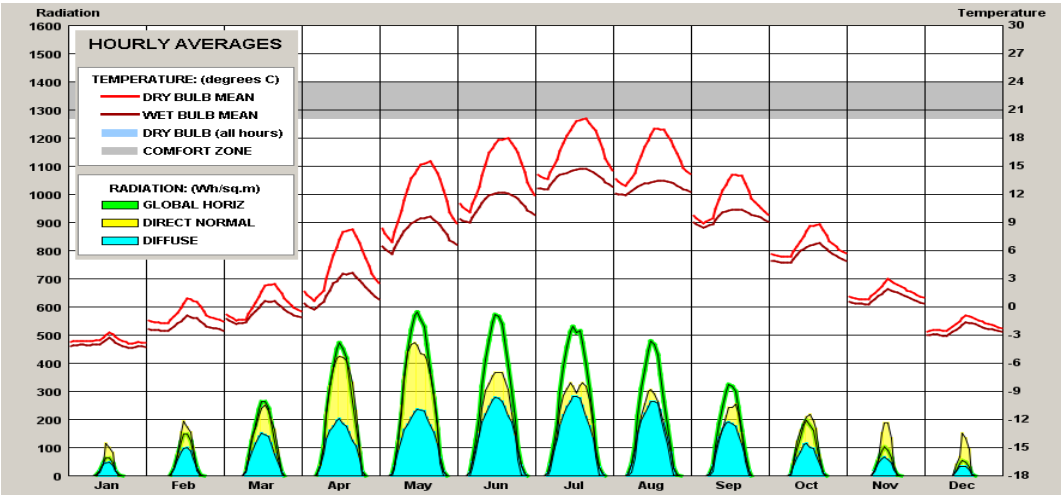

Figure 6–3: Weather data (Stockholm)

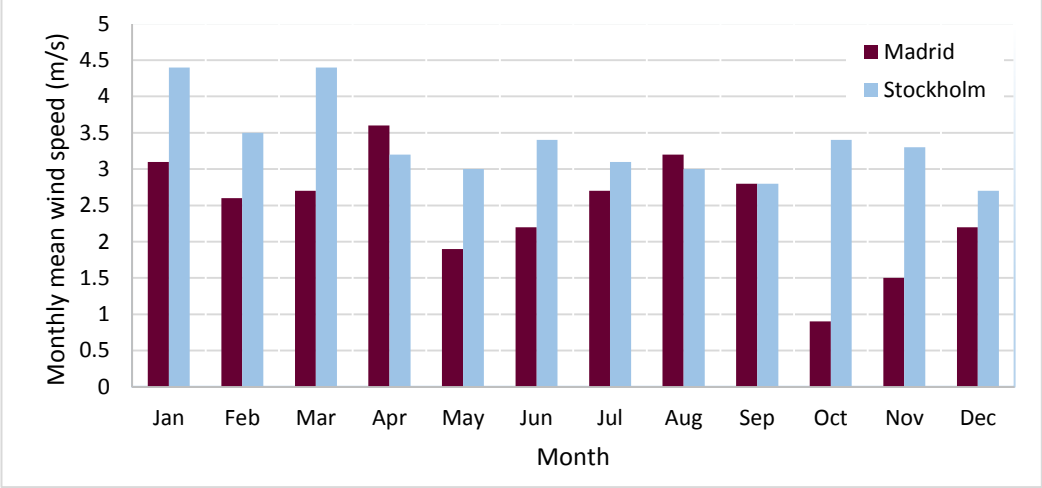

Figure 6–4: Monthly mean wind speed in Madrid and Stockholm

6.1.2 Simulation results of Electricity and Heat yields for slurry based system

By running the computerised simulation model from chapter 4 including the heat pump to guarantee the phase change of the PCM consequently guarantee the benefit of the material, depending on the weather data extracted from the Energy –Plus. Monthly and annual electricity and heat yields are calculated and shown in **Figure 6–5** and

Figure 6–6 for both cities. Generally, the outputs are affected by of the parameters such as air temperature, wind speed and the intensity of the radiation. The figures show that over the year, the electrical and heat yields of Madrid are higher than Stockholm, due to the higher radiation in Madrid. For both cities, the lowest electrical output is in January, because of the short daytime and lower sun angle, and consequently less radiation during this month. Stockholm has the highest electricity and heat output of (53.72 and 225.1 kWh) in May, because highest radiation about 700 kWh/m^2 in Stockholm is in May, that the air temperature could reach 15.6 $^{\circ}$C that is relatively high for Stockholm according to the data extracted from Energy- Plus but it is not the highest. These high yields in Stockholm in May are close to yields for Madrid in May. The latter however reaches higher electrical and heat yields of (57.10 and 290.73 kWh) in July.

The annual electricity and heat output were calculated, they are (488.29 and 2184.93 kWh) for Madrid and (323.12 and 1262.1 kWh) for Stockholm. The results prove that the MPCM-S based PV/T system located at the south can achieve more electricity and heat yields than the north because the south has a more intense radiance and higher temperature than the north. The current electricity tariff of 12.15p/kWh and gas tariff of 2.8p/kWh in the UK [171] excluding VAT. So depending on the current tariff, the annual saving cost for electricity and heat are (59.33 and 61.18 GBP) for Madrid and (39.26 and 35.34 GBP) for Stockholm.

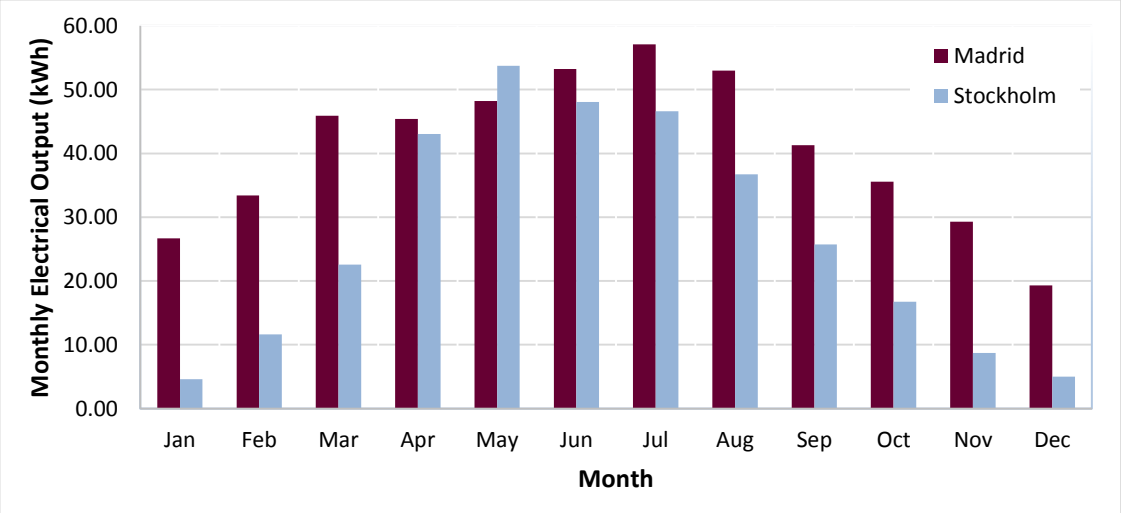

Figure 6–5: Monthly Electrical Output in Madrid and Stockholm

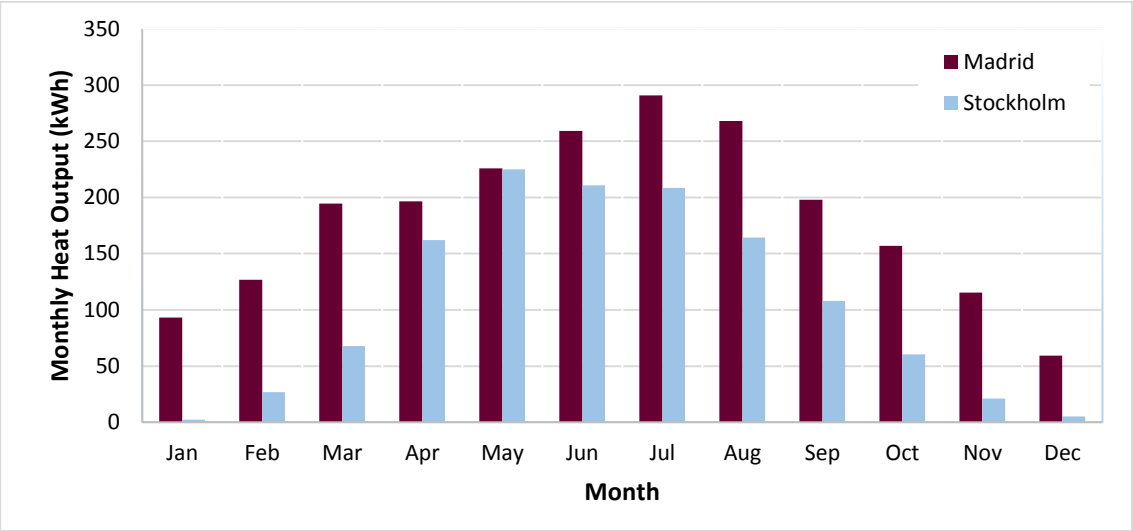

Figure 6–6: Monthly Heat yields for Madrid and Stockholm

6.1.3 Simulation results of Electricity and Heat yields for water-based system

To compare the MPCM-S system to the conventional water-based system. The computerized model was run with water and without the heat pump under two different climate conditions of Madrid and Stockholm from 6:00AM to 6:00 PM of typical days for12 months, following the same process done for the slurry based system. The results showed that the annual electrical yields are 240.32kWh and 171.19 kWh for Madrid and Stockholm respectively, and the annual heat yields are 861.43 kWh and 435.7kWh for Madrid and Stockholm respectively. For calculating the annual saving cost the same current electricity and gas tariff of (0.1215 and 0.028 GBP) were used. It is concluded that the annual saving of electricity and heat are (29.2 and 21.07 GBP) for Madrid, and (20.8 and 12.2 GBP) in Stockholm. Therefore, the total annual saving is (50.27 and 33 GBP) for Madrid and Stockholm respectively. The result confirms that even the water-based has higher outputs in Madrid than Stockholm.

The results showed that the annual electrical yields are 240.32kWh and 171.19 kWh for Madrid and Stockholm respectively, and the annual heat yields are 861.43 kWh and 435.7kWh for Madrid and Stockholm respectively. For calculating the annual saving cost the same current electricity and gas tariff of (0.1215 and 0.028 GBP) were used. It

is concluded that the annual saving of electricity and heat are (29.2 and 21.07 GBP) for Madrid, and (20.8 and 12.2 GBP) in Stockholm. Therefore, the total annual saving is (50.27 and 33 GBP) for Madrid and Stockholm respectively. The result confirms that even the water-based has higher outputs in Madrid than Stockholm.

6.2 Economic analysis

The economics of any energy system are vital to understand the cost of production and payback period on the investment to reduce the risk of the project failure. The capital and operational cost were calculated to analyse the economic aspect of the system, and same calculations were done for the conventional water-based PV/T system for further analyses and comparisons.

6.2.1 Estimated Capital Cost

This type of system was considered to have a life span of 25 years [172]. The capital cost includes all the individual component costs. The cost of solar technologies sharply descended due to the high market demand and competition. If it is assumed that the knowledge applied for a big project and the electrical output is connected to the British National Grid, then there will be no need for batteries and the prices of the components should be a wholesale price. The PV/T panel which represents the most expensive part of the system is assumed as 160-210 % of solar PV panel's price[83] . The MPCM-S, prepared from MPCM wet cake need to be changed twice a year (0.175kg) each time because the capsules are subject to fracture. The life of the other components of the system is assumed 25 years. Details of each item cost are presented in **Table 6-1**, giving a capital cost for the whole system of 510.27 GBP.

Table 6-1: Capital cost of the MPCM-S based PV/T system.

System Component	Unit price	Quantity	Cost (£)	Life period (years)
Slurry based PV/T module	128	1	128	25
MPCM-wet cake	13.82	0.175kg	2.42	0.5
Compressor	37.98	1	37.98	25
Flat-plate heat exchanger	20.5	1	20.5	25
Circulation pump	60	1	60	25
Tank	49.25	1	49.25	25
Expansion valve	15.5	1	15.5	25
Pipe lines and accessories	N/A	N/A	36.5	25
Micro-inverter	50	1	50	25
Installation and commissioning	110.12	N/A	110.12	25
Capital cost (GBP)				**510.27**

The conventional water-based PV/T systems are also expected to have a 25years life cycle [172]. Water-based system does not include the heat pump, also is simple and easy to install in comparison with MPCM-S based PV/T system, so installation cost then general capital cost of 415.12 GBP is much lower than the MPCM-S based PV/T system, as shown in **Table 6-2**.

Table 6-2: Capital cost of the water-based PV/T system

System Component	Unit price (£)	Quantity	Cost (£)	Life period(years)
Water-based PV/T module	128	1	128	25
Circulation pump	60	1	60	25
Tank	49.25	1	49.25	25
Pipe lines and accessories	N/A	N/A	30.5	25
Micro-inverter	50		50	25
Installation and commissioning	N/A	N/A	97.37	-
Capital cost (£)				**415.12**

6.2.2 Annual Operational Cost

The annual operational cost of the MPCM-S based PV/T system comprises the electricity costs consumed by the compressor of the heat pump and the maintenance cost. The electricity used by the MPCM-S based PV/T system and its cost for both cities (Madrid and Stockholm) are extracted from the computerised simulation and listed in **Figure 6–7**. The highest electrical used is in May (40.9 kWh) for Stockholm and in July (53.3 kWh) for Madrid due to the high radiation and temperature of both cities in these specific months, therefore need more cooling consequently more operation in these months . The annual electrical used for operating the system are 426.2 and 267 kWh that cost 51.78 and 32.44 GBP for Madrid and Stockholm respectively.

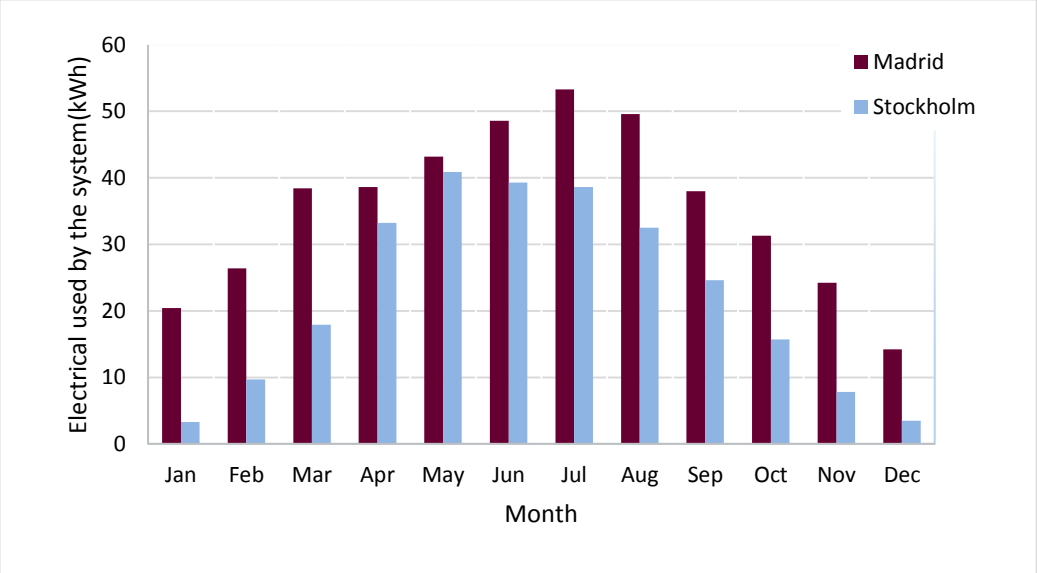

Figure 6–7: Annual Electricity used for the MPCM–S based PV/T system operation for Madrid and Stockholm

The maintenance cost of the system is estimated at 2% of the initial system cost [173], so the annual maintenance cost for both cities is 10.2 GBP. The MPCM-S need to be changed twice a year, the capital cost includes the slurry for the system operation that lasts for six months, so the system need one change of the slurry that costs 2.42 GBP for the second part of the year. The annual operational cost of the system for both cities is calculated, it comprises of annual electricity and annual maintenance cost. The

annual operational cost of the system for both cities is calculated, it comprises of annual electricity, the annual maintenance cost and the slurry cost. **Table 6-3** illustrates the annual operational cost and its parameters for both cities Madrid and Stockholm.

Table 6-3: Annual operational cost of the MPCM-S based PV/T and water-based systems (GBP) for Madrid and Stockholm

MPCM-S based PV/T system		
Items	**Madrid**	**Stockholm**
Annual MPCM wet cake(GBP)	2.42	2.42
Annual electricity cost (GBP)	51.78	32.44
Annual maintenance cost(GBP)	10.20	10.20
Annual operational cost(GBP)	**64.4**	**45.06**

For the conventional PV/T/water system, the electricity used for the circulation pump is 39 kWh which cost 4.7 GBP for Madrid and Stockholm respectively. The annual maintenance is 2% of the capital cost, so it is 8.3 GBP for both Madrid and Stockholm. Therefore, the overall operational cost for the water-based system is 13 GBP.

The MPCM-S based system is more expensive because it's accompanied with heat pump, which also led to an increase in installation in one hand, in the other hand it increased the operational cost in comparison with the water-based system. The system in Madrid was in need of cooling more than Stockholm so this is another reason for having higher operational cost in Madrid

6.2.3 Pay-back Time (PBT)

The pay-back time is the amount of time required to recoup the total capital cost of the system without any discounted costs. It was calculated by dividing the capital cost by the net income (value of energy savings minus operational costs). If the energy pay-back time is shorter than the life span of a system, the total energy saving can contribute the reduction of greenhouse gas GHG emission[174]. Payback time was calculated for

both MPCM–S and water-based PV/T systems for both cities Madrid and Stockholm as below:

$$\boldsymbol{PBT(years) = \frac{Capital\ Cost}{Annual\ Energy\ saving - Annual\ Operational\ cost}}$$

PBT was calculated for both cities Madrid and Stockholm. It is illustrated with the contributed data for its calculation in **Table 6-4** .

Table 6-4:The payback period in Madrid and Stockholm

Madrid	**MPCM-slurry- PV/T**	**Water-PV/T**
Initial capital cost GBP)	510.27	415.12
Annual Operational cost (GBP)	64.4	13
Annual electricity saving (GBP)	59.33	29.2
Annual heat saving (GBP)	61.16	24.12
Payback period (years)	**9.0**	**10.3**
Stockholm		
Initial capital cost (GBP)	510.27	415.12
Annual Operational cost (GBP)	45.06	13
Annual electricity yield saving (GBP)	39.26	20.8
Annual heat yield saving (GBP)	35.34	12.2
Payback period (years)	**17.3**	**20.75**

It is concluded that the MPCM-S based PV/T in Madrid has the lowest payback time of 9 years, and 10.3 years for the water-based system, with a difference of 1.3 years. At the same time, it is less than the MPCM-S based system in Stockholm by 8.3 years, which is a big difference that shows the advantage of the systems application in Madrid over Stockholm. The water-based system is economically more beneficial in Madrid than Stockholm according to the big difference in PBT, as it is 10.3 years in Madrid and 20.75 years in Stockholm. So the results confirm that generally both PV/T systems are more cost-effective in Madrid than Stockholm.

6.2.4 Life Cycle Cost (LCC) cost per kWhe generation

Life cycle cost is the sum of all the costs and income associated with an energy supply system at today's value (not discounted) over its lifetime [173]. It is an effective approach to evaluate and support a business case for emissions reduction initiatives like renewable energy projects as they have higher costs initially, but lower operating and maintenance costs, in investments it could be considered as an alert of future expenditure. The life cycle cost of the system can be calculated as below[175]:

$LCC = PCi + PCo - PSe - PSs$

Where; *PCi* : initial capital cost, , *PCm* : present value of maintenance cost, *PSe*: present value of energy saving, and PSs: present value of system's salvage.

The PV system's life cycle is usually 25years in European countries, the interest and inflation rate were assumed as 10% and 5% respectively, then the PCo, and PSe can be calculated using the same formula as below:

$$PCo = Co * \sum_{n=1}^{25} \frac{(1+f)^n}{(1+i)^n}$$

$$PSe = Se * \sum_{n=1}^{25} \frac{(1+f)^n}{(1+i)^n}$$

Where; Co is the annual operational cost, Se; is the annual energy saving cost, and Ss; is the scrap value of the equipment at the end of its service life, is ignored and excluded from the calculations.

The cost per kWh energy output and the parameters used for the calculation are shown in **Table 6-5** and for Madrid and Stockholm respectively

Table 6-5:The Life Cycle Cost per kWhe in Madrid and Stockholm

Present value of 25 years life cycle (Madrid)	**MPCM-S-PV/T**	**Water-PV/T**
Initial capital cost (GBP)	510.27	415.12
Operational cost (GBP)	929.94	187.72
Net cost	1440.2	602.84
Electricity and heat yield saving (GBP)	1740.02	769.94
Cost per kWhe(GBP/kWhe)	**-0.068**	**-0.038**
Present value of 25 years life cycle (Stockholm)		
Initial capital cost (GBP)	510	415.12
Operational cost (GBP)	650.67	187.72
Net cost	1160.94	602.84
Electricity and heat yield saving (GBP)	1077.22	476.52
Cost per kWhe(GBP/kWhe)	**0.019**	**0.028**

The results show that the LCC per kWhe in Madrid for MPCM-S and water-based PV/T, are -0.068 and -0.038 GBP respectively. The minus signifies that for generating each kWhe over 25 years' life, the system can cover all the cost and save the detached amount of 0.068 and 0.038 GBP as well for slurry based and water-based systems respectively. In Stockholm generating each kWhe over the systems life costs 0.019 and 0.028 GBP. So the cost difference in kWhe over 25 years life is 0.087GBP between the slurry based system in Madrid and Stockholm, which means that the slurry based system in Stockholm costs 0.087 GBP more for generating one kWhe than Madrid. The water-based system in Stockholm costs 0.066 GBP more for generating one kWhe than Madrid.

6.3 Environmental effects

Carbon dioxide (CO_2) is the most common greenhouse gases emitted by human being's activities, so for analysing the environmental effect of energy system s emission, usually CO_2 is the main greenhouse gas is taken into consideration as a main factor. In

terms of environmental effect of these PV/T systems, the annual CO_2 emission reduction could be determined from the annual energy save of the system multiplying by the electricity to the CO_2 conversion factor. Combined Heat and Power system yields both heat and electricity, and there are several conventions used to allocate emissions between these products. Emissions from these systems might be allocated entirely to electricity or entirely to heat. But to be more accurate it is better to separate the outputs to electricity and heat, each multiplied by its conversion factor. The electricity to CO_2 conversion factor for 2016 is 0.40957 kgCO_2 depending on the UK grid electricity, and heat to CO_2 conversion factor is 0.20405 [176] , this in case if compressed natural gas (CNG) is used for the electricity generation, because comparing to the other conventional energy production resources the (CNG) could be considered cleaner with less CO_2 emission. The UK grid electricity factor vagaries from year to year, because the fuel mix consumed for producing electricity in UK power stations changes, and as the proportion of net imported electricity changes. So the yearly changes can be big as the factor depends very greatly on the relative prices of natural gas and coal, in addition to variations in peak demand. The formula for calculating the CO_2 reduction will be as below [177] :

R.CO_2= CO_2 Reduction from Electricity generation + CO_2 Reduction from Heat generation

$$R.CO_2 = f\ CO_{2\,e}\,(E_o - E_u) + f\ CO_{2h}\,(H_o)$$

Where; $R.CO_2$ is the CO_2 emission reduction, $f\ CO2_e$ is the electricity to CO_2 conversion factor, E_o is the output energy of the system, and E_u is the energy used for the system operation, $f\ CO_{2h}$ is heat to CO_2 conversion factor and H_o is the heat output from the system.

The life cycle CO_2 emission for MPCM-S and water-based PV/T were calculated for Madrid and Stockholm and illustrated with all parameters used in the calculation in **Table 6-6**.

Table 6-6:CO2 Emission Reduction in Madrid and Stockholm

Madrid	**MPCM-S-PV/T**	**Water-PV/T**
Annual Electricity Yield(kWh)	488.29	240.32
Annual Electricity Used (kWh)	426.2	39
Annual heat Yield (kWh)	2184.6	861.43
Annual CO2 Emission (ton)	0.47	0.26
Total Life Cycle CO2 Emission Reduction (ton)	**11.75**	**6.46**
Stockholm		
Annual Electricity Yield(kWh)	323.14	171.19
Annual Electricity Used (kWh)	267	39
Annual heat Yield (kWh)	1262.1	435.7
Annual CO2 Emission Reduction(tons)	0.28	0.14
Total Life Cycle CO2 Emission Reduction (ton)	**7**	**3.5**

The highest CO2 emission reduction of 11.75 tons over 25 years' life cycle is in Madrid for the slurry based system, so even environmentally the novel slurry based system is more active than the water-based one which has the emission reduction of 6.46 tons by . In addition, it is higher than the emission reduction in Stockholm with a difference of 4.75 tons. The CO_2 reduction in Stockholm is doubled in case of MPCM-S based system in comparison with the conventional water-based system in the same city, so it is improved by 50%, in case this improvement is 55% in Madrid. Therefore, the slurry based is more environmentally friendly than the water-based system in both cities, but is friendlier in Madrid than Stockholm.

6.4 Chapter Summery

By running the computerised simulation module, depending on the weather data extracted from the Energy –Plus for Madrid and Stockholm. The annual electricity and heat output were calculated, they are (488.29 and 2184.93 kWh) for Madrid and (323.12 and 1262.1 kWh) for Stockholm. The results prove that the MPCM-S based PV/T

system located at the south can achieve more electricity and heat yields than the north because the south has a more intense radiance and higher temperature than the north. By depending on the current electricity tariff of 12.15p/kWh and gas tariff of 2.8p/kWh in the UK, the annual saving cost for electricity and heat are (59.33 and 61.18 GBP) for Madrid and (39.26 and 35.34 GBP) for Stockholm.

The capital cost of MPCM-S and water-based PV/T systems are 510.27 and 415.12 GBP respectively.The annual electrical used for operating the system are 426.2 and 267 kWh that cost 51.78 and 32.44 GBP for Madrid and Stockholm respectively. The economic investigation showed that the MPCM-S PV/T in Madrid has the lowest PBT of 9 years, and 10.3 years for the water-based system. The PBT of MPCM-S based system in Stockholm is 17.3 years, which is 8.3 years higher than the one in Madrid. The water-based system in Stockholm has 20.75 years PBT that is highest among all, in comparison with same system in Madrid it is higher by 10.45 years. So the PBT of both MPCM_S and water-based systems are higher in Stockholm than Madrid that proves the economic advantage of the systems application in Madrid over Stockholm. The LCC per kWhe in Madrid for MPCM-S and water-based PV/T, are -0.068 and -0.038 GBP/kWhe respectively. The minus signifies that for generating each kWhe over 25 years' life, the system can cover all the cost and save the detached amount of 0.068 and 0.038 GBP as well for slurry based and water-based systems respectively. In Stockholm generating each kWhe over the systems life costs 0.019 and 0.028 GBP. So the cost difference in kWhe over 25 years life is 0.087 GBP between the slurry based system in Madrid and Stockholm, which means that the slurry based system in Stockholm costs 0.087 GBP more for generating one kWhe than Madrid and water-based system costs 0.066 GBP more for generating one kWhe than Madrid.

The environmentally study showed that the highest CO_2 emission reduction of 11.75 tons over 25 years' life cycle is in Madrid for slurry based system, so even environmentally the novel slurry based system is more active than the water-based one which has the emission reduction of 6.46 tons .Also it is higher than the emission reduction in Stockholm with a difference of 4.75 tons. Therefore, the slurry based is more environmentally friendly than the water-based system in both cities, but is friendlier in Madrid than Stockholm.

CHAPTER 7: CONCLUSION AND FURTHER WORK

The research intensively investigated the novel MPCM-S based PV/T system, which was carried out through the literature review, optimum conceptual design, the development of simulation model based on theoretical analysis, laboratory-based experiments, and the economic and environmental study of the system's application. The main achievement of the research consists of the computerised simulation model, which was validated by the experiment outputs and the economic and environmental investigations of the different climates of Europe to predict the economic and environmental benefits of the system's application.

7.1 Computerised steady – state simulation module:

This task addressed the simulation model development and operation that is aimed to analyse the power generation, heat transfer and fluid flow problems occurring in various parts of the system, including PV/T module, heat exchanger and PCM. The validation of the simulation model was conducted using the experimental data of a previous study. The computerized module was run under specific operational conditions with concentrations of MPCM (0 %, 5%, 10%, 15%, and 20%) to test its influence on the performance of the system. The results showed that using 10% concentration slurry produce highest electrical and thermal outputs, because it gives the highest advantages of including PCM with reaching to the preferable turbulent flow state. In addition, the slurry over 10% concentration does not reach the turbulent flow state due to its high viscosity, and causes a sudden pressure drop in the serpentine pipe which increases the input electricity demand for the circulation pump.

To find the optimum diameter for the serpentine pipe the simulation was run under a specific condition with three different internal pipe diameter of 6, 7 and 8 mm. The smallest pressure drop occurs at the biggest diameter. Therefore, as a result of the investigation, the diameter of 8mm represents the better output of the system performance. The best operational case was identified with the highest net efficiency occurs at Reynolds number of 2600 and MPCM mass concentration of 10%, it achieves

highest net efficiency of 58.76%, and electrical, thermal and overall efficiency at this case are 15.6%, 43.8%, 59.4% respectively.

7.2 Experimental performance under laboratory conditions

Three steady state tests were run under laboratory condition to illustrate the impact of the radiation (I), the slurry flow state (Re) and the MPCM concentration in the slurry (MPCM%) on the performance of the PV/T system. The first test showed that with increasing the radiation from 500 W/m^2 to 900 W/m^2: The electrical and heat output increased, the pressure drop decreased, which indicates to lower viscosity with higher temperature, therefore decreasing the flow resistance of the slurry. The downward trend of the pressure drop is sharper with the radiation between 500-600 W/m^2. As a result, the net efficiency decreased smoothly from 83.9-78.5%.

The second test was run by varying the flow state, the test carried out with Reynolds numbers of 1508, 2600 and 3496 with remaining the other parameters unchanged. By increasing the Reynolds number; both electrical and thermal output were grown, this indicates to the enhanced heat transfer with trending toward turbulent flow condition. The growth of the Reynolds number reflected on the backplane temperature, it led to more cooling effectiveness, as the backplane temperature trend is downward with increasing the Reynolds number, but the pressure drop increased and it rises sharper with increasing the Reynolds number. As a result, the net efficiency rises, but the rise stopped at the Reynolds number of 3000 with a value of 81.6% and trended slightly downward to reach 81.3%. This happened when a sudden flow growth occurred in the serpentine pipe, which led to an apparent flow resistance, consequently the power consumption for the pump raised, that led to decreasing the net efficiency after the Reynolds number of 3000.

The third test was run by changing the MPCM concentration of the slurry from (0-15%) with remaining other parameters unchanged, it showed that with increasing the MPCM concentration: both electrical and heat output increased, with very slight increase from concentration 10% to 15%, which indicates to the minor positive effect of the slurry after 10% concentration pf MPCM. The backplane temperature decreased, again with

slightly decrease in temperature with concentration of 10 to 15%. The pressure drop of the slurry flow in the serpentine pipe raised, but it increased very rapidly from concentration 10 -15 %. This rapid increase in the pressure drop causes a struggle of the slurry flow, and then it diminishes the benefit of increasing the MPCM concentration after 10%. The net efficiency increased and reached the highest value of 80.8% with the concentration of 10%, later it trended downward to reach 78.18 when the concentration is 15 %. So it is proved that 10% is the perfect concentration with the best output. The mean uncertainty Ratio for the three set of tests ($\overline{U}$) were in the acceptable range of 1.5-10.6% and the maximum uncertainty ratio (Umax) also were in an acceptable range of 2 – 13 %. So generally, from the three tests, the best operational condition parameters were proved which are: 10% MPCM concentration slurry, 3000 Reynold number and 500-600W/m^2 solar radiation.

Comparison between the simulation and experimental results was investigated, for that the computer model run at the same operational conditions of the experiments to investigate the accuracy of the simulated module, as well as calculating the root mean square percentage error (RMSPE) to spot the discrepancy between the simulation and experimental outputs. The root mean square percentage deviation (RMSPE) were generally within the range of (1.1-6.1%), but most of them were under 4%, this difference probably because of measurement incorrectness or theoretical assumptions.

The system could produce hot water up to 55°C, with high radiation (900 to 1000 W/m^2) and the ambient temperatures as high as 25 to 30°C in case of using 10% slurry as cooling fluid. If the radiation and ambient temperature are low, a support heating device could be used to upgrade the water temperature to 45°C (the hot water criterion). The Investigation of the operational conditions of 10% MPCM concentration slurry, 3000 Reynold number and 600W/m^2 solar radiation, end up with electrical and heat output of 108 and 520 W respectively, the associated electrical and thermal efficiency of 14.1 and 68.8%, both efficiencies together form the overall efficiency of 82.9%, and finally (COP) of the PV/T system of (5.9).

7.3 Economic and environmental analyses

The annual electricity and heat output were calculated by running the simulation model relying on the weather data extracted from the Energy –Plus for Madrid and Stockholm. The annual electricity and heat output were calculated, they are (488 and 2184kWh) for Madrid and (323 and 1262 kWh) for Stockholm. The results prove that the MPCM-S based PV/T system located at the south can achieve more electricity and heat yields than the north because the south has a more intense radiance and higher temperature than the north.

The economic investigation started with calculating the capital cost of MPCM-S and water-based PV/T systems, they are 510.27 and 415.12 GBP respectively.The annual electrical used for operating the system are 426.2 and 267 kWh that cost 51.78 and 32.44 GBP for Madrid and Stockholm respectively. The economic investigation showed that the MPCM-S PV/T in Madrid has the lowest PBT of 9 years, and the highest one is the water-based system in Stockholm that has 20.75 years PBT. So the PBT of both MPCM_S and water-based systems are higher in Stockholm than Madrid that proves the economic advantage of the system's application in Madrid over Stockholm. The Life Cycle Cost (LCC) per kWhe in Madrid for MPCM-S and water-based PV/T, are -0.068 and -0.038 GBP/kWhe respectively. The minus signifies that for generating each kWhe over 25 years' life, the system can cover all the cost, with a surplus of 0.068 and 0.038 GBP as well for slurry based and water-based systems respectively. In Stockholm, generating each kWhe over the system's life costs 0.019 and 0.028 GBP for slurry based and water-based systems respectively.

The environmentally impact of the systems application indicated that the highest CO_2 emission reduction of 11.75 tons over 25 years' life cycle is in Madrid for slurry based system and the lowest is 3.5 tons for water-based system in Stockholm. Therefore, the slurry based is more environmentally friendly than the water-based system in both cities, and is better in Madrid than Stockholm.

The study outputs support the opportunity of the novel MPCM-S based PV/T application. As it is one of the very first studies using the slurry in this field, it outlined that 10% MPCM-S is the best concentration due to its highest outputs in comparison

with the other concentrations and water. Meaning higher energy save, consequently economic and more environmentally friendly.

7.4 Barrier and challenges remaining with the PV/T systems and MPCM-S application

7.4.1 Challenges facing PV/T systems

Technical challenges: There is no international standard for testing, monitoring and performance of the PV/T systems to value the advantages of the system over the separate PV and solar collectors. All the researches have done for studying this hybrid system are according to the different views of different researchers that affects negatively on the reliability and development speed of the technology.

Economic challenges: Despite the big range of developments have been done recently to improve the output of the combined PV/T technology, it still not as popular as the separate PV and thermal systems. The studies still have not reflected on the market of the technology. The price reduction in future is accompanied by the reliable enhancement and large-scale production of this combined technology stakeholders and the authorities could play a positive role in booming the PV/T market. Lack of assistance or grants especially from governments is another big challenge in font of this technology.

Other Challenges: Social aspect should not be ignored, the public acceptance level for this relatively new technology is low, so public awareness needs a big effort and wide range of studies. The PV/T systems produce electricity and heat, the former is always demanded everywhere in the world, but the latter (heat) should be employed depending on the need, because sometimes in hot climates there is no need for heat , therefor the employment of the heat should be investigated previously in any PV/T project to deliver the maximum benefit of the system.

7.4.2 Barriers to MPCM-S applications

Technical Barriers: Many barriers still facing the wide application of phase change materials in the solar energy field. A large number of experiments have investigated

limited properties of PCMs such as melting temperature and latent heat of fusion, ignoring to concentrate on other thermo-physical properties especially for pure substances. Two main express techniques, first is differential thermal analysis (DTA) and the second one is differential scanning calorimetry (DSC) are used to measure the basic properties like latent heat of fusion and melting temperature [13], the accuracy of the mentioned methods is not sufficiently high due to the obvious discrepancies in the data obtained from studies and researches. The absence of unified international standards for PCM products is deepens the problems accompanied with using them.

MPCM-S based system is much more complicated than the water-based system, because water is a simple fluid with certain and precise properties, so using water in any energy system simplifies the technical study of the system. There are a large number of factors affecting on MPCM-S properties such as different substances, preparation method, additives, core-to-shell percentage and MPCM mass fraction in the slurry. All these parameters effect properties of MPCM-S such as suspension stability, thermal and rheological properties. Due to this diversity and absence of a universal standard for determining MPCM-S properties, it is hard to compare results of different researches. Luckily, nowadays PCM is a desirable field for researchers due to the advantages of these materials; consequently, it enriches the related researches about building energy applications.

Economic Barriers: The economic aspect of any project is the base that is strictly limited and should not be exceeded. Beside the high cost of the PV/T technology, the high cost of the PCM products forms the biggest portion of the problem, particularly the organic PCMs which is one of the most suitable PCMs for HVAC and solar applications, however it is expected to be reduced with large scale production in future, but for now it is one of the biggest barriers in front of the phase change materials applications in buildings generally. For MPCM-S based PV/T system, the slurry needs to be changed in specified time intervals depending on the used PCM that adds an extra cost to the operational cost.

Other Barriers: Beside all previous barriers the PCMs themselves have such big problems like supercoiling and instability, that is a part of other problems which could be controlled easier. Despite the large number of PCMs , they are limited for solar

applications , due to the restriction with a melting temperature range, which is around 30ºC for solar applications, so just the low melting temperature phase change materials needed for this purpose, as well as that just few number of them have got investigated thermal and mechanical properties.

7.5 Contribution to knowledge

Despite growing number of studies using PCM in the solar energy field, using MPCM-S is still new and novel, it involved many technical challenges that been solved during implementing the research. So using MPCM-S as cooling fluid of the PV/T system instead of the conventional cooling fluids such as air and water is considered a major contribution to knowledge in PV/T engineering field.

The computerised module is validated twice. Firstly, it validated depending on an established experimental study of a similar water-based PV/T to predict the system's operating performance and optimise its configurations. Secondly, this module is validated depending on the reliable outputs of the current experiments for MPCM-S based PV/T system. So by using this validated computerised module, the feasibility of the MPCM-S based PV/T system has been tested for two different locations in Europe, and it could be used for any part of the world with different climates.

7.6 Recommendation for further research

Due to the importance of the renewable energy, extra works are demanded to be done on MPCM-S based PV/T system, further dynamic simulations need to be done for a precise presentation of the real climate condition and operational parameters. In case of building integrated PV/T, additional outdoor test chamber is required under real climate conditions and for longer period with a proper installation on a building façade. This could represent the entire system performance, and further economic and environmental investigations could be done depending on the output of these realistic kind of systems.

This study is considered as the first step of a wide field of investigations, as the used fluid is quite complex due to comprising of many parameters. Consequently, further investigations are required for each change of any parameter of the slurry such as PCM kind, shell material, carrier fluid, the percentage of substances of the slurry, etc. to

improve the performance of the PV/T system. Finally, Nano-PCM based slurry is another opportunity to be investigated in this field.

REFERENCES

[1] El Chaar L, Lamont L a., El Zein N. Review of photovoltaic technologies. Renew Sustain Energy Rev 2011;15:2165–75.

[2] Parida B, Iniyan S, Goic R. A review of solar photovoltaic technologies. Renew Sustain Energy Rev 2011;15:1625–36.

[3] Anderson TR, Hawkins E, Jones PD. sCO 2 , the greenhouse effect and global warming : from the pioneering work of Arrhenius and Callendar to today ' s Earth System Model. Endeavour 2016;xxx.

[4] Yang L, Xia J, Shen Q. Establishing target-oriented energy consumption quotas for buildings. Util Policy 2016:1–10.

[5] Allouhi a., El Fouih Y, Kousksou T, Jamil a., Zeraouli Y, Mourad Y. Energy consumption and efficiency in buildings: Current status and future trends. J Clean Prod 2015;109:1–13.

[6] Thomsen KE, Rose J, Mørck O, Jensen SØ, Østergaard I, Knudsen HN, et al. Energy consumption and indoor climate in a residential building before and after comprehensive energy retrofitting. Energy Build 2016;123:8–16.

[7] Cao X, Dai X, Liu J. Building energy-consumption status worldwide and the state-of-the-art technologies for zero-energy buildings during the past decade. Energy Build 2016;128:198–213.

[8] https://www.greenworldtrust.org.uk/Science/Curious.htm n.d.

[9] Knopf B, Nahmmacher P, Schmid E. The European renewable energy target for 2030 - An impact assessment of the electricity sector. Energy Policy 2015;85:50–60.

[10] https://ec.europa.eu/energy/en/topics/energy-strategy/2050-energy-strategy n.d.

[11] http://www.telegraph.co.uk/finance/newsbysector/energy/11129336/Solar-could-beat-coal-as-worlds-top-power-source-by-2050-says-IEA.html n.d.

[12] http://www.ren21.net/wp-content/uploads/2015/07/REN12-GSR2015_Onlinebook_low1.pdf n.d.

[13] Sharma RK, Ganesan P, Tyagi VV, Metselaar HSC, Sandaran SC. Developments in organic solid–liquid phase change materials and their applications in thermal energy storage. Energy Convers Manag 2015;95:193–228.

[14] Chen L, Wang T, Zhao Y, Zhang X-R. Characterization of thermal and hydrodynamic properties for microencapsulated phase change slurry (MPCS). Energy Convers Manag 2014;79:317–33.

[15] Kenisarin M, Mahkamov K. Solar energy storage using phase change

materials☆. Renew Sustain Energy Rev 2007;11:1913–65.

[16] Sharma A, Tyagi VV, Chen CR, Buddhi D. Review on thermal energy storage with phase change materials and applications. Renew Sustain Energy Rev 2009;13:318–45.

[17] Browne MC, Norton B, McCormack SJ. Phase change materials for photovoltaic thermal management. Renew Sustain Energy Rev 2015;47:762–82.

[18] Pasupathy a., Velraj R, Seeniraj RV. Phase change material-based building architecture for thermal management in residential and commercial establishments. Renew Sustain Energy Rev 2008;12:39–64.

[19] Sarı A. Thermal characteristics of a eutectic mixture of myristic and palmitic acids as phase change material for heating applications. Appl Therm Eng 2003;23:1005–17.

[20] Diaconu BM, Varga S, Oliveira AC. Experimental assessment of heat storage properties and heat transfer characteristics of a phase change material slurry for air conditioning applications. Appl Energy 2010;87:620–8.

[21] Kalnæs SE, Jelle BP. Phase Change Materials for Building Applications: A State-of-the-Art Review and Future Research Opportunities. Elsevier B.V.; 2015.

[22] Ho CJ, Lin JF, Chiu SY. Heat Transfer of Solid–Liquid Phase-Change Material Suspensions in Circular Pipes: Effects of Wall Conduction. Numer Heat Transf Part A Appl 2004;45:171–90.

[23] Yamagishi Y, Takeuchi H, Pyatenko AT, Kayukawa N. Characteristics of microencapsulated PCM slurry as a heat-transfer fluid. AIChE J 1999;45:696–707.

[24] Safari A, Saidur R, Sulaiman FA, Xu Y, Dong J. A review on supercooling of Phase Change Materials in thermal energy storage systems. Renew Sustain Energy Rev 2016:1–15.

[25] Design A. Latent heat storage in building materials n.d.:1–28.

[26] Zhou D, Zhao CY, Tian Y. Review on thermal energy storage with phase change materials (PCMs) in building applications. Appl Energy 2012;92:593–605.

[27] Wang X, Niu J, Zhang Y. Progresses of Thermal Energy Storage Using Microencapsulated PCM Slurry for Low Energy Building Applications Motivation Properties of MPCM slurry Heat transfer behaviors Applications of MPCM slurry Conclusions n.d.

[28] Tyagi VV, Kaushik SC, Tyagi SK, Akiyama T. Development of phase change materials based microencapsulated technology for buildings: A review. Renew Sustain Energy Rev 2011;15:1373–91.

[29] Zhai XQ, Wang XL, Wang T, Wang RZ. A review on phase change cold storage in air-conditioning system: Materials and applications. Renew Sustain Energy Rev 2013;22:108–20.

[30] Bayés-García L, Ventolà L, Cordobilla R, Benages R, Calvet T, Cuevas-Diarte MA. Phase Change Materials (PCM) microcapsules with different shell compositions: Preparation, characterization and thermal stability. Sol Energy Mater Sol Cells 2010;94:1235–40.

[31] Li W, Zhang XX, Wang XC, Tang GY, Shi HF. Fabrication and morphological characterization of microencapsulated phase change materials (MicroPCMs) and macrocapsules containing MicroPCMs for thermal energy storage. Energy 2012;38:249–54.

[32] Zhang X, Wang X, Wu D. Design and synthesis of multifunctional microencapsulated phase change materials with silver/silica double-layered shell for thermal energy storage, electrical conduction and antimicrobial effectiveness. Energy 2016;111:498–512.

[33] Alvarado JL, Marsh C, Sohn C, Phetteplace G, Newell T. Thermal performance of microencapsulated phase change material slurry in turbulent flow under constant heat flux. Int J Heat Mass Transf 2007;50:1938–52.

[34] https://www.aiaaustin.org/event/phase-change-materials-pcm-high-performance-enclosures n.d.

[35] Jamekhorshid a., Sadrameli SM, Farid M. A review of microencapsulation methods of phase change materials (PCMs) as a thermal energy storage (TES) medium. Renew Sustain Energy Rev 2014;31:531–42.

[36] Shukla A, Buddhi D, Sawhney RL. Thermal cycling test of few selected inorganic and organic phase change materials. Renew Energy 2008;33:2606–14.

[37] Cao F, Yang B. Supercooling suppression of microencapsulated phase change materials by optimizing shell composition and structure. Appl Energy 2014;113:1512–8.

[38] Yin D, Ma L, Liu J, Zhang Q. Pickering emulsion: A novel template for microencapsulated phase change materials with polymer-silica hybrid shell. Energy 2014;64:575–81.

[39] Delgado M, Lázaro A, Mazo J, Zalba B. Review on phase change material emulsions and microencapsulated phase change material slurries: Materials, heat transfer studies and applications. Renew Sustain Energy Rev 2012;16:253–73.

[40] BASF Factbook 2010, BASF, Ludwigshafen, Germany, 1-20, June 2010. n.d.

[41] Griffiths PW, Eames PC. Performance of chilled ceiling panels using phase change material slurries as the heat transport medium. Appl Therm Eng 2007;27:1756–60.

[42] Xiaoli Ma. Investigation of energy transportation capacity of a phase change slurry through a cold storage cooling coil system, International Journal of Energy Research. Int J Energy Res 2009;33:999–1004.

[43] Sari A, Alkan C, Karaipekli A, Uzun O. Microencapsulated n-octacosane as phase change material for thermal energy storage. Sol Energy 2009;83:1757–63.

[44] Wang X, Guo Q, Wang J, Zhong Y, Wang L, Wei X, et al. Thermal conductivity enhancement of form-stable phase-change composites by milling of expanded graphite, micro-capsules and polyethylene. Renew Energy 2013;60:506–9.

[45] Zhang Y, Wang S, Rao Z, Xie J. Experiment on heat storage characteristic of microencapsulated phase change material slurry. Sol Energy Mater Sol Cells 2011;95:2726–33.

[46] Li L, Yu H, Wang X, Zheng S. Thermal analysis of melting and freezing processes of phase change materials (PCMs) based on dynamic DSC test. Energy Build 2016;130:388–96.

[47] Sattari H, Mohebbi A, Afsahi MM, Azimi Yancheshme A. CFD simulation of melting process of phase change materials (PCMs) in a spherical capsule. Int J Refrig 2017;73:209–18.

[48] Tang F, Liu L, Alva G, Jia Y, Fang G. Synthesis and properties of microencapsulated octadecane with silica shell as shape???stabilized thermal energy storage materials. Sol Energy Mater Sol Cells 2017;160:1–6.

[49] Temirel M, Hu H, Shabgard H, Boettcher P, McCarthy M, Sun Y. Solidification of additive-enhanced phase change materials in spherical enclosures with convective cooling. Appl Therm Eng 2017;111:134–42.

[50] Liu L, Alva G, Jia Y, Huang X, Fang G. Dynamic thermal characteristics analysis of microencapsulated phase change suspensions flowing through rectangular mini-channels for thermal energy storage. Energy Build 2017;134:37–51.

[51] Zeng R, Wang X, Chen B, Zhang Y, Niu J, Wang X, et al. Heat transfer characteristics of microencapsulated phase change material slurry in laminar flow under constant heat flux. Appl Energy 2009;86:2661–70.

[52] Zhang GH, Zhao CY. Thermal and rheological properties of microencapsulated phase change materials. Renew Energy 36:2959–66.

[53] Jurkowska M, Szczygieł I. Review on properties of microencapsulated phase change materials slurries (mPCMS). Appl Therm Eng 2016;98:365–73.

[54] Y.Yamagishi,T.Sugeno,T.Ishige,H.Takeuchi ATP. An evaluation of microencapsulated PCM for use in cold energy transportation medium, 1996.

[55] Gschwander S, Schossig P, Henning H. Micro-encapsulated paraffin in phase-change slurries. Sol Energy Mater Sol Cells 2005;89:307–15.

[56] Wang X, Niu J, Li Y, Wang X, Chen B, Zeng R, et al. Flow and heat transfer behaviors of phase change material slurries in a horizontal circular tube. Int J Heat Mass Transf 2007;50:2480–91.

[57] Ma ZW, Zhang P. Modeling the heat transfer characteristics of flow melting of phase change material slurries in the circular tubes. Int J Heat Mass Transf

2013;64:874–81.

[58] Roy SK, Avanic BL. Laminar forced convection heat transfer with phase change material emulsions. Int Commun Heat Mass Transf 1997;24:653–62.

[59] Wang X. Heat Transfer of Microencapsulated PCM Slurry Flow in a circular Tube. AIChE J 2008;54:110–1120.

[60] Kong M, Alvarado JL, Terrell W, Thies C. Performance characteristics of microencapsulated phase change material slurry in a helically coiled tube. Int J Heat Mass Transf 2016;101:901–14.

[61] Wang L, Zhang J, Wang Y, Lin X, Xie N, Chen H. Experimental study on natural convective heat transfer of tube immersed in microencapsulated phase change material suspensions. Appl Therm Eng 2016;99:583–90.

[62] Gao C. Protective Clothing. Elsevier; 2014.

[63] Nejman A, Goetzendorf-Grabowska B. Heat balance of textile materials modified with the mixtures of PCM microcapsules. Thermochim Acta 2013;569:144–50.

[64] Sarier N, Onder E. The manufacture of microencapsulated phase change materials suitable for the design of thermally enhanced fabrics. Thermochim Acta 2007;452:149–60.

[65] Zhang P, Ma ZW, Wang RZ. An overview of phase change material slurries: MPCS and CHS. Renew Sustain Energy Rev 2010;14:598–614.

[66] Entrop a. G, Brouwers HJH, Reinders a. HME. Experimental research on the use of micro-encapsulated Phase Change Materials to store solar energy in concrete floors and to save energy in Dutch houses. Sol Energy 2011;85:1007–20.

[67] Tyagi VV, Kaushik SC, Tyagi SK, Akiyama T. Development of phase change materials based microencapsulated technology for buildings: A review. Renew Sustain Energy Rev 2011;15:1373–91.

[68] Rastogi M, Chauhan A, Vaish R, Kishan A. Selection and performance assessment of Phase Change Materials for heating, ventilation and air-conditioning applications. Energy Convers Manag 2015;89:260–9.

[69] Malvi CS, Dixon-Hardy DW, Crook R. Energy balance model of combined photovoltaic solar-thermal system incorporating phase change material. Sol Energy 2011;85:1440–6.

[70] Barreneche C, Navarro ME, Cabeza LF, Fernández AI. New database to select phase change materials: Chemical nature, properties, and applications. J Energy Storage 2015;3:18–24.

[71] Vitorino N, Abrantes JCC, Frade JR. UIDM - Quality criteria for phase change materials selection. Energy Convers Manag 2016;124:598–606.

[72] Li W, Zhang X, Wang X, Tang G, Shi H. Fabrication and morphological

characterization of microencapsulated phase change materials (MicroPCMs) and macrocapsules containing MicroPCMs for thermal energy storage. Energy 2012;38:249–54.

[73] Zhao L, Wang H, Luo J, Liu Y, Song G, Tang G. Fabrication and properties of microencapsulated n-octadecane with TiO2 shell as thermal energy storage materials. Sol Energy 2016;127:28–35.

[74] Madessa HB. A Review of the Performance of Buildings Integrated with Phase Change Material: Opportunities for Application in Cold Climate. Energy Procedia 2014;62:318–28.

[75] Chandel SS, Agarwal T. Review of current state of research on energy storage, toxicity, health hazards and commercialization of phase changing materials. Renew Sustain Energy Rev 2017;67:581–96.

[76] Nomura T, Sheng N, Zhu C, Saito G, Hanzaki D, Hiraki T, et al. Microencapsulated phase change materials with high heat capacity and high cyclic durability for high-temperature thermal energy storage and transportation. Appl Energy 2017;188:9–18.

[77] Jamekhorshid A, Sadrameli SM, Barzin R, Farid MM. Composite of wood-plastic and micro-encapsulated phase change material (MEPCM) used for thermal energy storage. Appl Therm Eng 2017;112:82–8.

[78] Jie L. Raising evaporative cooling potentials using combined cooled ceiling and MPCM slurry storage. 2nd Int Conf Inf Sci Eng 2010:1390–3.

[79] Wang X, Niu J. Performance of cooled-ceiling operating with MPCM slurry. Energy Convers Manag 2009;50:583–91.

[80] Kousksou T, Bruel P, Cherreau G, Leoussoff V, El Rhafiki T. PCM storage for solar DHW: From an unfulfilled promise to a real benefit. Sol Energy 2011;85:2033–40.

[81] Huang MJ, Eames PC, McCormack S, Griffiths P, Hewitt NJ. Microencapsulated phase change slurries for thermal energy storage in a residential solar energy system. Renew Energy 2011;36:2932–9.

[82] http://www.myershomes.com/solar-panels-are-gaining-ground/ n.d.

[83] Solar H, Thermal P. Evidence Gathering – Low Carbon Heating Technologies Hybrid Solar Photovoltaic Thermal Panels Evidence Gathering – Low Carbon Heating Technologies 2015.

[84] http://www.nef.org.uk/knowledge-hub/solar-energy/types-of-photovoltaic-pv-cells n.d.

[85] Tripathy M, Sadhu PK, Panda SK. A critical review on building integrated photovoltaic products and their applications. Renew Sustain Energy Rev 2016;61:451–65.

[86] Skoplaki E, Palyvos JA. On the temperature dependence of photovoltaic module

electrical performance: A review of efficiency/power correlations. Sol Energy 2009;83:614–24.

[87] Kant K, Shukla A, Sharma A, Biwole PH. Heat transfer studies of photovoltaic panel coupled with phase change material. Sol Energy 2016;140:151–61.

[88] http://www.thegreenage.co.uk/article/the-impact-of-temperature-on-solar-panels/ n.d.

[89] Roger A. Messenger, Jerry Ventre, Photovoltaic System Engineering, 2nd ed., Florida (USA): CRC Press; 2003, 54-55. n.d.

[90] Baloch AAB, Bahaidarah HMS, Gandhidasan P, Al-Sulaiman FA. Experimental and numerical performance analysis of a converging channel heat exchanger for PV cooling. Energy Convers Manag 2015;103:14–27.

[91] Sobhnamayan F, Sarhaddi F, Alavi M a., Farahat S, Yazdanpanahi J. Optimization of a solar photovoltaic thermal (PV/T) water collector based on exergy concept. Renew Energy 2014;68:356–65.

[92] Chow TT. A review on photovoltaic/thermal hybrid solar technology. Appl Energy 2010;87:365–79.

[93] Larsson S. Residential PV versus Ground Mounted PV Comparing the cost of produced electricity 2015.

[94] Cartmell B., Shankland N., Fiala D, Hanby V. A multi-operational ventilated photovoltaic and solar air collector: application, simulation and initial monitoring feedback. Sol Energy 2004;76:45–53.

[95] Tonui JK, Tripanagnostopoulos Y. Improved PV/T solar collectors with heat extraction by forced or natural air circulation. Renew Energy 2007;32:623–37.

[96] Zondag HA, de Vries DW, van Helden WGJ, van Zolingen RJC, van Steenhoven AA. The yield of different combined PV-thermal collector designs. Sol Energy 2003;74:253–69.

[97] Florschuetz LW. Extension of the Hottel-Whillier model to the analysis of combined photovoltaic/thermal flat plate collectors. Sol Energy 1979;22:361–6.

[98] Hottel HC WA. Evaluation of flat-plate solar collector performance. Trans. Conf. use Sol. energy, vol. 2, Tucson, Arizona: University of Arizona Press; 1958.

[99] Zondag HA, de Vries DW, van Helden WGJ, van Zolingen RJC, van Steenhoven AA. The thermal and electrical yield of a PV-thermal collector. Sol Energy 2002;72:113–28.

[100] Kalogirou S a., Tripanagnostopoulos Y. Hybrid PV/T solar systems for domestic hot water and electricity production. Energy Convers Manag 2006;47:3368–82.

[101] Yang T, Athienitis AK. A review of research and developments of building-integrated photovoltaic/thermal (BIPV/T) systems. Renew Sustain Energy Rev 2016;66:886–912.

[102] Moradi K, Ali Ebadian M, Lin CX. A review of PV/T technologies: Effects of control parameters. Int J Heat Mass Transf 2013;64:483–500.

[103] Krauter S, Araujo RG, Schroer S, Hanitsch R, Salhi MJ, Triebel C. COMBINED PHOTOVOLTAIC AND SOLAR THERMAL SYSTEMS 2000;67:239–48.

[104] Chow T-T, Qiu Z, Li C. Potential application of “see-through” solar cells in ventilated glazing in Hong Kong. Sol Energy Mater Sol Cells 2009;93:230–8.

[105] Qiu Z, Chow T, Li P, Li C, Ren J, Wang W, et al. PERFORMANCE EVALUATI ON OF THE PHOTOVOLTA IC DOUBLE-SKIN FACADES 2009:2251–7.

[106] Hussain F, Othman MY., Sopian K, Yatim B, Ruslan H, Othman H. Design development and performance evaluation of photovoltaic/thermal (PV/T) air base solar collector. Renew Sustain Energy Rev 2013;25:431–41.

[107] Daghigh R, Ruslan MH, Sopian K. Advances in liquid based photovoltaic/thermal (PV/T) collectors. Renew Sustain Energy Rev 2011;15:4156–70.

[108] Lamnatou C, Chemisana D. Photovoltaic/thermal (PVT) systems: A review with emphasis on environmental issues. Renew Energy 2017;105:270–87.

[109] Solanki SC, Dubey S, Tiwari A. Indoor simulation and testing of photovoltaic thermal (PV/T) air collectors. Appl Energy 2009;86:2421–8.

[110] http://www.creativeenergyengineering.net/solar.html n.d.

[111] Sopian K, Yigit KS, Liu HT, Kakaç S, Veziroglu TN. Performance analysis of photovoltaic thermal air heaters. Energy Convers Manag 1996;37:1657–70.

[112] Hussain, F., Othman, M. Y. H., Yatim B., Ruslan, H., Sopian, K., Anuar, Z., Khairuddin S. Comparison Study of Air-Based Photovoltaic / Thermal (PV/T) Collector with Different Designs of Heat Exchanger. World Renew Energy Forum, WREF 2012, Incl World Renew Energy Congr XII Color Renew Energy Soc Annu Conf 2012.

[113] Mojumder JC, Chong WT, Ong HC, Leong KY, Abdullah-Al-Mamoon. An experimental investigation on performance analysis of air type photovoltaic thermal collector system integrated with cooling fins design. Energy Build 2016;130:272–85.

[114] Farshchimonfared M, Bilbao JI, Sproul AB. Channel depth, air mass flow rate and air distribution duct diameter optimization of photovoltaic thermal (PV/T) air collectors linked to residential buildings. Renew Energy 2015;76:27–35.

[115] Ooshaksaraei P, Sopian K, Zaidi SH, Zulkifli R. Performance of four air-based photovoltaic thermal collectors configurations with bifacial solar cells. Renew Energy 2017;102:279–93.

[116] Yang T, Athienitis AK. Experimental investigation of a two-inlet air-based building integrated photovoltaic/thermal (BIPV/T) system. Appl Energy 2015;159:70–9.

[117] Solanki SC, Dubey S, Tiwari A. Indoor simulation and testing of photovoltaic thermal (PV/T) air collectors. Appl Energy 2009;86:2421–8.

[118] PVTWINS, < http://www.pvtwins.nl>, accessed at 10/06/2011. n.d.

[119] Tripanagnostopoulos Y, Souliotis M, Battisti R, Corrado a. Energy, cost and LCA results of PV and hybrid PV/T solar systems. Prog Photovoltaics Res Appl 2005;13:235–50.

[120] Tiwari A, Sodha MS. Performance evaluation of solar PV/T system: An experimental validation. Sol Energy 2006;80:751–9.

[121] Yazdanifard F, Ebrahimnia-Bajestan E, Ameri M. Investigating the performance of a water-based photovoltaic/thermal (PV/T) collector in laminar and turbulent flow regime. Renew Energy 2016;99:295–306.

[122] Huang B., Lin T., Hung W., Sun F. Performance evaluation of solar photovoltaic/thermal systems. Sol Energy 2001;70:443–8.

[123] Bahaidarah H, Subhan A, Gandhidasan P, Rehman S. Performance evaluation of a PV (photovoltaic) module by back surface water cooling for hot climatic conditions. Energy 2013;59:445–53.

[124] Jarimi H, Abu Bakar MN, Othman M, Din MH. Bi-fluid photovoltaic/thermal (PV/T) solar collector: Experimental validation of a 2-D theoretical model. Renew Energy 2016;85:1052–67.

[125] Ji J, Chow T-T, He W. Dynamic performance of hybrid photovoltaic/thermal collector wall in Hong Kong. Build Environ 2003;38:1327–34.

[126] He W, Zhang Y, Ji J. Comparative experiment study on photovoltaic and thermal solar system under natural circulation of water. Appl Therm Eng 2011;31:3369–76.

[127] Ji J, He H, Chow T, Pei G, He W, Liu K. Distributed dynamic modeling and experimental study of PV evaporator in a PV/T solar-assisted heat pump. Int J Heat Mass Transf 2009;52:1365–73.

[128] Bakker M, Zondag HA, Elswijk MJ, Strootman KJ, Jong MJM. Performance and costs of a roof-sized PV/thermal array combined with a ground coupled heat pump. Sol Energy 2005;78:331–9.

[129] Ji J, Pei G, Chow T, Liu K, He H, Lu J, et al. Experimental study of photovoltaic solar assisted heat pump system. Sol Energy 2008;82:43–52.

[130] Ji J, He H, Chow T, Pei G, He W, Liu K. Distributed dynamic modeling and experimental study of PV evaporator in a PV/T solar-assisted heat pump. Int J Heat Mass Transf 2009;52:1365–73.

[131] Tsai HL. Modeling and validation of refrigerant-based PVT-assisted heat pump water heating (PVTA-HPWH) system. Sol Energy 2015;122:36–47.

[132] Chen H, Zhang L, Jie P, Xiong Y, Xu P, Zhai H. Performance study of heat-pipe

solar photovoltaic/thermal heat pump system. Appl Energy 2017;190:960–80.

[133] Sharif MKA, Al-Abidi AA, Mat S, Sopian K, Ruslan MH, Sulaiman MY, et al. Review of the application of phase change material for heating and domestic hot water systems. Renew Sustain Energy Rev 2015;42:557–68.

[134] Sharaf OZ, Orhan MF. Concentrated photovoltaic thermal (CPVT) solar collector systems: Part II – Implemented systems, performance assessment, and future directions. Renew Sustain Energy Rev 2014;50:1566–633.

[135] Kibria MA, Saidur R, Al-Sulaiman FA, Aziz MMA. Development of a thermal model for a hybrid photovoltaic module and phase change materials storage integrated in buildings. Sol Energy 2016;124:114–23.

[136] Ma T, Yang H, Zhang Y, Lu L, Wang X. Using phase change materials in photovoltaic systems for thermal regulation and electrical efficiency improvement: A review and outlook. Renew Sustain Energy Rev 2015;43:1273–84.

[137] Hasan A, McCormack SJ, Huang MJ, Norton B. Characterization of phase change materials for thermal control of photovoltaics using Differential Scanning Calorimetry and Temperature History Method. Energy Convers Manag 2014;81:322–9.

[138] Browne MC, Norton B, McCormack SJ. Phase change materials for photovoltaic thermal management. Renew Sustain Energy Rev 2015;47:762–82.

[139] Noro M, Lazzarin R, Bagarella G. Advancements in Hybrid Photovoltaic-thermal Systems: Performance Evaluations and Applications. Energy Procedia 2016;101:496–503.

[140] Su D, Jia Y, Alva G, Liu L, Fang G. Comparative analyses on dynamic performances of photovoltaic-thermal solar collectors integrated with phase change materials. Energy Convers Manag 2017;131:79–89.

[141] Huang MJ, Eames PC, Norton B. Thermal regulation of building-integrated photovoltaics using phase change materials. Int J Heat Mass Transf 2004;47:2715–33.

[142] Elarga H, Goia F, Zarrella A, Dal Monte A, Benini E. Thermal and electrical performance of an integrated PV-PCM system in double skin facades: A numerical study. Sol Energy 2016;136:112–24.

[143] Hasan A, McCormack S, Huang M, Norton B. Energy and Cost Saving of a Photovoltaic-Phase Change Materials (PV-PCM) System through Temperature Regulation and Performance Enhancement of Photovoltaics. Energies 2014;7:1318–31.

[144] Park J, Kim T, Leigh SB. Application of a phase-change material to improve the electrical performance of vertical-building-added photovoltaics considering the annual weather conditions. Sol Energy 2014;105:561–74.

[145] Browne MC, Lawlor K, Kelly A, Norton B, Cormack SJM. Indoor Characterisation of a Photovoltaic/ Thermal Phase Change Material System. Energy Procedia 2015;70:163–71.

[146] Hasan A, Alnoman H, Rashid Y. Impact of integrated photovoltaic-phase change material system on building energy efficiency in hot climate. Energy Build 2016;130:495–505.

[147] Ho CJ, Jou BT, Lai CM, Huang CY. Performance assessment of a BIPV integrated with a layer of water-saturated MEPCM. Energy Build 2013;67:322–33.

[148] Ho CJ, Tanuwijava AO, Lai C-M. Thermal and electrical performance of a BIPV integrated with a microencapsulated phase change material layer. Energy Build 2012;50:331–8.

[149] Chow TT. A review on photovoltaic/thermal hybrid solar technology. Appl Energy 2010;87:365–79.

[150] http://sinovoltaics.com/learning-center/materials/tpt-tedlar-polyester-tedlar-what-is-it/ n.d.

[151] Zhennan Liang HQ and HS. The experimental study on backplane material influencing the performance of solar cell module. g 10 th China Sol. Photovolt. Conf., Changzhou, Jiangsu, China: n.d., p. 988–99.

[152] http://www.mpoweruk.com/heat_engines.htm n.d.

[153] DW. DV. Design of a photovoltaic/thermal combi-panel. PhD Report, EUT, 1998 n.d.

[154] http://www.thermaxxjackets.com/5-most-common-thermal-insulation-materials/ n.d.

[155] Amalfi RL, Vakili-Farahani F, Thome JR. Flow boiling and frictional pressure gradients in plate heat exchangers: part 1, review and experimental database. Int J Refrig 2015.

[156] Gong C, Zhang H, Wang X. Effect of shell materials on microstructure and properties of microencapsulated n-octadecane. Iran Polym J 2009;18:501–12.

[157] http://www.microteklabs.com/pdfs/MPCM-28%20Product%20Data%20Sheet.pdf. n.d.

[158] Goel M, Roy S, Sengupta S. Laminar forced convection heat transfer in microcapsulated phase change material suspensions. … J Heat Mass Transf 1994;37:593–604.

[159] Karaipekli A, Sari A, Kaygusuz K. Thermal conductivity improvement of stearic acid using expanded graphite and carbon fiber for energy storage applications. Renew Energy 2007;32:2201–10.

[160] Vand.V. Theory of Viscosity of Concentrated Suspensions. Nature n.d.;155:364–5.

[161] Duffles JA BW. Solar Engineering of Thermal Processes 2nd Edition. Newyork: 1991.

[162] A KS. Heat transfer of microencapsulated PCM slurry flow in a circular tube. 2009.

[163] Klein SA. Calculation of flat-plate collector loss coefficients. Sol Energy 1975;17:79–80.

[164] Nahar A, Hasanuzzaman M, Rahim NA. Numerical and experimental investigation on the performance of a photovoltaic thermal collector with parallel plate flow channel under different operating conditions in Malaysia. Sol Energy 2017;144:517–28.

[165] John A.Duffie & William A. Beckham. solar engineering of thermal processes. 2nd ed. Newyork: John willy and sons; 1991.

[166] Armstrong BJS, Collopy F. Error Measures For Generalizing About Forecasting Methods: Empirical Comparisons By J. Scott Armstrong and Fred Collopy Reprinted with permission form. Int J Forecast 1992;8:69–80.

[167] DRAFT_Legionella_Policy_V6_October_2014 n.d.

[168] Huang BJ, Chyng JP. Performance characteristics of integral type solar-assisted heat pump. Sol Energy 2001;71:403–14.

[169] http://web2.airmail.net/danb1/european.htm n.d.

[170] https://www.gearthblog.com/wp-content/uploads/2014/10/HistoricalImageryEurope_static.jpg n.d.

[171] https://www.ukpower.co.uk/home_energy/tariffs-per-unit-kwh n.d.

[172] <http://info.cat.org.uk/questions/pv/life-expectancy- solar-PV-panels n.d.

[173] Kalogirou S. Economic analysis of solar energy systems using spreadsheets. Renew Energy 1996;9:1303–7.

[174] Chan A. Energy and environmental performance of building façades integrated with phase change material in subtropical Hong Kong. Energy Build 2011;43:2947–55.

[175] Roger Flanagan. Life Cycle Costing. British library; 1989.

[176] https://www.gov.uk/government/uploads/system/uploads/attachment_data/file/553488/2016_methodology_paper_Final_V01-00.pdf 2016.

[177] https://www.gov.uk/government/uploads/system/uploads/attachment_data/file/69554/pb13773-ghg-conversion-factors-2012.pdf n.d.